Journal of Medicinal Chemistry

pubs.acs.org/jmc

Article

Impact of Combinatorial Histone Modifications on Acetyllysine Recognition by the ATAD2 and ATAD2B Bromodomains

Margaret Phillips,[△] Kiera L. Malone,[△] Brian W. Boyle, Cameron Montgomery, Isabelle A. Kressy, Faith M. Joseph, Kathleen M. Bright, Samuel P. Boyson, Sunsik Chang, Jay C. Nix, Nicolas L. Young, Victoria Jeffers, Seth Frietze, and Karen C. Glass*

Cite This: https://doi.org/10.1021/acs.jmedchem.4c00210

Read Online

ACCESS | Metrics & More | Article Recommendations | Supporting Information

ABSTRACT: The ATPase family AAA$^+$ domain containing 2 (ATAD2) protein and its paralog ATAD2B have a C-terminal bromodomain (BRD) that functions as a reader of acetylated lysine residues on histone proteins. Using a structure−function approach, we investigated the ability of the ATAD2/B BRDs to select acetylated lysine among multiple histone post-translational modifications. The ATAD2B BRD can bind acetylated histone ligands that also contain adjacent methylation or phosphorylation marks, while the presence of these modifications significantly weakened the acetyllysine binding activity of the ATAD2 BRD. Our structural studies provide mechanistic insights into how ATAD2/B BRD-binding pocket residues coordinate the acetyllysine group in the context of adjacent post-translational modifications. Furthermore, we investigated how sequence changes in amino acids of the histone ligands impact the recognition of an adjacent acetyllysine residue. Our study highlights how the interplay between multiple combinations of histone modifications influences the reader activity of the ATAD2/B BRDs, resulting in distinct binding modes.

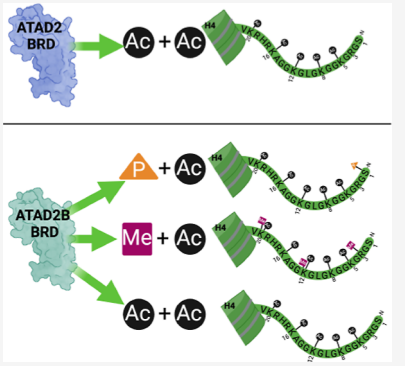

1. INTRODUCTION

DNA is tightly packaged within the eukaryotic nucleus in the form of chromatin. The primary units of chromatin are nucleosomes, composed of ∼146 base pairs of DNA wrapped around an octamer of histone proteins that includes two copies of each of histone H3, H4, H2A, and H2B.[1−3] Histones are subject to various post-translational modifications (PTMs) by the enzymatic addition of covalent chemical groups to their globular domain and to the amino-terminal tails that extrude from the nucleosome core particle.[4] Many histone PTMs, including methylation, phosphorylation, acetylation, ubiquitylation, SUMOylation, glycosylation, and ADP-ribosylation, govern different biological processes by regulating chromatin structure and function.[5−7] Distinctive combinations of multiple types of histone PTMs can be present simultaneously on histones, commonly referred to as forming the "histone code."[8] These unique patterns of histone PTMs serve as binding sites for various effector proteins that translate the histone code into biological readouts, including the activation and repression of gene expression.[9−12] Focused research efforts have allowed us to understand how the different histone "reader" proteins selectively recognize individual PTMs; however, much less is known about the combinatorial recognition of histone modifications.

Among the protein "reader" domains that bind various histone PTMs, bromodomains (BRDs) are acknowledged as the primary reader of acetylated lysine residues.[13] Histone acetylation regulates the relaxation of chromatin structure via repulsive electrostatic interactions between the acetyl group and the DNA phosphodiester backbone, permitting the accessibility of sequence-specific transcription factors to the DNA.[14,15]Histone acetylation also serves as a docking site for the recruitment and assembly of protein complexes at distinct regulatory elements within the chromatin.[16,17]The histone PTM ligand-binding specificity of BRDs is dictated by the amino acid sequence surrounding the acetyllysine modification on the histone protein and by the residues lining the BRD-binding pocket.[18] While high-resolution structures of various BRDs complexed with acetylated histone ligands have provided critical insights into ligand recognition, understanding how combinatorial patterns of multiple PTMs influence histone ligand selectivity remains an area of significant interest. The importance of multiple modifications on functional outcomes was recently highlighted by a study on the tandem-Tudor domain of human UHRF1, which demonstrated that the *in vivo* association of UHRF1 with chromatin is correlated with histone H3K9me2/3 in combination with H3K4me1 and that dual readout of these

Received: February 1, 2024
Revised: April 10, 2024
Accepted: April 19, 2024

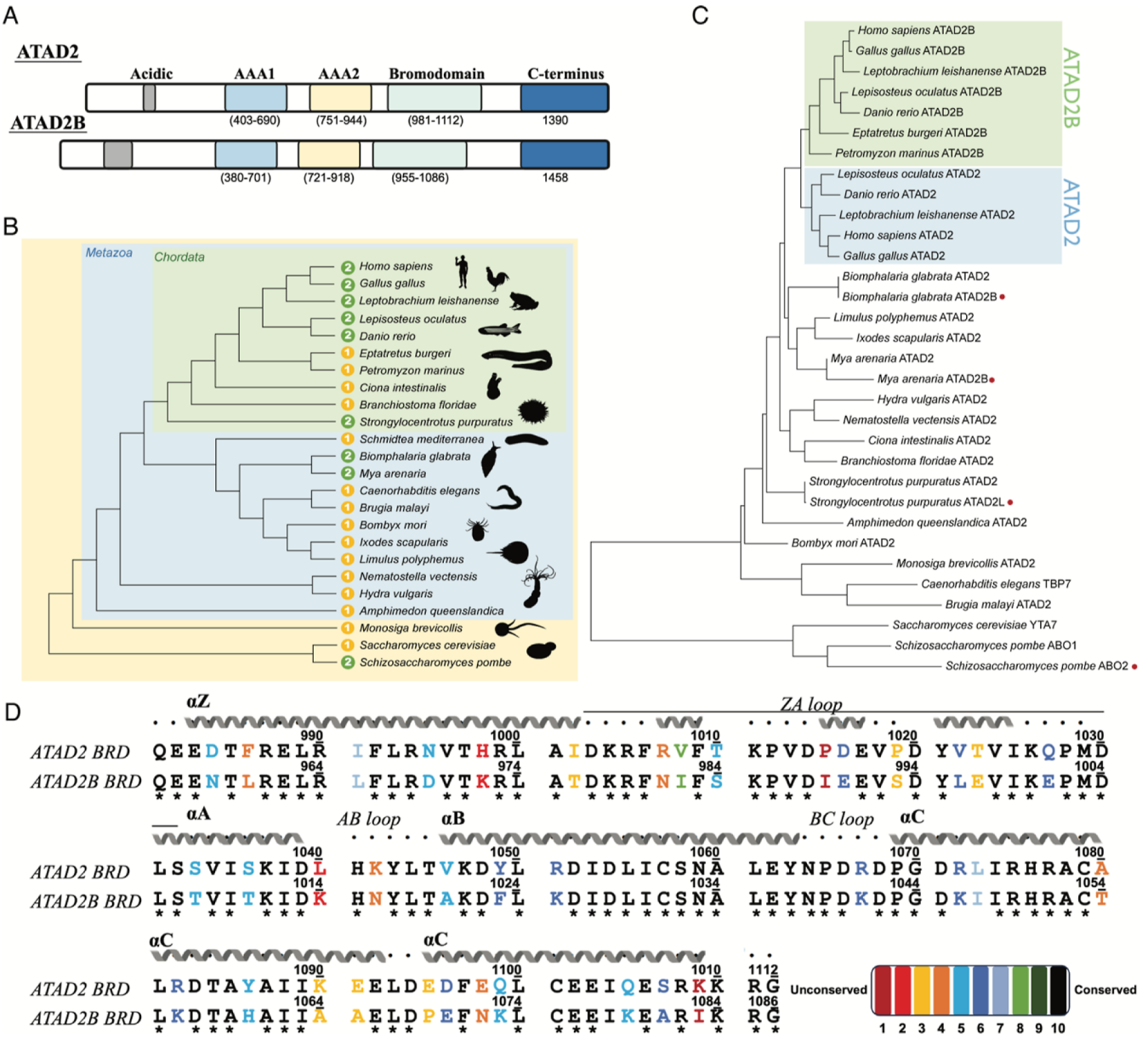

Figure 1. Evolution of ATAD2 homologues in animals. (A) Domain architecture of the human ATAD2 and ATAD2B proteins with the conserved functional domains highlighted. (B) Phylogeny of species within the Opisthokonta with the number of ATAD2 homologues indicated in the yellow (one homologue) or green (two homologues) circles. (C) Phylogenetic tree of the BRD sequences in ATAD2 homologues from species depicted in (A), inferred by using the maximum likelihood method and JTT matrix-based model. The branches representing the ATAD2 and ATAD2B lineages in vertebrates are highlighted in the blue and green shaded boxes, respectively. Red circles indicate predicted ATAD2 duplications that occurred independently of vertebrate ATAD2 and ATAD2B evolution. The tree is drawn to scale, with branch lengths measured in the number of substitutions per site. Animal silhouette images were obtained from http://www.phylopic.org/, where they are available under the public domain CC0 1.0 DEED. (D) Sequence alignment of the human ATAD2 and ATAD2B BRD region, residues 981−1112 and 955−1086, respectively. Sequence alignment and conservation analysis were performed with PRALINE.[19] Secondary structure alignments were performed using PROMALS3D.[20] The secondary structure features are annotated above the sequence. Identical residues are marked with an (*), and the conservation of residues is scored on a scale from 1 for the most unconserved residue, to 10 for the most conserved residue in the alignment.

modifications significantly increased its binding affinity for modified histone ligands.[21]

ATAD2 and ATAD2B are BRD-containing proteins that harbor conserved AAA$^+$ (ATPases associated with diverse cellular activities) ATPase domains.[22] As paralogs, ATAD2 and ATAD2B share a high degree of amino-acid similarity (97% similar in the ATPase domains and 74% in the BRDs).[23] Their BRDs also share high structural similarity and appear to have similar ligand-binding preferences.[24−27] While ATAD2 has been demonstrated to serve as a chromatin-binding protein and current research indicates it functions in regulating chromatin structure and transcription,[24,26] the function of ATAD2B remains elusive.

In this study, we investigated the similarities and differences between the ATAD2 and ATAD2B paralogs. First, we conducted an evolutionary analysis to identify when a gene duplication event occurred to produce these two paralogs. We compared the selectivity of the reader function of the ATAD2 and ATAD2B BRDs using different histone H4 ligands containing multiple combinations of PTMs, including

https://doi.org/10.1021/acs.jmedchem.4c00210
J. Med. Chem. XXXX, XXX, XXX−XXX

Table 1. Histone H4 N-Terminus Tail-Binding Affinities to the ATAD2 and ATAD2B BRD-Containing Proteins[a]

peptide	peptide sequence	K_D for ATAD2 (μM)	N	K_D for ATAD2B (μM)	N	% abundance
H4 unmodified (residues 1−24)	SGRGKGGKGLGKGGAKRHRKVLRD	no binding	NA	no binding	NA	53.17 ± 0.75
H4K5ac (1−24)	SGRG(Kac)GGKGLGKGGAKRHRKVLRD	57.7 ± 10.7	1.00	50.5 ± 4.4	1.00	3.62 ± 1.62
H4K8ac (1−24)	SGRGKGG(Kac)GLGKGGAKRHRKVLRD	no binding	NA	no binding	NA	6.69 ± 0.29
H4K12ac (1−24)	SGRGKGGKGLG(Kac)GGAKRHRKVLRD	65.6 ± 8.9	1.00	22.8 ± 2.1	1.00	8.52 ± 1.63
H4K16ac (1−24)	SGRGKGGKGLGKGGA(Kac)RHRKVLRD	no binding	NA	no binding	NA	9.77 ± 0.48
H4K20ac (1−24)	SGRGKGGKGLGKGGAKRHR(Kac)VLRD	no binding	NA	no binding	NA	*
H4K5acK8ac (1−24)	SGRGKGGKGLGKGGAKRHR(Kac)VLRD	273.7 ± 34.3	1.00	94.6 ± 17.2	1.00	2.25 ± 1.11
H4K5acK12ac (1−24)	SGRG(Kac)GGKGLG(Kac)GGAKRHRKVLRD	38.5 ± 5.4	1.03	25.9 ± 4.0	1.00	7.92 ± 0.23
H4K8acK12ac (1−24)	SGRGKGG(Kac)GLG(Kac)GGAKRHRKVLRD	52.1 ± 2.9	1.00	30.9 ± 1.6	1.00	11.95 ± 1.64
H4K12acK16ac (1−24)	SGRGKGGKGLG(Kac)GGA(Kac)RHRKVLRD	78.1 ± 8.9	1.00	35.6 ± 3.6	1.00	29.83 ± 7.03
H4K12acK20ac (1−24)	SGRGKGGKGLG(Kac)GGAKRHR(Kac)VLRD	41.0 ± 0.7[28]	1.00	29.1 ± 4.7	1.01	[a]
H4K5acK8acK12ac (1−24)	SGRG(Kac)GG(Kac)GLG(Kac) GGAKRHRKVLRD	64.9 ± 5.0	1.00	78.3 ± 2.9	1.00	6.44 ± 1.78
H4K5acK12acK16ac (1−24)	SGRG(Kac)GGKGLG(Kac)GGA(Kac) RHRKVLRD	84.0 ± 6.8	1.00	34.1 ± 6.3	1.00	7.84 ± 1.04
H4K8acK12acK16ac (1−24)	SGRGKGG(Kac)GLG(Kac)GGA(Kac) RHRKVLRD	20.8 ± 1.6	1.00	47.8 ± 7.2	1.00	25.18 ± 2.69
H4K5acK8acK12acK16ac (1−24)	SGRG(Kac)GG(Kac)GLG(Kac)GGA(Kac) RHRKVLRD	125.9 ± 26.6	0.99	62.8 ± 10.9	1.00	27.24 ± 4.11
H4R3me2aK5ac (1−24)	SG(Rme2a)G(Kac) GGKGLGKGGAKRHRKVLRD	211 ± 39.4	1.08	55.5 ± 11.2	1.00	[a]
H4K5acK8me1K12ac (1−24)	SGRG(Kac)GG(Kme1)GLG(Kac) GGAKRHRKVLRD	64.0 ± 10.1	0.93	48.2 ± 2.4	1.00	*
H4K5acK8me1K12acK16ac (1−24)	SGRG(Kac)GG(Kme1)GLG(Kac)GGA(Kac) RHRKVLRD	257 ± 40.5	1.00	47.9 ± 1.4	1.00	*
H4K16acK20me3 (1−24)	SGRGKGGKGLGKGGA(Kac)RHR(Kme3)VLRD	no binding	NA	no binding	NA	*
H4S1phK5ac (1−15)	SGRG(Kac)GGKGLGKGGA	439.0 ± 22.0	1.00	84.2 ± 13.1	1.00	*

[a]The dissociation constants (K_D) for the ATAD2 and ATAD2B BRD interaction with multiple modifications on histone H4 peptides as determined by isothermal calorimetry (ITC). The identity and abundance of specific PTMs in MCF7 cells were carried out using mass spectrometry. NA—not applicable. *—below detection limits.

acetylated lysine adjacent to another acetylation, phosphorylation, or methylation mark. Then, using X-ray crystallographic structural approach, we solved five, novel, high-resolution structures of the ATAD2 and ATAD2B BRDs in complex with multivalent histone H4 ligands. Additionally, using ligands from mutant onco-histones and histone variants, we investigated how changes in the histone tail sequence affect the recognition of adjacent acetylated lysine modifications. These results provide new insights into the interaction of the understudied ATAD2B BRD with histone H4 PTMs and highlight how combinations of histone modifications regulate BRD selectivity. Our comparative analysis of the ATAD2 and ATAD2B BRDs reveals their unique binding activities and sheds light on their possible nonredundant biological functions, providing new insights into their evolution and functional divergence.

2. RESULTS

2.1. Gene Duplication of *ATAD2* Occurred Several Times during Eukaryotic Evolution. The *ATAD2* gene encodes for two AAA$^+$ ATPase domains and a C-terminal BRD (Figure 1A) that is thought to play an essential role in chromatin remodeling. *ATAD2* is found in a diverse variety of organisms ranging from yeast to humans. A gene duplication event resulting in two paralogous proteins, ATAD2 and ATAD2B, is found in humans and many other higher eukaryotic organisms. However, the origin and conservation of ATAD2/B are unclear.

Evolutionary analysis of ATAD2 homologues across eukaryotes identifies at least a single homologue of ATAD2 in all species within the opisthokonts, the major eukaryote supergroup representing fungi and metazoans (Figure 1B). Within the vertebrates, most species contain both ATAD2 and ATAD2B homologues, with the exception of the early branching chordates, suggesting that the gene duplication occurred more recently during vertebrate evolution. One of the early branching chordates, the purple sea urchin (*Strongylocentrotus purpuratus*), also contains two ATAD2 homologues. Further comparison of the protein sequences of the purple sea urchin homologues with ATAD2 and ATAD2B sequences from other vertebrates reveals that these are more divergent from the mammalian ATAD2 proteins. This comparison also indicates a more recent expansion of ATAD2 in the Chordata after divergence from the evolutionary trajectory of mammals.

To determine how the evolution of ATAD2 orthologues might have functional implications for the BRD, we performed a phylogenetic analysis of ATAD2 BRD sequences from the selected species within the Opisthokonta. ATAD2 and ATAD2B BRDs assemble into two distinct groups in the vertebrates, supporting the hypothesis that the second paralog derived from a single gene duplication event. Interestingly, we identified the single ATAD2 homologues in jawless fish (*Eptatretus burgeri* and *Petromyzon marinus*) group with the ATAD2B homologues from other species (Figure 1C, green shaded box). This presents two possibilities that either ATAD2B was the original ATAD2 in vertebrates that was later duplicated to form ATAD2 after the divergence of the jawless fish or that the ATAD2 homologue was lost at some point during the jawless fish evolutionary trajectory. This

https://doi.org/10.1021/acs.jmedchem.4c00210
J. Med. Chem. XXXX, XXX, XXX−XXX

analysis also reveals evidence of multiple independent duplications of ATAD2 in many of the other species we examined (*Mya arenaria*, *Biomphalaria glabrata* and *Schiz. pombe*), suggesting that expansion of ATAD2 variants is a relatively common evolutionary event and might represent a beneficial strategy for dealing with increasing transcriptional complexity.

Gene duplication and retention of the ATAD2 orthologs in vertebrates suggest that the ATAD2 and ATAD2B proteins may have independent functions. As paralogs, human ATAD2 and ATAD2B share a high degree of amino-acid similarity (97% similarity in the ATPase domains and 74% in the BRDs) (Figure 1D).[23] Their BRDs also share high structural similarity and have similar ligand-binding preferences. Their conserved structural features make it difficult to determine if ATAD2 and ATAD2B have independent or redundant functions. In cells, the ATAD2 protein has been shown to associate with newly synthesized histones,[26,29] which is characterized by the presence of diacetylated H4 histones containing H4K5acK12ac. ATAD2 has been demonstrated to serve as a chromatin-binding protein, and current research indicates that it regulates chromatin structure and transcription.[24,26] Expression of ATAD2 is restricted to S-phase,[26] indicating a cell cycle-specific function of the ATAD2 complex. However, the cellular function(s) of ATAD2B is still unknown. We conducted an in-depth structure−function analysis of the ATAD2 and ATAD2B BRDs to characterize the unique features of these two BRDs and elucidate how they contribute to distinct histone ligand recognition and binding activity.

2.2. Combinatorial Histone PTMs Influence "Kac" Recognition by the ATAD2/B BRDs. Our previous study compared the recognition of acetylated histone ligands by the ATAD2 and ATAD2B BRDs using an unbiased histone PTM ligand-binding dCypher screen that included 288 distinct peptides with both single and combinatorial histone modifications.[27] We found that the ATAD2 BRD preferred a select subset of acetyllysine modifications, recognizing 11 histone ligands within the context of adjacent acetylation, phosphorylation, and methylation modifications.[27] In contrast, the ATAD2B BRD is more promiscuous and could recognize 39 different acetylated histone ligands, including many with multiple adjacent PTMs.[27] While the BRDs recognize only acetylation marks, we hypothesized that neighboring PTMs (of varying shape, size, and charge) would impact the acetyllysine insertion into the BRD-binding pocket. Thus, to understand how adjacent PTMs modulate the binding activities of the ATAD2 and ATAD2B BRDs, we first performed a quantitative analysis using ITC (isothermal titration calorimetry) of the ligand-binding activity of these two BRDs with histone H4 peptides containing combinatorial PTMs. The histone peptides used in the experiments were selected from the top histone H4 ligands identified previously[27] and were designed to have uniform amino-acid sequence lengths to allow for a direct comparison (Table 1 and Figures S1 and S2).

Among the monoacetylated histone H4 ligands tested, the ATAD2 BRD prefers the H4K5ac modification binding with an affinity of K_D = 57.7 ± 10.7 μM compared to the ATAD2B BRD, which demonstrates the highest binding affinity for the H4K12ac ligand (K_D = 22.8 ± 2.1 μM). Neither of the ATAD2/B BRDs bind to H4K8ac, H4K16ac, and H4K20ac peptides.

Among the diacetylated histone H4 peptides tested, both ATAD2/B BRDs prefer the H4K5acK12ac modification, binding with affinities of K_D = 38.5 ± 5.4 and 25.9 ± 4.0 μM, respectively. In contrast, significantly reduced binding affinities are observed for recognition of the H4K5acK8ac combinatorial marks by the ATAD2/B BRDs (K_D = 273.7 ± 34.3 and 94.6 ± 17.2 μM, respectively), when compared to H4K5ac alone.

For the three triacetylated H4 peptides tested, the ATAD2 BRD binds to H4K8acK12acK16ac peptide with the highest affinity (K_D = 20.8 ± 1.6 μM) but displays an almost fourfold decrease in affinity for H4K5acK12acK16ac (K_D = 84.0 ± 6.8 μM). In contrast, the ATAD2B BRD shows the tightest binding to the H4K5acK12acK16ac combinatorial modifications (K_D = 34.1 ± 6.3 μM).

The differences in ATAD2 and ATAD2B BRD-binding selectivity are most noticeable in H4 peptides carrying hydrophobic methyl modifications in combination with acetylation marks. Overall, the binding affinity of the ATAD2 BRD for acetyllysine marks near mono- and dimethylation modifications is reduced, while the presence of adjacent methyl groups has an insignificant effect on the ATAD2B BRD activity (Table 1). For example, the addition of bulky dimethyl groups at Arg 3 significantly reduces the affinity of the ATAD2 BRD for the "K5ac" mark in H4R3me2aK5ac (K_D = 211 ± 39.4 μM compared to the H4K5ac K_D = 57.7 ± 10.7 μM). However, the ATAD2B BRD tolerates the presence of adjacent methyl groups, with no notable change in its affinity for the H4R3me2aK5ac (K_D = 55.5 ± 11.2 μM) compared to H4K5ac alone (K_D = 50.5 ± 4.4 μM).

Histone post-translational modifications are dynamic and often found in different abundances on the N- and C-terminal regions of histone proteins.[8,30−35] The modified histone ligands in the dCypher screen were designed and synthesized to cover known post-translational modifications on the canonical and variant histones in a combinatorial manner. However, it does not necessarily represent the physiologically relevant combinations of modifications on individual histone molecules (also known as histone proteoforms) that are biologically available within the cell. To assess this, we used a top-down proteomic approach, which omits protein digestion, to identify and quantify the abundance of intact histone H4 proteoforms in MCF7 human breast cancer cells (Table 1, right column). This proteoform profile confirms that mono-, di-, tri-, and tetra-acetylated histone H4 are biologically relevant ligands and that phosphorylation and methylation marks surrounding the acetylated lysine modifications are also available within these cells. Thus, the combination(s) of physiologically relevant combinations of histone PTMs likely influences the histone recognition activity of the ATAD2 and ATAD2B BRDs within the cell.

2.3. Molecular Basis of Acetyllysine Recognition by the ATAD2/B BRDs. *2.3.1. Distinct Recognition of Monoacetylated Histone H4.* While recognition of monoacetylated histone ligands such as H4K5ac and H4K12ac by the ATAD2 BRD is established,[24,31] there is little information on how its paralog, the ATAD2B BRD, coordinates acetylated lysine modifications. To elucidate the molecular mechanisms involved in acetyllysine recognition by the lesser-studied ATAD2B, we co-crystallized the ATAD2B BRD with the monoacetylated histone H4K12ac (residues 4−17) ligand. The X-ray crystal structure of this complex was solved to a resolution of 2.0 Å (PDB ID: 8UHL) by molecular replacement using the apo ATAD2B BRD crystal structure (PDB ID:3LXJ) as the search model (Figure 2A and Table

https://doi.org/10.1021/acs.jmedchem.4c00210
J. Med. Chem. XXXX, XXX, XXX−XXX

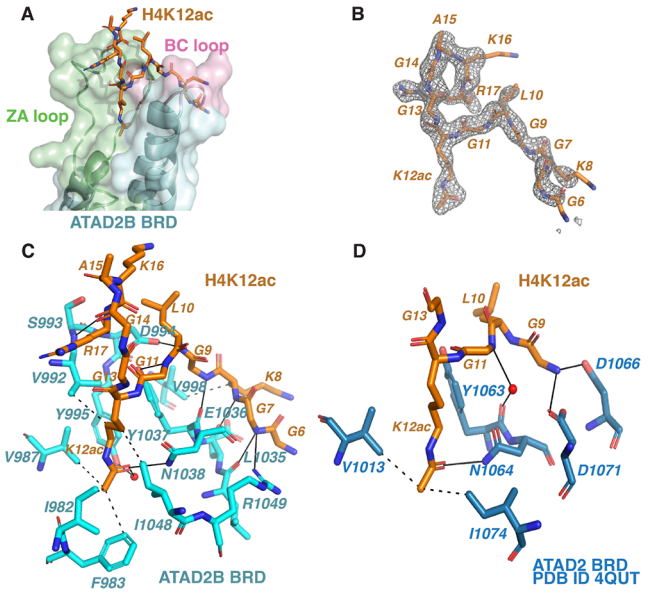

Figure 2. Coordination of the histone H4K12ac ligand by the ATAD2/B BRDs. (A) Surface representation of the ATAD2B BRD in complex with the H4K12ac ligand (residues 4−17) (PDB ID: 8EOQ). The H4K12ac ligand residues are shown as orange sticks, while the cartoon representation of BRD (cyan) highlights the ZA and BC loops in green and pink, respectively. (B) An isolated image of the simulated annealing composite omit map (gray) around the histone ligand H4K12ac (orange) contoured at 1σ. The composite omit map was calculated before building the histone ligand into the structure. (C) Coordination of the H4K12ac ligand by the ATAD2B BRD. Residues lining the BRD pocket involved in ligand coordination are displayed in cyan, while the H4K12ac ligand residues are displayed in orange. Hydrogen bonds are represented by solid black lines, while dashed black lines show hydrophobic interactions. Water molecules are shown in red. (D) Coordination of the H4K12ac ligand (residues 9−16) by the ATAD2 BRD as obtained from the previously solved crystal structure (PDB ID: 4QUT).[24,31] Residues lining the BRD pocket involved in ligand coordination are displayed in dark blue, while the H4K12ac ligand residues are indicated in orange. Hydrogen bonds are represented by solid black lines, while dashed black lines show hydrophobic interactions. Water molecules are shown in red.

S1). Good ligand density is observed for residues Gly 6 to Arg 17 of the histone H4 peptide within the canonical ATAD2B BRD pocket (Figure 2B). Multiple hydrogen bonds and hydrophobic interactions contribute to the histone H4K12ac ligand coordination (Figure 2C). Although the ATAD2 and ATAD2B BRDs share a conserved acetyllysine recognition pattern, their coordination of adjacent histone residues in the BRD-binding pocket is starkly different. This distinction is evident through the divergent binding affinities observed with an identical H4K12ac ligand as determined by ITC (ATAD2 K_D: 65.6 ± 8.9 μM; ATAD2B K_D: 22.8 ± 2.1 μM). A detailed comparison of the ATAD2 BRD in complex with the H4K12ac ligand solved previously (PDB ID: 4QUT)[24] (shown in Figure 2D), with our ATAD2B BRD complex structure, highlights some of the features of H4K12ac recognition by the two BRDs (compare Figure 2C and D). Coordination of the acetyllysine moiety carbonyl group occurs via a direct hydrogen bond to the conserved N1038 and N1064 of the ATAD2B and ATAD2 BRDs, respectively. Similarly, the hydrophobic interaction between V987 and the gatekeeper residue I1048 of ATAD2B with the acetyllysine group of the histone ligand is similar to the hydrophobic interaction made by the corresponding V1013 and I1074 residues in the ATAD2 BRD. However, major differences in the coordination of the histone H4K12ac ligand by the two BRDs lie in the extent of the histone tail readout. In ATAD2B, multiple hydrogen bonds are formed between the ZA/BC loop region of the BRD and residues within the histone ligand, while only three hydrogen bonds (one through water) are observed with the same ligand in the ATAD2 BRD pocket. In our ATAD2B structure, the conserved tyrosine (Y1037) makes direct hydrogen bonds with the histone residues Gly 9 and Gly 11. In contrast, in the ATAD2 structure (4QUT), there is only one water-mediated bond to Gly 11 of the histone ligand through the backbone carbonyl group of the conserved tyrosine Y1063. Furthermore, we observe several additional protein−ligand contacts in the ATAD2B−H4K12ac BRD structure that are not seen in the ATAD2−H4K12ac structure. These include Gly 7 of histone H4 and L1035 and R1049 of ATAD2B, Lys 8 and Gly 9 with ATAD2B E1036, Leu 10 with ATAD2B D994, and Arg 17 with ATAD2B S993 for a total of nine direct hydrogen bonds coordinating the ATAD2B BRD−H4K12ac ligand interaction in addition to contacts with the acetyllysine group. Thus, our crystal structure illustrates how the ATAD2B BRD uses a canonical binding pocket to "read" acetylated histone H4K12. It also highlights the diverse network of polar and nonpolar interactions that guide the selection of this modification. Importantly, our results show that despite sharing high structural similarity in recognition of acetylated lysine, the ATAD2 and ATAD2B BRDs coordinate the histone H4 protein using distinct binding modes that are fine-tuned through specific interactions between the BRD-binding pocket and the histone H4 tail residues.

2.3.2. Effect of Adjacent Modifications on "Kac" Recognition. Based on the ATAD2B−H4K12ac structure, where several polar contacts are observed between the BRD and histone residues surrounding the acetyllysine mark, we hypothesized that neighboring PTMs would impact acetyllysine recognition by the ATAD2/B BRDs. Our previous research highlighted the importance of the first three residues, "SGR," in coordinating acetyllysine on the histone H4 tail as their deletion completely abolished H4K5ac and H4K8ac ligand binding.[27] Based on this, we selected the histone H4S1phK5ac (residues 1−15) ligand as we hypothesized that a negatively charged phosphoryl group (ph) at Ser 1 would impact recognition of the adjacent H4K5ac group by the two BRDs. To characterize how this H4S1ph modification alters the molecular mechanism of acetyllysine coordination, we co-crystallized the ATAD2 and ATAD2B BRDs with the H4S1phK5ac peptide. We solved the crystal structures of the ATAD2 and ATAD2B BRDs−ligand complexes at resolutions of 1.85 Å (PDB ID: 8SDQ) and 1.4 Å (PDB ID: 8UK5), respectively (Figure 3 and Tables S2 and S3, respectively). Electron density for histone H4 residues 1−7 is observed within the ATAD2 BRD-binding pocket (Figure 3A,C), whereas electron density for H4 residues 1−6 is seen in the ATAD2B BRD pocket (Figure 3B,D). Similar to H4K12ac, the coordination of H4K5ac by both BRDs involves a combination of hydrogen bonds and hydrophobic contacts. In our ATAD2/B structures, direct hydrogen bonds are observed between the conserved N1064 of ATAD2 and the corresponding N1038 in ATAD2B and the carbonyl oxygen atom of the H4K5ac group (Figure 3C,D). This acetyllysine residue is further stabilized by hydrophobic contacts between its side chain and residues

https://doi.org/10.1021/acs.jmedchem.4c00210
J. Med. Chem. XXXX, XXX, XXX−XXX

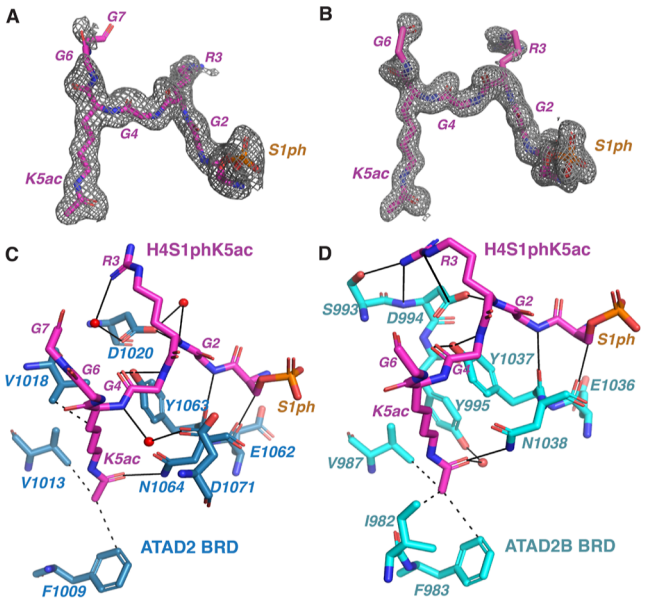

Figure 3. Coordination of the histone H4S1phK5ac ligand by the ATAD2A and ATAD2B BRDs. (A) An isolated image of the simulated annealing composite omit map (gray) around the histone ligand H4S1phK5ac (magenta, residues 1−7) contoured at 1σ observed in the ATAD2 BRD−H4S1phK5ac complex (PDB ID: 8SDQ). The composite omit map was calculated before building the histone ligand into the structure. (B) An isolated image of the simulated annealing composite omit map (gray) around the histone ligand H4S1phK5ac (magenta, residues 1−6) contoured at 1σ observed in the ATAD2B BRD−H4S1phK5ac complex. (C) Coordination of the H4S1phK5ac ligand (residues 1−7) by the ATAD2 BRD. Residues lining the BRD pocket involved in ligand coordination are displayed in dark blue, while the H4S1phK5ac ligand residues are shown in magenta. (D) Coordination of the H4S1phK5ac ligand (residues 1−6) by the ATAD2B BRD (PDB ID: 8UK5). Residues lining the BRD pocket involved in ligand coordination are displayed in cyan, while the H4S1phK5ac ligand residues are shown in magenta. Hydrogen bonds are represented by solid black lines, while dashed black lines show hydrophobic interactions. Water molecules are shown in red.

F1009, V1013, and V1018 of the ATAD2 BRD (Figure 3C) and the corresponding residues F983 and V987 in the ATAD2B BRD (Figure 3D). The conserved tyrosine residue (Y1063 in ATAD2 and Y1037 in ATAD2B BRD) is also crucial for coordinating the histone H4 ligand as seen by the hydrogen bonds between this tyrosine residue and Gly 2 and Gly 4 of the H4 ligand in the two structures (Figure 3C,D). Similarly, coordination of the adjacent phosphorylated Ser 1 in the histone H4 ligand is comparable between the two BRDs where the backbone carbonyl of the glutamic acid residue (E1062 in ATAD2 and E1036 in ATAD2B) interacts with the backbone amide of the Ser1ph group. Interestingly, while the ATAD2 BRD coordinates several residues in the histone H4 ligand via water-mediated hydrogen bonds (D1020 with Arg 3 and Gly 2 and D1071 with Gly 4), all of these parallel interactions in the ATAD2B BRD occur through direct hydrogen bonds (Figure 3D). Notably, the direct hydrogen-bond interactions between the ATAD2B BRD−H4S1phK5ac ligand appear to exclude water from the binding pocket and stabilize ligand coordination, resulting in a significantly increased binding affinity of K_D = 84.2 ± 13.1 μM when compared with the ATAD2 BRD−H4S1phK5ac K_D = 439.0 ± 22.0 μM (Table 1). Despite the high structural similarity between the BRDs, slight differences in the amino acid sequence between the ATAD2/B paralogs likely play a role in their ligand-binding specificity. For example, ATAD2B makes direct hydrogen-bond contacts to the side chain of Arg 3 in the histone ligand with residues S993 and D994. In ATAD2 however, these residues are P1019 and D1020. D1020 of the ATAD2 BRD makes a water-mediated hydrogen-bond contact to Arg 3 in the histone ligand, but P1019 in ATAD2 is unable to form a hydrogen bond with this residue. Thus, the sequence divergence between ATAD2 and ATAD2B BRDs appears to alter the side chain conformations and orientation of the histone ligand in the binding pocket. Overall, our structure−function analysis of the ATAD2 and ATAD2B BRDs demonstrates that in the context of multiple post-translational modifications, such as a phosphorylated serine adjacent to acetyllysine, differences in the amino acid sequence of the BRD-binding pocket can result in significant changes in ligand coordination. These differences in histone-binding modes contribute to the distinct binding specificities and affinities observed by BRDs and result in altered functional activities of BRD region, which would then influence the chromatin targets of the associated BRD-containing proteins, in this case, the full-length ATAD2 and ATAD2B proteins.

2.4. Histone Amino Acid Sequence Regulates BRD Activity. Our crystal structures highlight the importance of specific BRD residues in coordinating the "Kac" mark by participating in water-mediated or direct polar contacts with the amino acid residues in the histone tail ligands in the BRD-binding pocket. We hypothesized that any changes to the sequence of the N-terminal histone tail would impact the recognition of nearby acetylated lysine modifications by the BRD.

2.4.1. Mutations in the H4 N-Terminal Tail Alter the ATAD2/B BRD Activity. A recent study identified "onco" mutations in the histone genes associated with cancer.[36] Several of these mutations occur at or adjacent to sites of known PTMs.[36,37] We hypothesized that these "onco"

Table 2. Binding Affinities of the ATAD2/B BRD with the Histone H4 Oncohistone Peptides with an Acetyllysine Modification on K5 as Measured by ITC[a]

peptide	peptide sequence	K_D for ATAD2 (μM)	N	K_D for ATAD2B (μM)	N
H4K5ac (1−15)	SGRG(Kac)GGKGLGKGGA	39.4 ± 6.0[41]	1.04	5.2 ± 1.0[27]	1.00
H4**S1C**K5ac (1−15)	**C**GRG(Kac)GGKGLGKGGA	12.9 ± 2.5	1.00	19.4 ± 2.9	1.00
H4**R3C**K5ac (1−15)	SG**C**G(Kac)GGKGLGKGGA	22.8 ± 2.0	1.00	22.9 ± 1.4	1.07
H4**G4D**K5ac (1−15)	SGR**D**(Kac)GGKGLGKGGA	no binding	NA	no binding	NA
H4**G4S**K5ac (1−15)	SGR**S**(Kac)GGKGLGKGGA	no binding	NA	no binding	NA

[a]The apparent dissociation constants (K_D) are given in micromolar. Amino acid mutations are highlighted in bold and underlined in the sequence. NA—not applicable.

https://doi.org/10.1021/acs.jmedchem.4c00210
J. Med. Chem. XXXX, XXX, XXX−XXX

mutations would affect how the ATAD2/B BRDs "read" the closely associated histone acetylation marks. In this study, we selected the top four N-terminal mutations near the site of Lys 5 acetylation and assessed their impact on ATAD2/B BRD-binding activity.

Surprisingly, our ITC data demonstrate a threefold increase in binding affinity of the ATAD2 BRD for the onco-histone H4S1C with a K5ac modification when compared to the wild-type histone H4K5ac ligand[31] (Table 2 and Figure S3). However, the ATAD2B BRD binding activity decreases in response to the same onco-histone mutation (Table 2 and Figure S4).[27] The onco-histone H4R3C mutation also increases the binding affinity of the ATAD2 BRD for H4K5ac but decreases the binding affinity of the ATAD2B BRD for H4K5ac. Interestingly, mutation of histone H4G4 to either Asp or Ser abolishes the recognition of K5ac by both the ATAD2 and ATAD2B BRDs (Table 2).

To further investigate the molecular mechanisms involved in the acetyllysine recognition of the mutated onco-histone H4 tail, we solved X-ray crystal structures of the ATAD2 and ATAD2B BRDs in complex with H4S1CK5ac (residues 1−15) at resolutions of 2.01 Å (PDB ID: 8SDO, Figure 4A,C and Table S4) and 2.79 Å (PDB ID: 8SDX, Figure 4B,D and Table S5), respectively. As shown in Figure 4A,B, the $2F_o-F_c$ composite omit maps show that ligand density is observed for the first six residues in the ATAD2 BRD pocket and the first seven residues of the ATAD2B BRD pocket. The coordination of the K5ac group of the onco-histone H4S1CK5ac ligand is well conserved between the ATAD2 and ATAD2B BRDs (Figure 4C,D). The higher affinity of the ATAD2 BRD for the S1C mutant compared to the wild-type H4K5ac (PDB ID: 7M98) (Figure S6)[31] can be explained by the increased number of water-mediated hydrogen bonds observed between Cys 1 of the histone H4 ligand and the E1062 residue in the ATAD2 BRD, along with an additional hydrophobic contact between the K5ac group and the gatekeeper residue I1074 in ATAD2 BRD.

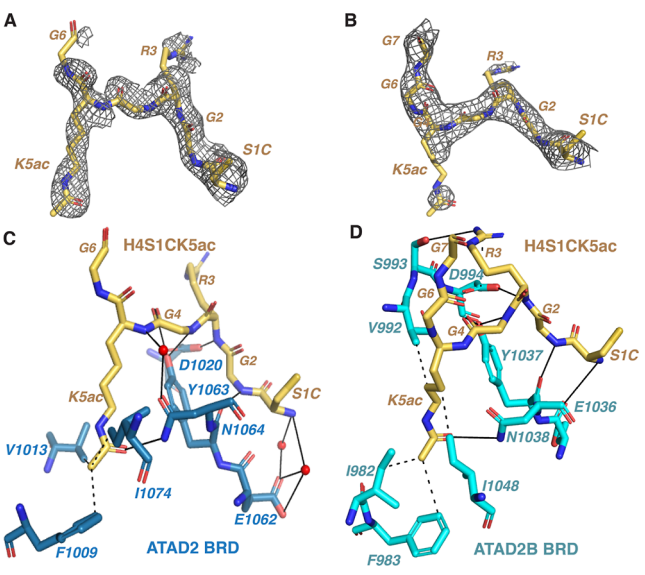

Figure 4. Coordination of the oncohistone H4S1C with K5ac modification by the ATAD2/B BRDs. (A) Isolated image of the simulated annealing composite omit map (gray) around the oncohistone H4S1C with K5ac (yellow, residues 1−6) contoured at 1σ observed in the ATAD2 BRD−H4S1CK5ac complex (PDB ID: 8SDO). The composite omit map was calculated before building the histone ligand into the structure. (B) Isolated image of the simulated annealing composite omit map (gray) around the histone ligand oncohistone H4S1C with K5ac (yellow, residues 1−7) contoured at 1σ observed in the ATAD2B BRD−H4S1phK5ac complex. (C) Coordination of the H4S1C with the K5ac ligand (residues 1−6) by the ATAD2 BRD. Residues lining the BRD pocket involved in ligand coordination are displayed in dark blue, while the H4S1CK5ac ligand residues are shown in yellow. (D) Coordination of the H4S1CK5ac ligand (residues 1−7) by the ATAD2B BRD (PDB ID: 8SDX). Residues lining the BRD pocket involved in ligand coordination are displayed in cyan, while the H4S1CK5ac ligand residues are shown in yellow. Hydrogen bonds are represented by solid black lines, while dashed black lines show hydrophobic interactions. Water molecules are shown in red.

Due to the lack of an ATAD2B BRD−H4K5ac structure, we cannot directly ascertain how the H4S1C onco-histone mutation affects the K5ac insertion within the ATAD2B binding pocket. However, our structure reveals that K5ac is coordinated by at least four hydrophobic contacts, one of which involves the ATAD2B BRD gatekeeper residue I1048 (Figure 4D). Conserved N1038 and Y1037 of ATAD2B BRD form direct hydrogen bonds with the K5ac side chain and the adjacent Gly 4. The N-terminus of the H4S1CK5ac ligand is stabilized via hydrogen-bond formation with the Y1037 and E1036 residues in the ATAD2B BRD. Additional hydrogen bonds are observed between Gly 2 and Arg 3 of the histone H4 ligand and residues D994 and S993 of ATAD2B BRD, respectively. When comparing the coordination of H4K12ac and H4S1CK5ac by ATAD2B, it is notable that several hydrogen-bond contacts between the BRD-binding pocket and the histone tail are lost due to this "onco" mutation. Overall, our structural and ITC data demonstrate that "onco" mutations within the histone H4 tail can influence the recognition of adjacent post-translational modifications and would likely affect the ATAD2/B BRD-binding activity in a cellular context.

2.4.2. Histone Variants H2A.X and H2A.Z Demonstrate Distinct ATAD2/B BRD Activity. Histone variants have unique amino acid sequences compared to canonical histones and play distinct roles in various cellular processes.[38] Histone variants differ in the co-translational and post-translational modifications they harbor.[39] While many H2A sequences are quite similar, H2A.X and H2A.Z.1 and H2A.Z.2 are more distinct.[40] The first five amino acids of H2A.X, 'SGRGK', are identical to the canonical H2A sequences. Histone H4 also shares an identical starting sequence. This preserves the constitutive N-terminal acetylation and the more-abundant K5ac between sequence.[39] However, starting at the sixth amino acid, the sequences diverge slightly between H2A (QGGK), H2A.X (TGGK), and H4 (GGK). H2A.Z shares far less sequence homology near common modification sites and has not been observed to be N-terminally acetylated.[39,40]How the differences between these variants modulate BRD-binding activity is understudied. Among the histone variants tested in our previous dCypher screen, only the ATAD2B BRD appeared to bind H2A.X in its acetylated form.[27]

To further investigate how changes in histone amino acid sequence influence acetyllysine recognition, we used ITC to calculate the binding affinities of the ATAD2/B BRDs with histone variants H2A.X and H2A.Z that carry mono- and diacetylated lysine modifications (Table 3 and Figure S5). Compared to binding with the canonical histone H2AK5ac modification, the ATAD2B BRD shows a two-fold higher

https://doi.org/10.1021/acs.jmedchem.4c00210
J. Med. Chem. XXXX, XXX, XXX−XXX

Table 3. Histone Variant H2A.X and H2A.Z N-Terminus Tail-Binding Affinities to the ATAD2 and ATAD2B BRD-Containing Proteins[a]

peptide	peptide sequence	K_D for ATAD2 (μM)	K_D for ATAD2B (μM)
H2AK5ac (1−12)	SGRG**Kac**QGGKARA	38.9 ± 5.9[31]	42.5 ± 2.9[27]
H2A.X unmodified (1−17)	SGRGKTGGKARAKAKSR	no binding	no binding
H2A.XK5ac (1−17)	SGRG**Kac**TGGKARAKAKSR	160.3 ± 19.4	28.6 ± 2.0
H2A.XK9ac (1−17)	SGRGKTGG**Kac**ARAKAKSR	51.1 ± 5.4	90.0 ± 12.8
H2A.XK5acK9ac (1−17)	SGRG**Kac**TGG**Kac**ARAKAKSR	82.0 ± 11.0	66.6 ± 10.5
H2A.Z unmodified (1−15)	AGGKAGKDSGKAKTK	no binding	no binding
H2A.ZK4ac (1−15)	AGG**Kac**AGKDSGKAKTK	no binding	79.3 ± 4.2
H2A.ZK4acK7ac (1−15)	AGG**Kac**AG**Kac**DSGKAKTK	no binding	no binding

[a]The apparent dissociation constants (K_D) are given in micromolar. Amino acid mutations are highlighted in bold and underlined in the sequence.

affinity for the H2A.XK5ac mark (K_D = 28.6 ± 2.0 μM), whereas the ATAD2 BRD demonstrates a four-fold decrease in binding affinity for the same modification (K_D = 160.3 ± 19.4 μM). Interestingly, while the ATAD2 and ATAD2B BRDs can interact with modified histone H2A.X, the ATAD2B BRD preferentially binds the modified histone H2A.XK5ac, while the ATAD2 BRD prefers the canonical H2A histone acetylated at K5. When we tested the binding activity of the ATAD2 and ATAD2B BRDs with modifications on histone variant H2A.Z, the ATAD2B BRD binds with moderate affinity to the H2A.Z.K4ac ligand (K_D = 79.3 ± 4.2 μM). Interestingly, the ATAD2 BRD does not bind the mono- or the di-acetylated histone H2A.Z ligands. Overall, our ITC data suggest that the ATAD2 BRD is more sensitive to changes in the histone H2A N-terminal amino acid sequence than the ATAD2B BRD, which exhibits a broader ligand-binding specificity for acetylated lysine modifications on canonical and variant histones.

3. DISCUSSION AND CONCLUSIONS

ATAD2 and its closely related paralog ATAD2B belong to subfamily IV of the human BRDs.[22] The BRDs of these related proteins share a high degree of structural similarity and exhibit comparable ligand preferences for histone H4 acetylation modifications *in vitro*.[24,27,34,35] Previous studies have found that the ATAD2 and ATAD2B BRDs preferentially recognize diacetylated histone H4K5acK12ac.[26,27] However, a high-throughput combinatorial dCypher screen to identify post-translationally modified histone ligands of the ATAD2/B BRDs indicated that the ATAD2B BRD was more promiscuous, binding 39 unique ligands, versus 11 bound by the ATAD2 BRD.[27] Interestingly, the ATAD2 and ATAD2B BRDs could bind to acetylated histone ligands containing distinctive arrangements of PTMs, including those that contained adjacent acetylation and methylation modifications.[27] This result prompted us to further characterize the structural and functional differences between the ATAD2 and ATAD2B BRDs to determine if they have distinctive histone-binding properties. These unique properties provide new insights into their unique cellular functions and may facilitate the development of specific agents that can target each protein by blocking their BRD acetyllysine-binding activity.

ATAD2 has been widely studied in the context of cancer and is thought to be involved in chromatin-remodeling activities associated with transcription, DNA damage repair, and cell cycle progression.[24,26,41,42] However, the precise role of histone ligand recognition by the ATAD2 BRD in these various processes still needs further characterization. A recent study by Lazarchuk et al. showed that ATAD2 might play a role in DNA replication during the S phase of the cell cycle by protecting newly synthesized histones containing H4K5acK12ac modifications from the histone deacetylases HDAC1 and HDAC2 until they are incorporated into chromatin.[29] Yet, the cellular function of ATAD2B is still unknown. Understanding the similarities and differences between the ATAD2 and ATAD2B BRD−histone PTM interactions may shed light on the unique functions of the ATAD2B protein.

In this study, we directly measured the binding affinities of the ATAD2/B BRDs to histone H4 peptide ligands containing different combinations of PTMs. Our results demonstrated that the ATAD2 and ATAD2B BRDs recognize distinct subsets of histone modifications. For example, the preferred mono-acetylated histone H4 ligand was H4K5ac for the ATAD2 BRD, whereas the ATAD2B BRD preferred H4K12ac. Structural analysis of the ATAD2/B BRDs in complex with the histone H4K12ac ligand (Figure 2) confirms that coordination of the acetyllysine moiety is consistent between the ATAD2 and ATAD2B BRDs.[24] However, we found that there are distinct variations in how the histone tail residues are coordinated by the BRDs of ATAD2 and ATAD2B. For the ATAD2 BRD bound to H4K12ac (PDB ID: 4QUT, Figure 2D), the histone ligand was coordinated mainly through water-mediated interactions between the protein and the histone peptide, except for histone residue Gly 9, which forms hydrogen bonds with D1066 and D1071 of the ATAD2 BRD.[24] Alternatively, in the ATAD2B BRD−H4K12ac structure (PDB ID: 8UHL), we observe an intricate network of direct hydrogen bonds between the histone ligand and the BRD-binding pocket residues. These direct interactions exclude water from the ATAD2B-binding pocket and stabilize the protein−ligand interaction. A sequence alignment of the ATAD2/B BRDs shows that while the BC-loop regions of these two BRDs are well-conserved, the amino acid sequence of the ZA loop differs between ATAD2 and ATAD2B. The sequence differences change the structural features of the ZA loop and result in new contacts between nonconserved residues I982 and S993 in ATAD2B that facilitate a stronger interaction with the histone H4K12ac ligand (Figure 1D). These distinctive differences in histone H4K12ac coordination by the ATAD2 and ATAD2B BRDs indicate that they are utilizing unique binding modes to recognize and select for histone ligands.

Among the diacetylated histone H4 ligands, both the ATAD2 and ATAD2B BRDs show the strongest affinity for histone H4K5acK12ac (Table 1). This di-acetylated lysine combination is known to be highly enriched in newly synthesized histones in the nascent chromatin,[43,44] and the full-length ATAD2 and ATAD2B proteins have also been

https://doi.org/10.1021/acs.jmedchem.4c00210
J. Med. Chem. XXXX, XXX, XXX−XXX

shown to localize with newly synthesized chromatin.[26,28] Thus, our ITC data demonstrating a preference for the histone H4K5acK12ac ligand by these two BRDs also supports their biological role in the regulation of nascent chromatin via interaction with di-acetylated H4 histones. Moreover, the di-acetylated H4K5acK12ac modification has been identified as an abundant proteoform in acute myeloid leukemia cells,[45] which may recruit their activity in disease.

Within the chromatin, histones often contain multiple PTMs in various combinations.[46−48] Hyper-acetylation of the histone H4 N-terminal tail has been associated with chromatin decompaction and transcriptional activation.[49−51] Our ITC data demonstrated how multiple PTMs on the histone H4 N-terminus modulate the BRD-binding activity of ATAD2 and ATAD2B. Within the multi-acetylated histone H4 peptides tested, the ATAD2 BRD strongly preferred the H4K8acK12-acK16ac ligand, while the ATAD2B BRD selected the H4K5acK12acK16ac combination (Table 1). Interestingly, H4K8acK12acK16ac is one of the histone H4 hyper-acetylated proteoforms shown to increase dramatically upon HDAC inhibitor treatment of breast cancer cell lines SUM159 and MCF-7,[52] which would be predicted to increase the interaction of ATAD2 with chromatin. Another histone modification associated with transcriptional activation is H4R3me2a,[53] where the Arg residue becomes asymmetrically dimethylated through addition of two methyl groups on the same nitrogen atom in the guanidino group.[54] Our ITC data shows that the presence of bulky methyl groups on histone H4 inhibits the ATAD2 BRD activity, as demonstrated by the several-fold reduction in binding affinity of the histone H4R3me2aK5ac ligand when compared to the H4K5ac ligand (Table 1). Conversely, the ATAD2B BRD is more tolerant of the methylation modifications tested and showed no significant changes in binding affinity (Table 1). Since ATAD2 protein is up-regulated in breast cancer and higher expression is correlated with poor patient prognosis,[55] understanding how its activity is modulated by changes in the epigenetic landscape could have important implications for treatment strategies.

Elucidating the molecular mechanisms regulating how the ATAD2 and ATAD2B BRDs recognize distinctive subsets of multivalent histones is essential for understanding their function as putative chromatin regulators. For example, histone H4 phosphorylation at Ser 1 (H4S1ph) is associated with newly synthesized histones, and it is most abundant during the mitotic and S phases of the cell cycle.[56] Phosphorylation of S1 on histone H4 is also induced following DNA damage and is possibly associated with DNA double-strand break repair.[57] Our high-resolution crystal structures of ATAD2 and ATAD2B BRDs in complex with the histone H4S1phK5ac ligand provide residue-specific information on how the addition of a negatively charged, bulky phosphoryl group at the N-terminus of histone H4 impacts the insertion of H4K5ac into the BRD pocket, resulting in altered BRD-binding activity. The several-fold reduced binding affinity of the ATAD2 BRD for the H4S1phK5ac peptide likely originates from the reduced number of contacts between the histone ligand and the BRD. These include a loss of water-mediated hydrogen bonds between H4K5ac and the Y1021 residue in ATAD2 (Figure S6) and between H4R3 and the R1067 residue in ATAD2.[31] Another factor that could contribute to the differences in affinity for these peptide ligands is altered dynamics of the ZA/BC loop regions in ATAD2 vs ATAD2B. Amino acid sequence differences in the loop regions may affect the "opening" and "closing" of the BRD pockets.[58,59] Ultimately, the large difference in affinity observed for the ATAD2−BRD interaction with H4K5ac (K_D = 57.7 μM) and H4S1phK5ac (K_D = 439.0 μM) may function as an important regulatory mechanism to release ATAD2 from newly synthesized histones or to inhibit its interaction with transcriptionally active chromatin in the context of DNA damage.

Onco-histones have been described in various tumors where histone genes harbor mutations in regions encoding both the tail and core residues.[36,37] Within histone H4, the most frequently observed mutations occur at the N-terminal tail. Our binding analyses demonstrated that mutations around the "Kac" mark significantly impact the BRD activity (Table 2). Interestingly, mutations to cysteine (e.g., S1C and R3C) increased the binding affinity for the "K5ac" group by the ATAD2 BRD but reduced the binding affinity of the ATAD2B BRD. However, mutations to charged/polar residues (G4D and G4S) abolished binding to the adjacent K5ac mark by both BRDs. Based on our ATAD2 and ATAD2B BRD structures in complex with the histone H4S1CK5ac ligand, the altered binding affinities for these mutated onco-histones likely result from changes in the polar and hydrophobic contacts between the histone ligand and BRD. Our structure−function analysis suggests that onco-histone mutations changing Gly 4 to an Asp or Ser residue would cause steric clashes from unfavorable orientations of their bulky side chains within the BRD-binding pocket, prohibiting histone recognition. Thus, onco-histone mutations have the potential to play a significant role in inhibiting the activity of BRD-containing proteins in cancer.

Like the canonical histones H3, H4, H2A, and H2B, histone protein variants can also have a variety of post-translational modifications.[39,60] However, due to variations in their amino acid sequence, the histone variants create unique binding sites for proteins that read post-translational modifications. Despite the importance of histone variants in essential cellular processes, including the regulation of transcription, DNA repair, and mitosis,[61,62] information on the molecular mechanisms driving the interaction of chromatin "readers" with modified histone variants is still limited. We focused on the interaction of acetylated histone H2A.X and H2A.Z variants with the ATAD2 and ATAD2B BRDs and demonstrated how changes in the histone tail sequence modulate the recognition of the "Kac" PTM. The ATAD2 BRD was found to be more selective, and changes in the histone sequence surrounding the "Kac" modification resulted in much weaker binding affinities for ATAD2 with PTM histone variants. Notably, the ATAD2B BRD is preferentially bound to the H2A.XK5ac modification over the canonical histone H2AK5ac mark, and it was also able to interact with the acetylated histone variant H2A.ZK4ac, while the ATAD2 BRD was not. Our results align with the cell-cycle expression pattern of ATAD2, which is predominantly expressed during the S phase when newly synthesized histones are most abundant.[26] In contrast, the histone variants are expressed throughout the cell cycle.[63,64] Notably, insertion and acetylation of H2A.Z at K4, K7, and K11 are associated with actively transcribed chromatin at promoter regions, where it functions to destabilize DNA wrapping and opening the nucleosome stacks.[65−67] Recently Kim et al. reported a nonhomologous end-joining DNA repair phenotype associated with ATAD2B in a BRD-containing protein-wide siRNA screen.[68] This result was not followed up, but the data suggest

https://doi.org/10.1021/acs.jmedchem.4c00210
J. Med. Chem. XXXX, XXX, XXX−XXX

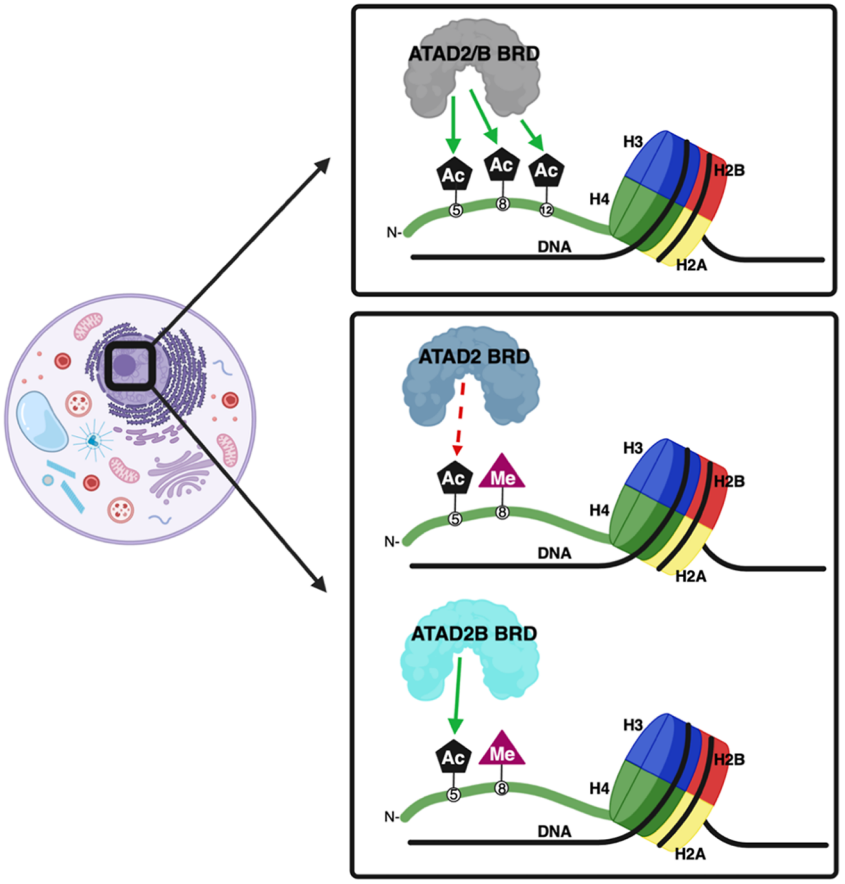

Figure 5. Multiple modifications on individual histone tails of the nucleosome modulate the ATAD2/B BRD activity. In the cell, ATAD2/B is localized at the chromatin, which is enriched with histone PTMs. These modifications influence the ATAD2/B BRD activity. Adjacent methyl groups negatively impact the ATAD2 BRD's ability to recognize the "Kac" mark but do not significantly affect the ATAD2B BRD activity.

that unlike its ATAD2 paralog, ATAD2B may have activity outside of the S phase. The histone H2A.X variant is strongly associated with DNA damage repair through the crucially important S139ph signaling event, also known as γ-H2A.X.[69] The abundance of H2A.X relative to total cellular H2A varies greatly, from 2 to 36%, in the sparse reports available. Histone acetyltransferase TIP60 also acetylates histone H2A.X at the K5 position after DNA damage, creating H2A.XK5ac, which accelerates histone exchange at sites of DNA double-strand breaks (DSBs).[70,71] Moreover, the turnover of NBS1, a primary sensor of DSBs at DNA damage sites, depends on the acetylation state of histone H2A.X.[72] Our ITC binding data demonstrates that the ATAD2 and ATAD2B BRDs have the ability to interact with N-terminally acetylated H2A.X, which is consistent with their potential roles in DNA damage repair.[68,73]

The interplay between diverse histone PTMs forms the "histone code," which drives the recruitment of reader proteins to the chromatin and ultimately dictates specific cellular outcomes. Our current study highlights the importance of studying crosstalk between various histone post-translational modifications to understand how they modulate BRD-containing protein-binding activity. Adjacent histone PTMs can either promote or inhibit the affinity of BRDs with chromatin, which, in turn, regulates essential cellular processes such as gene transcription (Figure 5). Future investigations on how individual and combinatorial histone modifications direct the localization of ATAD2 and ATAD2B to specific regulatory sites along the genome are needed to understand how epigenetic signals created by the "histone code" drives gene regulation in specific biological contexts.

ATAD2 is an attractive therapeutic target due to its role in cancer, and several studies have focused on the development of BRD inhibitors to block its activity.[74−76] Currently, small-molecule inhibitors targeting the ATAD2 BRD include the GlaxoSmithKline compound 38 (GSK C-38),[77] a potent and ATAD2 isoform-selective inhibitor developed by Bayer Pharmaceuticals (BAY-850),[78] GSK8814,[79] GSK388,[80] AM879,[81] and AZ13824374.[82] While many ATAD2 inhibitors have been developed, their potency and antiproliferative effects have been disappointing.[76] At this time, there are no small-molecule inhibitors specifically targeting the ATAD2B paralog. Considering the high degree of conservation between the ATAD2 and ATAD2B BRD-binding pockets, it is not surprising that ATAD2 inhibitors can have overlapping inhibitory effects on the ATAD2B BRD;[83] but in most cases, their ATAD2B-binding activity has not been specifically measured. One exception is BAY-850, which induces dimerization of the ATAD2 BRD to block binding to acetylated histones.[78] BAY-850 is a potent inhibitor with an IC_{50} value of 0.02 μM, and it was validated as an ATAD2 only inhibitor without any off-target effects or binding to the ATAD2B BRD.[78] The AstraZeneca inhibitor AZ13824374 is a recently developed compound with selective binding to the ATAD2 and ATAD2B BRDs that has shown promising

https://doi.org/10.1021/acs.jmedchem.4c00210
J. Med. Chem. XXXX, XXX, XXX−XXX

antiproliferative effects in several cellular models of breast cancer.[82]

The results presented herein provide crucial new information on the histone ligand-binding preferences for the two closely related BRDs found in the ATAD2 and ATAD2B paralogs, thereby shedding light on their potential roles in chromatin regulation. However, focusing on the BRD region alone introduces some limitations to the scope and implications of the results. It is essential to keep in mind that these domains function within the larger multidomain context of the full-length ATAD2 and ATAD2B proteins, which also contain an AAA^+ ATPase domain. Additionally, while the use of modified histone peptides to identify and characterize ligand specificity has become standard in structure−function studies on chromatin reader domains, this approach does not fully capture the intricacies of how numerous modifications function in the context of the intact histone proteins and/or the nucleosome. Thus, our current work establishes a promising starting point for deeper investigations into how these multidomain proteins contribute to specific cellular processes.

In summary, a comparative evolutionary analysis of ATAD2 and ATAD2B highlights their high conservation as paralogues, characterized by gene duplication and subsequent evolution in chordates to acquire distinct BRD-binding activities. Our findings strongly suggest the likelihood of nonredundant functions for the ATAD2 and ATAD2B BRD-containing proteins and emphasize the important role their BRDs likely play in directing their unique biological functions. BRD inhibitors have emerged as a primary research focus and given the association of ATAD2 as a key player in cancer, targeting the specific BRD activities of ATAD2 and ATAD2B which could be vital for developing potent therapeutic interventions.

4. EXPERIMENTAL SECTION

4.1. Evolutionary Analysis of ATAD2 Proteins. ATAD2 homologues were identified by BLAST searches of type species representing the major clades of the Opisthokonta using the human ATAD2 and ATAD2b protein sequences. Accession numbers for each homologue from NCBI, UniProt, or Ensembl databases are as follows: *Saccharomyces cerevisiae*, P40340; *Schizosaccharomyces pombe*, Q9C0W2, O14114; *Monosiga brevicollis*, A9 V250; *Amphimedon queenslandica*, XP_011407258.2; *Hydra vulgaris*, XP_002159335.4; *Nematostella vectensis*, XP_032233592.1; *Limulus polyphemus*, XP_013776023.1; *Ixodes scapularis*, XP_029837885.2; *Bombyx mori*, XP_037874642.1; *B. glabrata*, XP_013075716.1, XP_013075717.1; *M. arenaria*, WAR24384.1, XP_052778215.1; *Ciona intestinalis*, XP_026691996.1; *Branchiostoma floridae*, XP_035667749.1; *Leptobrachium leishanense*, A0A8C5MV52, A0A8C5M7M0; *Gallus*, XP_040553931.1, XP_040520727.1; *Lepisosteus oculatus*, XP_015207022.1, XP_015213378.1; *Danio rerio*, E7FE14, E7EXJ5; *Schmidtea mediterranea*, SMED30003605; *Caenorhabditis elegans*, NP_502289.2; *Brugia malayi*, XP_042930281.1; *Strongylocentrotus purpuratus*, XM_030982860, XM_030982840; *E. burger*, A0A8C4Q726; *P. marinus*, S4RMC5; and *Homo sapiens*, Q9ULI0, Q6PL18. The regions containing the BRD sequences were identified in the full-length protein using NCBI Conserved domain database and confirmed by protein alignment. The evolutionary relationship of BRD sequences was determined using the maximum likelihood method and JTT matrix-based model. The tree with the highest log likelihood was selected. Initial trees for the heuristic search were obtained automatically by applying Neighbor-Join and BioNJ algorithms to a matrix of pairwise distances estimated using the JTT model and then selecting the topology with superior log likelihood value. Evolutionary analyses were conducted in MEGA11.[84]

4.2. Plasmid Construction and Protein Purification. Human ATAD2 BRD-containing protein (residues 966−1112, UniProt code: Q6PL18) and human ATAD2B BRD-containing protein (residues 953−1085, Uniprot code: Q9ULI0) were expressed and purified as described previously in refs 31 and 27. More details can be found in the Supporting Information.

4.3. Histone Peptide Synthesis. All histone H4, H2A.X, and H2A.Z N-terminal tail peptides with and without modifications were purchased from GenScript (Piscataway, NJ, USA). Amino-acid sequence information on each peptide is available in the corresponding ITC-binding tables. All H4 peptides were synthesized with N-terminal acetylation (Nα-ac) and C-terminal amidation, while H2A.X and H2A.Z peptides were synthesized with a C-terminal amidation. All peptides used in this study are >95% pure by high-performance liquid chromatography analysis. Mass Spectrometry was used to confirm their identity.

4.4. Isothermal Titration Calorimetry. ITC experiments for the ATAD2/B BRDs [in 20 mM sodium phosphate buffer, pH 7.0, 150 mM NaCl, and 1 mM tris(2-carboxyethyl) phosphine (TCEP)] (Thermo Scientific) were carried out at 5 °C using a MicroCal iTC200 or a MicroCal PEAQ-ITC instrument (Malvern Analytical). The calorimetric titrations were performed with a histone tail ligand in the syringe (at concentrations of 1.25−5 mM) and BRD-containing protein ATAD2/B in the sample cell (at concentrations ranging from 0.05 to 0.2 mM). All data were fitted using a single set of binding site models to calculate the stoichiometry (N) and the binding constant (K_D). All experiments where binding occurred were performed in triplicate, while runs without binding were performed in duplicate. To calculate the K_D, the average of the three runs was taken as the mean K_D, and the standard deviation was calculated from the mean. All K_D values and standard deviations for each ligand tested are reported in Table 1.

4.5. X-ray Crystallography and Structure Determination. For all crystallization experiments, ATAD2 and ATAD2B BRDs were purified through size-exclusion chromatography using a Superdex 75 16/60 Sephacryl S-100 high-resolution gel filtration column (GE/Cytiva) on an ÄktaPrime system (GE/Cytiva) in buffer containing 25 mM *N*-(2-hydroxyethyl)-piperazine-*N*′-ethanesulfonic acid (HEPES) at pH 7.5, 150 mM NaCl, and 1 mM DTT and concentrated to 15 mg/mL with Amicon Ultra (MILLIPORE) concentrators with a 3 kDa MW cutoff (3 MWCO). Protein concentration was estimated using a UV−vis spectrophotometer at A_{280} nm.

All BRD−histone ligand complexes were prepared in a 1:10 molar ratio with the BRD at 10 mg/mL and histone ligand at 10 times the molar concentration.

For the ATAD2B−H4K12ac (4−17) complex, the crystal was obtained in 1.8 M ammonium citrate tribasic at pH 7.0 and was mounted on B1A (ALS style) reusable goniometer bases inserted with a 75 μm Dual Thickness Microloop LD built on 18 mm/SPINE length rods (pins) from MiTeGen (Ithaca, NY, USA).

For the ATAD2B−H4S1phK5ac (1−15) complex, the final crystal was obtained from a condition containing 0.2 M ammonium sulfate, 0.1 M Bis−Tris (pH 5.5), and 25% w/v PEG 3350 and was cryoprotected by sweeping the crystal in the loop through LV oil. The crystal was harvested using a 300 μm Dual Thickness Microloop LD built on an 18 mm/SPINE length rod (pin) with a B1A (ALS style) reusable goniometer base from MiTeGen.

For the ATAD2 BRD H4S1phK5ac (1−15) complex, the crystal grew in 60% v/v Tascimate pH 7.0 (Hampton HT screen). The crystal was harvested in a 75 μm Dual Thickness Microloop LD built on 18 mm/SPINE length rods (pins) from MiTeGen (Ithaca, NY, USA). The crystal was cryoprotected with a sweep through 5 μL of LV oil and then was flash frozen in liquid nitrogen.

For the ATAD2B−H4S1CK5ac (1−15) complex, the crystal grew in 0.2 M ammonium sulfate, 0.1 M Tris pH 8.5, and 25% w/v PEG 3350 and was harvested using a 200 μm Dual Thickness Microloop LD built on an 18 mm/SPINE length rod (pin) inserted in a B1A

https://doi.org/10.1021/acs.jmedchem.4c00210
J. Med. Chem. XXXX, XXX, XXX−XXX

(ALS style) reusable goniometer base from MiTeGen. An LV oil sweep was used for cryoprotection.

For the ATAD2 BRD H4S1CK5ac (1−15) complex, we screened against pH in hanging-drop 24-well VDX plates (Hampton Research, Aliso Viejo, CA, USA) over 500 μL of mother liquor solution. In each 2 μL drop, there was 1 μL of the protein−peptide solution and 1 μL of the mother liquor. The optimal crystallization condition was 1.42 M sodium phosphate monobasic monohydrate and 0.976 M potassium phosphate dibasic pH 6.4. The crystal was harvested in a 50 μm Dual Thickness Microloop LD built on 18 mm/SPINE length rods (pins) from MiTeGen (Ithaca, NY, USA). The crystal was cryoprotected with a sweep through 28% ethylene glycol in mother liquor and then was flash frozen in liquid nitrogen.

Data were collected at the Advanced Light Source at the Lawrence Berkeley National Lab on beamline 4.2.2, equipped with an RDI CMOS-8 M detector. The diffraction data were processed using XDS,[85] and the structure was solved by a molecular replacement using PHASER.[86] For all ATAD2 structures, the starting model was a structure of the apo ATAD2 BRD, PDB ID: 3DAI. For all ATAD2B structures, the starting model was the apo ATAD2B BRD PDB ID: 3LXJ.[87] After obtaining an initial solution, several rounds of structure refinement and building were carried out with PHENIX-1.19.2[88] and COOT 0.8.9.3. Structural models of the ATAD2/B BRDs in complex with their histone ligands were built into the composite omit map, which showed clear density for the ligand using COOT 0.8.9.3,[89] followed by iterative rounds of refinement and rebuilding in PHENIX-1.19.2[88] and COOT 0.8.9.3. The final structures were deposited into the Protein Data Bank. PDB IDs: 8SDQ (ATAD2−H4S1phK5ac), 8SDO (ATAD2−S1CK5ac (1−15)), 8UHL (ATAD2B−H4K12ac), 8UK5 (ATAD2B−H4S1phK5ac), and 8SDX (ATAD2B−H4S1CK5ac), respectively, after validation using MolProbity.[90] The hydrogen bonds and hydrophobic interactions were determined using the PLIP program.[91]

■ ASSOCIATED CONTENT

Data Availability Statement

The atomic coordinates and structure factors for the ATAD2 BRD in complex with H4S1phK5ac (1−15), H4S1CK5ac (1−15), and ATAD2B BRD in complex with histones H4K12ac (4−17), H4S1phK5ac (1−15), and H4S1CK5ac (1−15) have been deposited with the Protein Data Bank under the accession numbers (PDBID)—8sdq, 8sdo, 8uhl, 8uk5, and 8sdx, respectively. The mass spectrometry data are publicly available through the MassIVE repository at MSV000090397.

Supporting Information

The Supporting Information is available free of charge at https://pubs.acs.org/doi/10.1021/acs.jmedchem.4c00210.

Supplemental methods; ATAD2 BRD ITC binding data; ATAD2B BRD ITC binding data; crystallographic data collection and refinement statistics: ATAD2B BRD and H4K12ac; crystallographic data collection and refinement statistics: ATAD2 BRD and H4S1phK5ac; crystallographic data collection and refinement statistics: ATAD2B BRD and H4S1phK5ac; ATAD2 BRD oncohistone ITC binding data; ATAD2B BRD oncohistone ITC binding data; crystallographic data collection and refinement statistics: ATAD2 BRD and H4S1CK5ac; crystallographic data collection and refinement statistics: ATAD2B BRD and H4S1CK5ac; ITC binding data of ATAD2/B BRDs with histone H2A.X and H2A.Z ligands; coordination of histone H4K5ac ligands by the ATAD2 BRD; supplemental references; and histone peptide purification and identification data (PDF)

■ AUTHOR INFORMATION

Corresponding Author

Karen C. Glass − *Department of Pharmacology, Larner College of Medicine, University of Vermont, Burlington, Vermont 05405, United States; Department of Pharmaceutical Sciences, Albany College of Pharmacy and Health Sciences, Colchester, Vermont 05446, United States;* orcid.org/0000-0002-2761-733X; Phone: +1(802) 656-5760; Email: karen.glass@med.uvm.edu; Fax: +1(802) 656-4523

Authors

Margaret Phillips − *Department of Pharmacology, Larner College of Medicine, University of Vermont, Burlington, Vermont 05405, United States; Department of Pharmaceutical Sciences, Albany College of Pharmacy and Health Sciences, Colchester, Vermont 05446, United States*

Kiera L. Malone − *Department of Pharmacology, Larner College of Medicine, University of Vermont, Burlington, Vermont 05405, United States*

Brian W. Boyle − *Department of Pharmacology, Larner College of Medicine, University of Vermont, Burlington, Vermont 05405, United States*

Cameron Montgomery − *Department of Pharmaceutical Sciences, Albany College of Pharmacy and Health Sciences, Colchester, Vermont 05446, United States*

Isabelle A. Kressy − *Department of Pharmacology, Larner College of Medicine, University of Vermont, Burlington, Vermont 05405, United States*

Faith M. Joseph − *Verna & Marrs McLean Department of Biochemistry & Molecular Pharmacology, Baylor College of Medicine, Houston, Texas 77030, United States; Translational Biology and Molecular Medicine Graduate Program, Baylor College of Medicine, Houston, Texas 77030, United States*

Kathleen M. Bright − *Department of Biomedical and Health Sciences, University of Vermont, Burlington, Vermont 05405, United States*

Samuel P. Boyson − *Department of Pharmaceutical Sciences, Albany College of Pharmacy and Health Sciences, Colchester, Vermont 05446, United States*

Sunsik Chang − *Department of Pharmaceutical Sciences, Albany College of Pharmacy and Health Sciences, Colchester, Vermont 05446, United States*

Jay C. Nix − *Molecular Biology Consortium, Advanced Light Source, Berkeley, California 94720, United States*

Nicolas L. Young − *Verna & Marrs McLean Department of Biochemistry & Molecular Pharmacology, Baylor College of Medicine, Houston, Texas 77030, United States; Translational Biology and Molecular Medicine Graduate Program, Baylor College of Medicine, Houston, Texas 77030, United States;* orcid.org/0000-0002-3323-2815

Victoria Jeffers − *Department of Molecular, Cellular and Biomedical Sciences, University of New Hampshire, Durham, New Hampshire 03824, United States;* orcid.org/0000-0003-1233-1088

Seth Frietze − *Department of Biomedical and Health Sciences, University of Vermont, Burlington, Vermont 05405, United States*

Complete contact information is available at: https://pubs.acs.org/10.1021/acs.jmedchem.4c00210

https://doi.org/10.1021/acs.jmedchem.4c00210
J. Med. Chem. XXXX, XXX, XXX−XXX

Author Contributions

△M.P. and K.L.M. share first authorship. Conceptualization: M.P., K.L.M., S.F., and K.C.G.; investigation and validation: M.P., K.L.M., B.W.B., C.M., I.A.K., F.M.J., K.M.B., S.P.B., S.C., J.C.N., N.L.Y., V.J., and K.C.G.; writing: M.P., reviewing and editing: M.P., K.L.M., F.M.J., K.M.Q., N.L.Y., V.J., S.F., and K.C.G.; supervision: N.L.Y., and K.C.G.; and funding acquisition: K.C.G., N.L.Y., V.J., and S.F. All authors have read and agreed to the final version of the manuscript.

Notes

The authors declare no competing financial interest.

■ ACKNOWLEDGMENTS

All figures were made using the PyMOL Molecular Graphics system using version 2.3, Schrödinger, LLC, and all contacts were determined using the PLIP program.[91] BioRender.com was used to create the graphical abstract and Figure 5. Research reported in this study was supported by the National Institute of General Medical Sciences and the National Cancer Institute of the National Institutes of Health under award numbers (R15GM104865 to K.C.G.) and (R01GM129338 and P01CA240685 to K.C.G. and S.F.). This work was also supported by a U.S. National Sciene Foundation award 2321501 to K.C.G. and National Institutes of Health grants to N.L.Y. (R01GM139295, P01AG066606, 1R01AG074540, R56HG012206, R01CA276663 and R01CA193235) and V.J. (P20GM113131). The content is solely the responsibility of the authors and does not necessarily represent the official views of the National Institutes of Health. This study used the Advanced Light Source in Berkeley, CA, Beamline 4.2.2, a DOE Office of Science User Facility under Contract no. DE-AC02-05CH11231 which is partly supported by the ALS-ENABLE program funded by the National Institutes of Health and National Institute of General Medical Sciences grant number (P30GM124169). Automated DNA sequencing was performed in the Vermont Integrative Genomics Resource DNA Facility and was supported by the University of Vermont Cancer Center, the Lake Champlain Cancer Research Organization, and the UVM Larner College of Medicine.

■ ABBREVIATIONS

AAA$^+$, ATPases associated with diverse cellular activities; ac, acetylation/acetyl group; ALS, advanced light source; Arg, arginine; Asp, aspartate; ATAD2, ATPase family AAA$^+$ domain-containing protein 2; ATAD2B, ATPase family AAA$^+$ domain-containing protein 2B; ATP, adenosine triphosphate; BRD, bromodomain; Cys, cysteine; DSB, double-strand break; Gly, glycine; GST, glutathione-*S*-transferase; H2A, histone 2A; H2A.X, histone 2A variant X; H2A.Z, histone 2A variant Z; H2B, histone 2B; H3, histone 3; H4, histone 4; HDAC, histone deacetylase; HEPES, *N*-(2-hydroxyethyl)-piperazine-*N*′-ethanesulfonic acid; ITC, isothermal titration calorimetry; K_D, binding/dissociation constant; kDa, kilodaltons; Leu, leucine; Lys, lysine; me, methylation/methyl group; me2a, asymmetric dimethylation; MW, molecular weight; PDB, protein data bank; ph, phosphorylation/phosphoryl group; NBS1, Nijmegan breakage syndrome; PLIP, protein−ligand interaction profiler; PTMs, post-translational modifications; S phase, synthesis phase of the cell cycle; Ser, serine; siRNA, small interfering RNA; TCEP, tris(2-carboxyethyl) phosphine; UHRF1, ubiquitin-like with PHD and ring finger domains 1

■ REFERENCES

(1) Luger, K.; Mader, A. W.; Richmond, R. K.; Sargent, D. F.; Richmond, T. J. Crystal structure of the nucleosome core particle at 2.8 A resolution. *Nature* **1997**, *389* (6648), 251−260.
(2) McGinty, R. K.; Tan, S. Nucleosome structure and function. *Chem. Rev.* **2015**, *115* (6), 2255−2273.
(3) Pei, J.; Grishin, N. V. PROMALS3D: multiple protein sequence alignment enhanced with evolutionary and three-dimensional structural information. *Methods Mol. Biol.* **2014**, *1079*, 263−271.
(4) Huang, H.; Sabari, B. R.; Garcia, B. A.; Allis, C. D.; Zhao, Y. SnapShot: histone modifications. *Cell* **2014**, *159* (2), 458−458.e1.
(5) Strahl, B. D.; Allis, C. D. The language of covalent histone modifications. *Nature* **2000**, *403* (6765), 41−45.
(6) Iizuka, M.; Smith, M. M. Functional consequences of histone modifications. *Curr. Opin. Genet. Dev.* **2003**, *13* (2), 154−160.
(7) Peterson, C. L.; Laniel, M. A. Histones and histone modifications. *Curr. Biol.* **2004**, *14* (14), R546−R551.
(8) Jenuwein, T.; Allis, C. D. Translating the histone code. *Science* **2001**, *293* (5532), 1074−1080.
(9) Lachner, M.; O'Carroll, D.; Rea, S.; Mechtler, K.; Jenuwein, T. Methylation of histone H3 lysine 9 creates a binding site for HP1 proteins. *Nature* **2001**, *410* (6824), 116−120.
(10) Nakayama, J.; Rice, J. C.; Strahl, B. D.; Allis, C. D.; Grewal, S. I. Role of histone H3 lysine 9 methylation in epigenetic control of heterochromatin assembly. *Science* **2001**, *292* (5514), 110−113.
(11) Bernstein, B. E.; Humphrey, E. L.; Erlich, R. L.; Schneider, R.; Bouman, P.; Liu, J. S.; Kouzarides, T.; Schreiber, S. L. Methylation of histone H3 Lys 4 in coding regions of active genes. *Proc. Natl. Acad. Sci. U.S.A.* **2002**, *99* (13), 8695−8700.
(12) Kanno, T.; Kanno, Y.; Siegel, R. M.; Jang, M. K.; Lenardo, M. J.; Ozato, K. Selective recognition of acetylated histones by bromodomain proteins visualized in living cells. *Mol. Cell* **2004**, *13* (1), 33−43.
(13) Zeng, L.; Zhou, M. M. Bromodomain: an acetyl-lysine binding domain. *FEBS Lett.* **2002**, *513* (1), 124−128.
(14) Grunstein, M. Histone acetylation in chromatin structure and transcription. *Nature* **1997**, *389* (6649), 349−352.
(15) Bannister, A. J.; Kouzarides, T. Regulation of chromatin by histone modifications. *Cell Research* **2011**, *21* (3), 381−395.
(16) Paradowska, A. S.; Miller, D.; Spiess, A. N.; Vieweg, M.; Cerna, M.; Dvorakova-Hortova, K.; Bartkuhn, M.; Schuppe, H. C.; Weidner, W.; Steger, K. Genome wide identification of promoter binding sites for H4K12ac in human sperm and its relevance for early embryonic development. *Epigenetics* **2012**, *7* (9), 1057−1070.
(17) Raisner, R.; Kharbanda, S.; Jin, L.; Jeng, E.; Chan, E.; Merchant, M.; Haverty, P. M.; Bainer, R.; Cheung, T.; Arnott, D.; et al. Enhancer Activity Requires CBP/P300 Bromodomain-Dependent Histone H3K27 Acetylation. *Cell Rep.* **2018**, *24* (7), 1722−1729.
(18) Mujtaba, S.; Zeng, L.; Zhou, M. M. Structure and acetyl-lysine recognition of the bromodomain. *Oncogene* **2007**, *26* (37), 5521−5527.
(19) Simossis, V. A.; Heringa, J. PRALINE: a multiple sequence alignment toolbox that integrates homology-extended and secondary structure information. *Nucleic Acids Res.* **2005**, *33*, W289−W294.
(20) Van Hoide, K.E.; Sahasrabuddhe, C.G.; Shaw, B. R. A model for particulate structure in chromatin. *Nucleic Acids Res.* **1974**, *1* (11), 1579−1586.
(21) Choudalakis, M.; Kungulovski, G.; Mauser, R.; Bashtrykov, P.; Jeltsch, A. Refined read-out: The hUHRF1 Tandem-Tudor domain prefers binding to histone H3 tails containing K4me1 in the context of H3K9me2/3. *Protein Sci.* **2023**, *32*, No. e4760.
(22) Boyson, S. P.; Gao, C.; Quinn, K.; Boyd, J.; Paculova, H.; Frietze, S.; Glass, K. C. Functional Roles of Bromodomain Proteins in Cancer. *Cancers* **2021**, *13* (14), 3606.
(23) Leachman, N. T.; Brellier, F.; Ferralli, J.; Chiquet-Ehrismann, R.; Tucker, R. P. ATAD2B is a phylogenetically conserved nuclear protein expressed during neuronal differentiation and tumorigenesis. *Dev., Growth Differ.* **2010**, *52* (9), 747−755.

https://doi.org/10.1021/acs.jmedchem.4c00210
J. Med. Chem. XXXX, XXX, XXX−XXX

(24) Morozumi, Y.; Boussouar, F.; Tan, M.; Chaikuad, A.; Jamshidikia, M.; Colak, G.; He, H.; Nie, L.; Petosa, C.; de Dieuleveult, M.; et al. Atad2 is a generalist facilitator of chromatin dynamics in embryonic stem cells. *J. Mol. Cell Biol.* **2016**, *8* (4), 349−362.
(25) Caron, C.; Lestrat, C.; Marsal, S.; Escoffier, E.; Curtet, S.; Virolle, V.; Barbry, P.; Debernardi, A.; Brambilla, C.; Brambilla, E.; et al. Functional characterization of ATAD2 as a new cancer/testis factor and a predictor of poor prognosis in breast and lung cancers. *Oncogene* **2010**, *29* (37), 5171−5181.
(26) Koo, S. J.; Fernandez-Montalvan, A. E.; Badock, V.; Ott, C. J.; Holton, S. J.; von Ahsen, O.; Toedling, J.; Vittori, S.; Bradner, J. E.; Gorjanacz, M. ATAD2 is an epigenetic reader of newly synthesized histone marks during DNA replication. *Oncotarget* **2016**, *7* (43), 70323−70335.
(27) Lloyd, J. T.; McLaughlin, K.; Lubula, M. Y.; Gay, J. C.; Dest, A.; Gao, C.; Phillips, M.; Tonelli, M.; Cornilescu, G.; Marunde, M. R.; et al. Structural Insights into the Recognition of Mono- and Diacetylated Histones by the ATAD2B Bromodomain. *J. Med. Chem.* **2020**, *63* (21), 12799−12813.
(28) Alabert, C.; Bukowski-Wills, J. C.; Lee, S. B.; Kustatscher, G.; Nakamura, K.; de Lima Alves, F.; Menard, P.; Mejlvang, J.; Rappsilber, J.; Groth, A. Nascent chromatin capture proteomics determines chromatin dynamics during DNA replication and identifies unknown fork components. *Nat. Cell Biol.* **2014**, *16* (3), 281−291.
(29) Lazarchuk, P.; Hernandez-Villanueva, J.; Pavlova, M. N.; Federation, A.; MacCoss, M.; Sidorova, J. M. Mutual Balance of Histone Deacetylases 1 and 2 and the Acetyl Reader ATAD2 Regulates the Level of Acetylation of Histone H4 on Nascent Chromatin of Human Cells. *Mol. Cell. Biol.* **2020**, *40* (9), 004211-19.
(30) Aebersold, R.; Agar, J. N.; Amster, I. J.; Baker, M. S.; Bertozzi, C. R.; Boja, E. S.; Costello, C. E.; Cravatt, B. F.; Fenselau, C.; Garcia, B. A.; et al. How many human proteoforms are there? *Nat. Chem. Biol.* **2018**, *14* (3), 206−214.
(31) Evans, C. M.; Phillips, M.; Malone, K. L.; Tonelli, M.; Cornilescu, G.; Cornilescu, C.; Holton, S. J.; Gorjanacz, M.; Wang, L.; Carlson, S.; et al. Coordination of Di-Acetylated Histone Ligands by the ATAD2 Bromodomain. *Int. J. Mol. Sci.* **2021**, *22* (17), 9128.
(32) Jiang, T.; Hoover, M. E.; Holt, M. V.; Freitas, M. A.; Marshall, A. G.; Young, N. L. Middle-Down Characterization of the Cell Cycle Dependence of Histone H4 Posttranslational Modifications and Proteoforms. *Proteomics* **2018**, *18* (11), No. e1700442.
(33) Leroy, G.; Dimaggio, P. A.; Chan, E. Y.; Zee, B. M.; Blanco, M. A.; Bryant, B.; Flaniken, I. Z.; Liu, S.; Kang, Y.; Trojer, P.; et al. A quantitative atlas of histone modification signatures from human cancer cells. *Epigenet. Chromatin* **2013**, *6* (1), 20.
(34) Taylor, B. C.; Young, N. L. Combinations of histone post-translational modifications. *Biochem. J.* **2021**, *478* (3), 511−532.
(35) Wang, T.; Holt, M. V.; Young, N. L. The histone H4 proteoform dynamics in response to SUV4−20 inhibition reveals single molecule mechanisms of inhibitor resistance. *Epigenet. Chromatin* **2018**, *11* (1), 29.
(36) Nacev, B. A.; Feng, L.; Bagert, J. D.; Lemiesz, A. E.; Gao, J.; Soshnev, A. A.; Kundra, R.; Schultz, N.; Muir, T. W.; Allis, C. D. The expanding landscape of 'oncohistone' mutations in human cancers. *Nature* **2019**, *567* (7749), 473−478.
(37) Amatori, S.; Tavolaro, S.; Gambardella, S.; Fanelli, M. The dark side of histones: genomic organization and role of oncohistones in cancer. *Clin. Epigenet.* **2021**, *13* (1), 71.
(38) Buschbeck, M.; Hake, S. B. Variants of core histones and their roles in cell fate decisions, development and cancer. *Nat. Rev. Mol. Cell Biol.* **2017**, *18* (5), 299−314.
(39) Joseph, F. M.; Young, N. L. Histone variant-specific post-translational modifications. *Semin. Cell Dev. Biol.* **2023**, *135*, 73−84.
(40) Dang, X.; Singh, A.; Spetman, B. D.; Nolan, K. D.; Isaacs, J. S.; Dennis, J. H.; Dalton, S.; Marshall, A. G.; Young, N. L. Label-Free Relative Quantitation of Isobaric and Isomeric Human Histone H2A and H2B Variants by Fourier Transform Ion Cyclotron Resonance Top-Down MS/MS. *J. Proteome Res.* **2016**, *15* (9), 3196−3203.
(41) Mjelle, R.; Hegre, S. A.; Aas, P. A.; Slupphaug, G.; Drablos, F.; Saetrom, P.; Krokan, H. E. Cell cycle regulation of human DNA repair and chromatin remodeling genes. *DNA Repair* **2015**, *30*, 53−67.
(42) Liu, Q.; Liu, H.; Huang, X.; Fan, X.; Xiao, Z.; Yan, R.; Yao, J.; An, G.; Ge, Y.; Miao, J.; et al. A targetable MYBL2-ATAD2 axis governs cell proliferation in ovarian cancer. *Cancer Gene Ther.* **2023**, *30*, 192−208.
(43) Sobel, R. E.; Cook, R. G.; Perry, C. A.; Annunziato, A. T.; Allis, C. D. Conservation of deposition-related acetylation sites in newly synthesized histones H3 and H4. *Proc. Natl. Acad. Sci. U.S.A.* **1995**, *92* (4), 1237−1241.
(44) Hammond, C. M.; Stromme, C. B.; Huang, H.; Patel, D. J.; Groth, A. Histone chaperone networks shaping chromatin function. *Nat. Rev. Mol. Cell Biol.* **2017**, *18* (3), 141−158.
(45) Jiang, Y.; Hu, T.; Wang, T.; Shi, X.; Kitano, A.; Eagle, K.; Hoegenauer, K. A.; Konopleva, M. Y.; Lin, C. Y.; Young, N. L.; et al. AMP-activated protein kinase links acetyl-CoA homeostasis to BRD4 recruitment in acute myeloid leukemia. *Blood* **2019**, *134* (24), 2183−2194.
(46) Young, N. L.; DiMaggio, P. A.; Plazas-Mayorca, M. D.; Baliban, R. C.; Floudas, C. A.; Garcia, B. A. High throughput characterization of combinatorial histone codes. *Mol. Cell. Proteomics* **2009**, *8* (10), 2266−2284.
(47) (a) Barlesi, F.; Giaccone, G.; Gallegos-Ruiz, M. I.; Loundou, A.; Span, S. W.; Lefesvre, P.; Kruyt, F. A.; Rodriguez, J. A. Global histone modifications predict prognosis of resected non small-cell lung cancer. *J. Clin. Oncol.* **2007**, *25* (28), 4358−4364.
(48) Barski, A.; Cuddapah, S.; Cui, K.; Roh, T. Y.; Schones, D. E.; Wang, Z.; Wei, G.; Chepelev, I.; Zhao, K. High-resolution profiling of histone methylations in the human genome. *Cell* **2007**, *129* (4), 823−837.
(49) Tse, C.; Sera, T.; Wolffe, A. P.; Hansen, J. C. Disruption of higher-order folding by core histone acetylation dramatically enhances transcription of nucleosomal arrays by RNA polymerase III. *Mol. Cell. Biol.* **1998**, *18* (8), 4629−4638.
(50) Allahverdi, A.; Yang, R.; Korolev, N.; Fan, Y.; Davey, C. A.; Liu, C. F.; Nordenskiold, L. The effects of histone H4 tail acetylations on cation-induced chromatin folding and self-association. *Nucleic Acids Res.* **2011**, *39* (5), 1680−1691.
(51) Dhar, S.; Gursoy-Yuzugullu, O.; Parasuram, R.; Price, B. D. The tale of a tail: histone H4 acetylation and the repair of DNA breaks. *Philos. Trans. R. Soc., B* **2017**, *372* (1731), 20160284.
(52) Wang, T.; Holt, M. V.; Young, N. L. Early butyrate induced acetylation of histone H4 is proteoform specific and linked to methylation state. *Epigenetics* **2018**, *13* (5), 519−535.
(53) Beacon, T. H.; Xu, W.; Davie, J. R. Genomic landscape of transcriptionally active histone arginine methylation marks, H3R2me2s and H4R3me2a, relative to nucleosome depleted regions. *Gene* **2020**, *742*, 144593.
(54) Bedford, M. T. Arginine methylation at a glance. *J. Cell Sci.* **2007**, *120* (24), 4243−4246.
(55) Kalashnikova, E. V.; Revenko, A. S.; Gemo, A. T.; Andrews, N. P.; Tepper, C. G.; Zou, J. X.; Cardiff, R. D.; Borowsky, A. D.; Chen, H. W. ANCCA/ATAD2 overexpression identifies breast cancer patients with poor prognosis, acting to drive proliferation and survival of triple-negative cells through control of B-Myb and EZH2. *Cancer Res.* **2010**, *70* (22), 9402−9412.
(56) Barber, C. M.; Turner, F. B.; Wang, Y.; Hagstrom, K.; Taverna, S. D.; Mollah, S.; Ueberheide, B.; Meyer, B. J.; Hunt, D. F.; Cheung, P.; et al. The enhancement of histone H4 and H2A serine 1 phosphorylation during mitosis and S-phase is evolutionarily conserved. *Chromosoma* **2004**, *112* (7), 360−371.
(57) Cheung, W. L.; Turner, F. B.; Krishnamoorthy, T.; Wolner, B.; Ahn, S. H.; Foley, M.; Dorsey, J. A.; Peterson, C. L.; Berger, S. L.; Allis, C. D. Phosphorylation of histone H4 serine 1 during DNA damage requires casein kinase II in S. cerevisiae. *Curr. Biol.* **2005**, *15* (7), 656−660.

https://doi.org/10.1021/acs.jmedchem.4c00210
J. Med. Chem. XXXX, XXX, XXX−XXX

(58) Zhang, X.; Chen, K.; Wu, Y. D.; Wiest, O. Protein dynamics and structural waters in bromodomains. *PLoS One* **2017**, *12* (10), No. e0186570.
(59) Langini, C.; Caflisch, A.; Vitalis, A. The ATAD2 bromodomain binds different acetylation marks on the histone H4 in similar fuzzy complexes. *J. Biol. Chem.* **2017**, *292* (46), 19121.
(60) El Kennani, S.; Adrait, A.; Permiakova, O.; Hesse, A. M.; Ialy-Radio, C.; Ferro, M.; Brun, V.; Cocquet, J.; Govin, J.; Pflieger, D. Systematic quantitative analysis of H2A and H2B variants by targeted proteomics. *Epigenet. Chromatin* **2018**, *11* (1), 2.
(61) Talbert, P. B.; Henikoff, S. Histone variants at a glance. *J. Cell Sci.* **2021**, *134* (6), jcs244749.
(62) Henikoff, S.; Smith, M. M. Histone variants and epigenetics. *Cold Spring Harbor Perspect. Biol.* **2015**, *7* (1), a019364.
(63) Walkiewicz, M. P.; Bui, M.; Quenet, D.; Dalal, Y. Tracking histone variant nucleosomes across the human cell cycle using biophysical, biochemical, and cytological analyses. *Methods Mol. Biol.* **2014**, *1170*, 589−615.
(64) Zink, L. M.; Hake, S. B. Histone variants: nuclear function and disease. *Curr. Opin. Genet. Dev.* **2016**, *37*, 82−89.
(65) Valdes-Mora, F.; Song, J. Z.; Statham, A. L.; Strbenac, D.; Robinson, M. D.; Nair, S. S.; Patterson, K. I.; Tremethick, D. J.; Stirzaker, C.; Clark, S. J. Acetylation of H2A.Z is a key epigenetic modification associated with gene deregulation and epigenetic remodeling in cancer. *Genome Res.* **2012**, *22* (2), 307−321.
(66) Bruce, K.; Myers, F. A.; Mantouvalou, E.; Lefevre, P.; Greaves, I.; Bonifer, C.; Tremethick, D. J.; Thorne, A. W.; Crane-Robinson, C. The replacement histone H2A.Z in a hyperacetylated form is a feature of active genes in the chicken. *Nucleic Acids Res.* **2005**, *33* (17), 5633−5639.
(67) Ishibashi, T.; Dryhurst, D.; Rose, K. L.; Shabanowitz, J.; Hunt, D. F.; Ausio, J. Acetylation of vertebrate H2A.Z and its effect on the structure of the nucleosome. *Biochemistry* **2009**, *48* (22), 5007−5017.
(68) Kim, J. J.; Lee, S. Y.; Gong, F.; Battenhouse, A. M.; Boutz, D. R.; Bashyal, A.; Refvik, S. T.; Chiang, C. M.; Xhemalce, B.; Paull, T. T.; et al. Systematic bromodomain protein screens identify homologous recombination and R-loop suppression pathways involved in genome integrity. *Genes Dev.* **2019**, *33* (23−24), 1751−1774.
(69) Rogakou, E. P.; Pilch, D. R.; Orr, A. H.; Ivanova, V. S.; Bonner, W. M. DNA double-stranded breaks induce histone H2AX phosphorylation on serine 139. *J. Biol. Chem.* **1998**, *273* (10), 5858−5868.
(70) Ikura, T.; Tashiro, S.; Kakino, A.; Shima, H.; Jacob, N.; Amunugama, R.; Yoder, K.; Izumi, S.; Kuraoka, I.; Tanaka, K.; et al. DNA damage-dependent acetylation and ubiquitination of H2AX enhances chromatin dynamics. *Mol. Cell. Biol.* **2007**, *27* (20), 7028−7040.
(71) Kusch, T.; Florens, L.; Macdonald, W. H.; Swanson, S. K.; Glaser, R. L.; Yates, J. R.; Abmayr, S. M.; Washburn, M. P.; Workman, J. L. Acetylation by Tip60 is required for selective histone variant exchange at DNA lesions. *Science* **2004**, *306* (5704), 2084−2087.
(72) Ikura, M.; Furuya, K.; Matsuda, S.; Matsuda, R.; Shima, H.; Adachi, J.; Matsuda, T.; Shiraki, T.; Ikura, T. Acetylation of Histone H2AX at Lys 5 by the TIP60 Histone Acetyltransferase Complex Is Essential for the Dynamic Binding of NBS1 to Damaged Chromatin. *Mol. Cell. Biol.* **2015**, *35* (24), 4147−4157.
(73) Duan, Z.; Andrews, N. P.; Chen, C. Z.; Fan, M.; Wang, J.; Shen, J.; Li, J. J.; Chen, H. W. Targeting bromodomain protein ANCCA/ATAD2 enhances the efficacy of DNAdamaging chemotherapy agents and radiation. *Oncol. Rep.* **2019**, *43* (1), 318−327.
(74) Ciro, M.; Prosperini, E.; Quarto, M.; Grazini, U.; Walfridsson, J.; McBlane, F.; Nucifero, P.; Pacchiana, G.; Capra, M.; Christensen, J.; et al. ATAD2 is a novel cofactor for MYC, overexpressed and amplified in aggressive tumors. *Cancer Res.* **2009**, *69* (21), 8491−8498.
(75) Hussain, M.; Zhou, Y.; Song, Y.; Hameed, H. A.; Jiang, H.; Tu, Y.; Zhang, J. ATAD2 in cancer: a pharmacologically challenging but tractable target. *Expert Opin. Ther. Targets* **2018**, *22* (1), 85−96.
(76) Fu, J.; Zhang, J.; Chen, X.; Liu, Z.; Yang, X.; He, Z.; Hao, Y.; Liu, B.; Yao, D. ATPase family AAA domain-containing protein 2 (ATAD2): From an epigenetic modulator to cancer therapeutic target. *Theranostics* **2023**, *13* (2), 787−809.
(77) Bamborough, P.; Chung, C. W.; Demont, E. H.; Bridges, A. M.; Craggs, P. D.; Dixon, D. P.; Francis, P.; Furze, R. C.; Grandi, P.; Jones, E. J.; et al. A Qualified Success: Discovery of a New Series of ATAD2 Bromodomain Inhibitors with a Novel Binding Mode Using High-Throughput Screening and Hit Qualification. *J. Med. Chem.* **2019**, *62* (16), 7506−7525.
(78) Fernandez-Montalvan, A. E.; Berger, M.; Kuropka, B.; Koo, S. J.; Badock, V.; Weiske, J.; Puetter, V.; Holton, S. J.; Stockigt, D.; Ter Laak, A.; et al. Isoform-Selective ATAD2 Chemical Probe with Novel Chemical Structure and Unusual Mode of Action. *ACS Chem. Biol.* **2017**, *12* (11), 2730−2736.
(79) Bamborough, P.; Chung, C. W.; Furze, R. C.; Grandi, P.; Michon, A. M.; Watson, R. J.; Mitchell, D. J.; Barnett, H.; Prinjha, R. K.; Rau, C.; et al. Aiming to Miss a Moving Target: Bromo and Extra Terminal Domain (BET) Selectivity in Constrained ATAD2 Inhibitors. *J. Med. Chem.* **2018**, *61* (18), 8321−8336.
(80) Lucas, S. C. C.; Atkinson, S. J.; Bamborough, P.; Barnett, H.; Chung, C. W.; Gordon, L.; Mitchell, D. J.; Phillipou, A.; Prinjha, R. K.; Sheppard, R. J.; et al. Optimization of Potent ATAD2 and CECR2 Bromodomain Inhibitors with an Atypical Binding Mode. *J. Med. Chem.* **2020**, *63* (10), 5212−5241.
(81) Yao, D.; Zhang, J.; Wang, J.; Pan, D.; He, Z. Discovery of novel ATAD2 bromodomain inhibitors that trigger apoptosis and autophagy in breast cells by structure-based virtual screening. *J. Enzyme Inhib. Med. Chem.* **2020**, *35* (1), 713−725.
(82) Winter-Holt, J. J.; Bardelle, C.; Chiarparin, E.; Dale, I. L.; Davey, P. R. J.; Davies, N. L.; Denz, C.; Fillery, S. M.; Guerot, C. M.; Han, F.; et al. Discovery of a Potent and Selective ATAD2 Bromodomain Inhibitor with Antiproliferative Activity in Breast Cancer Models. *J. Med. Chem.* **2022**, *65* (4), 3306−3331.
(83) Lloyd, J. T.; Glass, K. C. Biological function and histone recognition of family IV bromodomain-containing proteins. *J. Cell. Physiol.* **2018**, *233* (3), 1877−1886.
(84) Tamura, K.; Stecher, G.; Kumar, S. MEGA11: Molecular Evolutionary Genetics Analysis Version 11. *Mol. Biol. Evol.* **2021**, *38* (7), 3022−3027.
(85) Kabsch, W. Xds. *Acta Crystallogr., Sect. D: Biol. Crystallogr.* **2010**, *66* (2), 125−132.
(86) McCoy, A. J.; Grosse-Kunstleve, R. W.; Adams, P. D.; Winn, M. D.; Storoni, L. C.; Read, R. J. Phaser crystallographic software. *J. Appl. Crystallogr.* **2007**, *40* (4), 658−674.
(87) Filippakopoulos, P.; Picaud, S.; Mangos, M.; Keates, T.; Lambert, J. P.; Barsyte-Lovejoy, D.; Felletar, I.; Volkmer, R.; Muller, S.; Pawson, T.; et al. Histone recognition and large-scale structural analysis of the human bromodomain family. *Cell* **2012**, *149* (1), 214−231.
(88) Adams, P. D.; Afonine, P. V.; Bunkoczi, G.; Chen, V. B.; Davis, I. W.; Echols, N.; Headd, J. J.; Hung, L. W.; Kapral, G. J.; Grosse-Kunstleve, R. W.; et al. PHENIX: a comprehensive Python-based system for macromolecular structure solution. *Acta Crystallogr., Sect. D: Biol. Crystallogr.* **2010**, *66* (2), 213−221.
(89) Emsley, P.; Cowtan, K. Coot: model-building tools for molecular graphics. *Acta Crystallogr., Sect. D: Biol. Crystallogr.* **2004**, *60* (12), 2126−2132.
(90) Chen, J.; Ghazawi, F. M.; Li, Q. Interplay of bromodomain and histone acetylation in the regulation of p300-dependent genes. *Epigenetics* **2010**, *5* (6), 509−515.
(91) Adasme, M. F.; Linnemann, K. L.; Bolz, S. N.; Kaiser, F.; Salentin, S.; Haupt, V. J.; Schroeder, M. PLIP 2021: expanding the scope of the protein-ligand interaction profiler to DNA and RNA. *Nucleic Acids Res.* **2021**, *49* (W1), W530−W534.

https://doi.org/10.1021/acs.jmedchem.4c00210
J. Med. Chem. XXXX, XXX, XXX−XXX

SUPPLEMENTARY INFORMATION

Impact of combinatorial histone modifications on acetyllysine recognition by the ATAD2 and ATAD2B bromodomains

‡Margaret Phillips[1,2], ‡Kiera L. Malone[1], Brian W. Boyle[1], Cameron Montgomery[2], Isabelle A. Kressy[1], Faith M. Joseph[3,4], Kathleen M. Bright[5], Samuel P. Boyson[2], Sunsik Chang[2], Jay C. Nix[6], Nicolas L. Young[3,4], Victoria Jeffers[7], Seth Frietze[5] and Karen C. Glass*[1,2]

[1]Department of Pharmacology, Larner College of Medicine, University of Vermont, Burlington, VT, 05405, USA

[2]Department of Pharmaceutical Sciences, Albany College of Pharmacy and Health Sciences, Colchester, VT, 05446, USA

[3]Verna & Marrs McLean Department of Biochemistry & Molecular Pharmacology, Baylor College of Medicine, Houston, TX, 77030, USA

[4]Translational Biology and Molecular Medicine Graduate Program, Baylor College of Medicine, Houston, TX, 77030, USA

[5]Department of Biomedical and Health Sciences, University of Vermont, Burlington, VT, 05405, USA

[6]Molecular Biology Consortium, Advanced Light Source, Berkeley, CA, 94720, USA

[7]Department of Molecular, Cellular and Biomedical Sciences, University of New Hampshire, Durham, NH, 03824, USA.

‡M.P. and K.L.M. share first authorship

*To whom correspondence should be addressed. Tel: +1(802) 656-5760; Fax: +1(802) 656-4523; Email: karen.glass@med.uvm.edu

Table of Contents

Plasmid construction and protein purification

Human ATAD2 bromodomain-containing protein (residues 966-1112, UniProt code: Q6PL18) and was cloned into a pGEX-6P-1 plasmid containing an N-terminal GST tag and a PreScission Protease cleavage site followed by the bromodomain sequence that had been codon optimized by DAPCEL (Cleveland, OH, USA) and synthesized by GenScript (Piscataway, NJ, USA). Human ATAD2B bromodomain-containing protein (residues 953−1085, Uniprot code: Q9ULI0) was a gift from Nicole Burgess-Brown (Addgene plasmid # 39046) was PCR-amplified and cloned into pDEST15 (GlaxoSmithKline) vector containing an N-terminal GST tag and a PreScission Protease cleavage site followed by the bromodomain sequence. Both plasmids (ATAD2/B) were transformed into *Escherichia coli* BL21(DE3) pLysS competent cells (Novagen, MA, USA) for protein expression.

The GST-ATAD2 and GST-ATAD2B bromodomain-containing plasmids in BL21(DE3) pLysS cells were grown and purified according to our established protocol (22, 24). Briefly, the transformed cells were grown at 37 °C in 2 L of Terrific broth (TB) media supplemented with ampicillin and chloramphenicol antibiotics. The cells were grown to an O.D.600 of ~0.6, and then the temperature was reduced to 20°C. The cells were grown to an O.D.600 between 0.8-1.0 and induced with 0.5 mM and 0.25 mM isopropyl β-D-1-thiogalactopyranoside (IPTG) for GST-ATAD2 and GST-ATAD2B respectively and grown at 20°C overnight. Next, the cells were harvested at 5,000 RPM for 10 min at 4°C. The cell pellet was suspended in 100 mL of lysis buffer containing 50 mM Tris−HCl pH 7.5, 500 mM NaCl, 5% glycerol, 0.05% Nonidet P-40 alternative, 1 mM dithiothreitol (DTT) and supplemented with 0.1 mg/mL of lysozyme, and 1 tablet of protease inhibitor (Pierce protease inhibitor tablets, EDTA-free, Thermo Fisher). The cells were lysed by sonication, and cell lysate was centrifuged at 10,000 RPM for 20 minutes. The supernatant was incubated with glutathione agarose resin (Thermo Scientific) at 4°C with gentle agitation for 1 hour and 30 minutes. The suspension was poured into 25 mL Econo-Column Chromatography Columns (Bio-Rad) and washed with ten times the resin volume of wash buffer (20 mM Tris−HCl, pH 7.5, 500 mM NaCl, 5% glycerol, 1 mM DTT). The GST tag was cleaved off by incubating the washed beads in wash buffer supplemented with PreScission Protease (~100 mL at 76 mg/mL) (GE Healthcare) overnight at 4°C. The eluted ATAD2/B bromodomain proteins were concentrated to a total volume of approximately 3 mL. The protein concentration was determined using a Pierce BCA protein assay kit (Thermo Scientific) or by measuring the protein absorbance at 280 nM (20, 23). The purity of the ATAD2/B bromodomain was confirmed by sodium dodecyl sulfate-polyacrylamide gel electrophoresis (SDS-PAGE) gels stained with GelCode Blue Safe protein stain (Thermo Scientific) (25, 26).

Isothermal titration calorimetry

For the Isothermal titration calorimetry (ITC) experiments, proteins ATAD2 and ATAD2B bromodomains were dialyzed for 48 h in 20 mM sodium phosphate buffer, pH 7.0, 150 mM NaCl, and 1 mM tris(2-carboxyethyl) phosphine (TCEP) (Thermo Scientific) and protein concentration was estimated on a UV-Vis Spectrophotometer at 280 nm. All ITC experiemnts were carried out at 5°C using a MicroCal iTC200 or a MicroCal PEAQ-ITC instrument (Malvern Analytical).

The histone ligand was added to the sample cell through a series of 20 individual 2 mL injections spaced at time intervals of 150 s while maintaining a continuous stirring speed of 750 RPM. These were preceded by a 0.4 mL preliminary injection of the peptide ligand, excluded from the data integration and binding constant calculation. Control runs of histone peptide into the protein buffer were conducted under identical conditions and subtracted from the ligand into protein runs to correct for the heat of dilution for each peptide. MicroCal PEAQ-ITC software was used for data analysis. All data were fitted using a single set of binding site models to calculate the stoichiometry (N) and the binding constant (K_D). All experiments where binding occurred were performed in triplicate, while runs without binding were performed in duplicate. To calculate the K_D, the average of the three runs was taken as the mean K_D, and the standard deviation was calculated from the mean.

X-ray crystallography and structure determination

The ATAD2 and ATAD2B bromodomains were further purified for all crystallization experiments through size exclusion chromatography using a Superdex 75 16/60 Sephacryl S-100 high-resolution gel filtration column (GE/Cytiva) on an ÄktaPrime system (GE/Cytiva) in buffer containing 25 mM N-(2-hydroxyethyl)- piperazine-N′-ethane sulfonic acid (HEPES) at pH 7.5, 150 mM NaCl, and 1 mM DTT, and concentrated to 15 mg/mL with Amicon® Ultra (MILLIPORE) concentrators with a 3 kDa MW cut-off (3 MWCO). Protein concentration was estimated using a UV-Vis spectrophotometer at A_{280} nm.

The BRD-histone ligand complex was prepared in a 1:10 molar ratio with the bromodomain at 10 mg/mL and histone ligand at 10 times the molar concentration. For the ATAD2B-H4K12ac (4-17) complex, sitting-drop trays were set up using the Hampton Research Index HT screen in a 96-well VDX plate (Hampton Research, Aliso Viejo, CA, USA) at 4°C. Each 2 mL drop contained 0.5 mL of the complex and 1.5 mL of the mother liquor with a 25 mL reservoir volume. Cryoprotection was achieved by dragging the crystal through LV oil added to the drop. The crystal used for the structure solution grew in 1.8 M ammonium citrate tribasic at pH 7.0 and was mounted on B1A (ALS style) reusable goniometer bases inserted with a 75 mm Dual Thickness Microloop LD built on 18 mm / SPINE length rods (pins) from MiTeGen (Ithaca, NY, USA).

For the ATAD2B-H4S1phK5ac (1-15) complex, sitting drop trays were set up using the Hampton Research Index HT screen in a 96-well VDX plate at 4°C. The 2 mL crystal drop contained 0.5 mL of the complex and 1.5 mL of the mother liquor with a 25 mL reservoir volume. The crystal was harvested using a 300 mm Dual Thickness Microloop LD built on an 18 mm / SPINE length rod (pin) with a B1A (ALS style) reusable goniometer base from MiTeGen. The final crystal was obtained from a condition containing 0.2 M ammonium sulfate, 0.1 M BIS-TRIS (pH 5.5), 25% w/v PEG 3350, and was cryoprotected by sweeping the crystal in the loop through LV oil.

For the ATAD2 BRD H4S1phK5ac (1-15) complex, the ATAD2 BRD protein (10 mg/mL, 0.573 mM) was incubated with the histone peptide (5.73 mM) on ice at a 1:10 molar protein:peptide ratio. Crystallization screens were set up using the Hampton Research Index HT screen in a 96-well, sitting drop VDX plate at 4°C. Each drop (2 µL) consisted of 1 µL of the protein-peptide complex and 1 µL of the mother liquor solution, with a 25 µL reservoir volume. Crystals grew in condition 29 of the Hampton Index HT screen (60% v/v Tascimate™ pH 7.0). The crystal was harvested in a 75 µm Dual

Thickness Microloop LD built on 18 mm/SPINE length rods (pins) from MiTeGen (Ithaca, NY, USA). The crystal was cryoprotected with a sweep through 5 µL of LV oil and then was flash frozen in liquid nitrogen.

For the ATAD2B-H4S1CK5ac (1-15) complex, a sitting drop 96 well tray was set up using the Hampton Research Index HT screen, in a 96-well VDX plate at 4°C. The crystal used for structure determination grew in 0.2 M ammonium sulfate, 0.1 M Tris pH 8.5, 25% w/v PEG 3350. Each drop was 2 mL volume made from 0.5 mL of the complex and 1.5 mL of the mother liquor with a 25 mL reservoir volume. The crystal was harvested using a 200 mm Dual Thickness Microloop LD built on an 18 mm / SPINE length rod (pin) inserted in a B1A (ALS style) reusable goniometer base from MiTeGen. An LV oil sweep was used for cryoprotection.

For the ATAD2 BRD H4S1CK5ac (1-15) complex, the ATAD2 BRD protein (10 mg/mL, 0.573 mM) was incubated with the histone peptide (5.73 mM) on ice at a 1:10 molar protein:peptide ratio. Crystallization screens were set up using the Molecular Dimensions JCSG-plus™ screen and Hampton Index HT screen in a 96-well, sitting drop VDX plate at 4°C. Each drop (2 µL) consisted of 1 µL of the protein-peptide complex and 1 µL of the mother liquor solution, with a 25 µL reservoir volume. Small crystals grew in multiple conditions, but none were satisfactory for collection. Therefore, we set up a separate crystal screen based off a previously successful condition (44). Briefly, we modeled the screen after the Hampton Research Index HT screen conditions 17-18 (1.26 M Sodium phosphate monobasic monohydrate, 0.14 M potassium phosphate dibasic, pH 5., and 0.49 M sodium phosphate monobasic monohydrate, 0.91 M potassium phosphate dibasic, pH 6.9). We screened against pH in hanging drop 24-well VDX plates (Hampton Research, Aliso Viejo, CA, USA) over 500 µL of mother liquor solution. In each 2 µL drop, there was 1 µL of the protein-peptide solution and 1 µL of the mother liquor. The optimal crystallization condition was 1.42 M sodium phosphate monobasic monohydrate and 0.976 M potassium phosphate dibasic pH 6.4. The crystal was harvested in a 50 µm Dual Thickness Microloop LD built on 18 mm/SPINE length rods (pins) from MiTeGen (Ithaca, NY, USA). The crystal was cryoprotected with a sweep through 28% ethylene glycol in mother liquor, and then was flash frozen in liquid nitrogen.

Data were collected at the Advanced Light Source at the Lawrence Berkeley National Lab on beamline 4.2.2, equipped with an RDI CMOS-8M detector. The diffraction data were processed using XDS (1), and the structure was solved by a molecular replacement using PHASER (2). Structural models of the ATAD2/B bromodomains in complex with their histone ligands were built into the composite omit map, which showed clear density for the ligand using COOT 0.8.9.3 (3), followed by iterative rounds of refinement and rebuilding in PHENIX-1.19.2 (4) and COOT 0.8.9.3. The final structures were deposited into the Protein Data Bank. PDB IDs: 8sdq (ATAD2-H4S1phK5ac), 8sdo (ATAD2-S1CK5ac (1-15)), 8uhl (ATAD2B-H4K12ac), 8uk5 (ATAD2B -H4S1phK5ac) , and 8sdx (ATAD2B-H4S1CK5ac), respectively, after validation using MolProbity (5). The hydrogen bonds and hydrophobic interactions were determined using the PLIP (6) program.

Mass Spectrometry and H4 proteoform quantitation

Cell pellets were collected from plates of MCF-7 cells, and the histones were acid extracted after nuclei isolation as described above and previously in (7). Isolated histones were then resuspended in 85 mL 5% acetonitrile and 0.2% trifluoroacetic acid (TFA) to

prepare for high-performance liquid chromatography (HPLC) separation. The histones were separated by type into families and specific variants as described previously (Holt et al., 2021). Briefly, Reverse Phase HPLC fractionation was performed with a Thermo U3000 HPLC system (Thermo Fisher Scientific, Waltham, MA) with a 150 × 2.1–mm Vydac 218TP 3-µm C18 column (HiChrom, Reading, UK, part. no. 218TP3215), using a linear gradient at a flowrate of 0.2 mL/min from 25% B to 60% B for 60 min. The composition of buffers used were A: 5% acetonitrile and 0.2% TFA; B: 95% acetonitrile and 0.188% TFA. After chromatographic separation and histone fraction collection, histone H4 was selected for further study, dried down and resuspended in additional MS buffer A (2% acetonitrile, 0.1% formic acid) for mass spectrometric analysis.

Dried H4 fractions were then diluted using the following calculation, mg H4 = (Peak area –6.0114)/31.215 to calculate the dilution to 200 ng H4/mL in MS buffer A (2% acetonitrile, 0.1% formic acid). 1 mL (200 ng) histone H4 was then loaded onto a 10 cm, 100 mm inner diameter C3 column (ZORBAX 300SB-C3 300 Å 5 mm) for online high-performance liquid chromatography (HPLC) on a Thermo U3000 RSLC nano Pro-flow system. A 70-minute linear gradient using buffer A: 2% acetonitrile, 0.1% formic acid, and B: 98% acetonitrile and 0.1% formic acid was used, and the samples were maintained at a temperature of 4°C. The column eluant was introduced into a Thermo Scientific Orbitrap Fusion Lumos by nanoelectrospray ionization. A static spray voltage of 1800 V and an ion transfer tube temperature of 320°C were set for the source. The MS1 experiment used a 60-k resolution setting in positive mode. An AGC target of 5.0e5 with 200 ms maximum injection time, three micro scans, and a scan range of 700-1400 m/z were used. A targeted charge state of +15 was selected for histone H4. An intensity threshold of 1e5 was set for the selection of ions for fragmentation. The target precursor selected for MS2 fragmentation included all major H4 peaks and chose the top 20 most abundant m/z. ETD fragmentation at a 14 ms reaction time, 5.0e5 reagent target with 200 ms injection time was used. MS2 acquisition was performed using the orbitrap with the 60 k resolution setting, an AGC target of 5.0e5, a max injection time of 200 ms, a ‘normal’ scan range, and three micro scans.

Identification of H4 at the desired charge state of +15 was observed in mass spectra. Raw files were converted to mzXML. Data processing was performed by a custom analysis suite as previously described (7, 8).

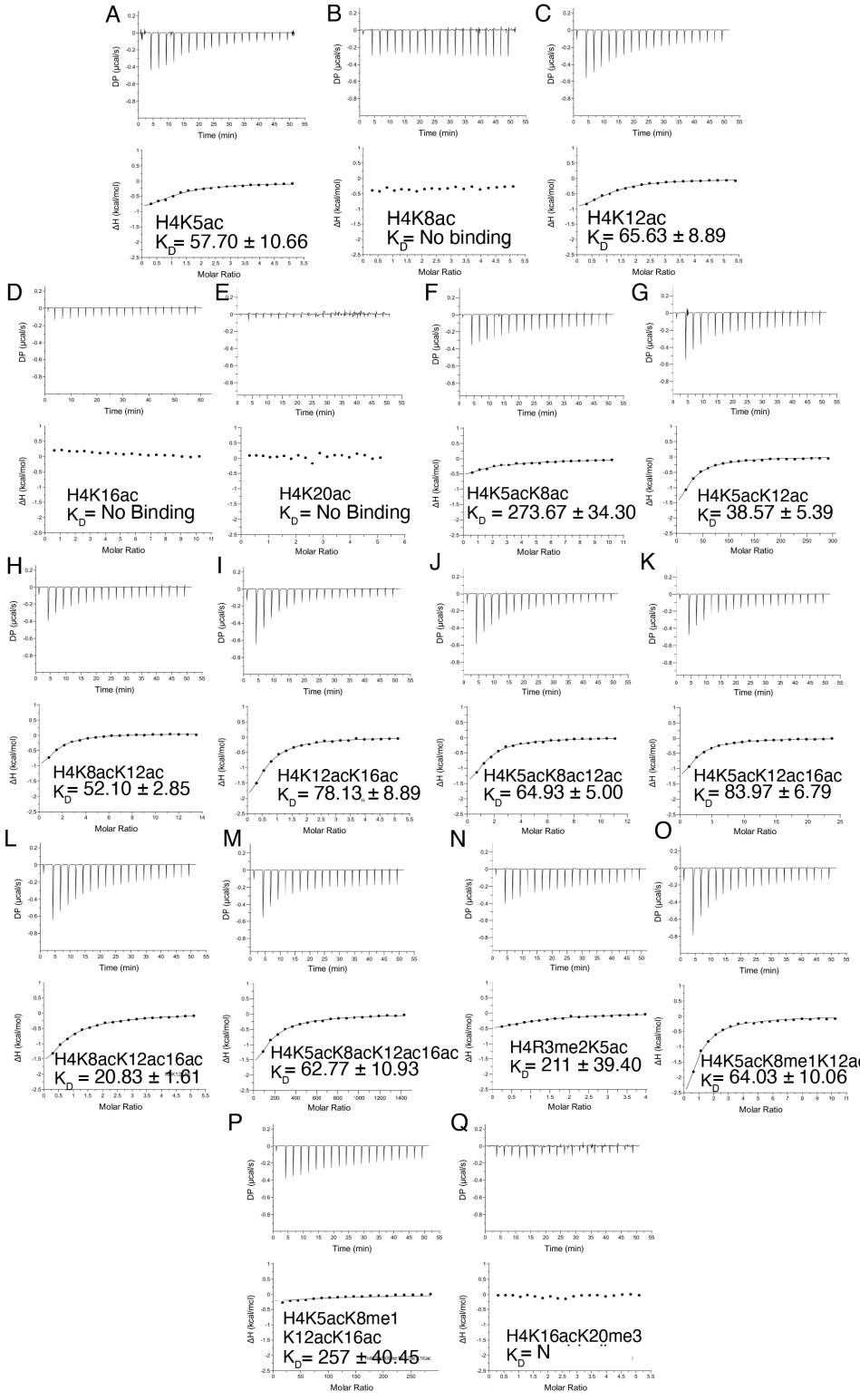

Fig. S1: Histone H4 peptides with combinatorial PTMs binding to the ATAD2 bromodomain. A-Q) Exothermic enthalpy ITC curves for the H4 peptides with various combinations of acetylation, methylation, and phosphorylation. The calculated binding constant is given in mM as K_D for each peptide. All peptides are 1-24 amino acids in length.

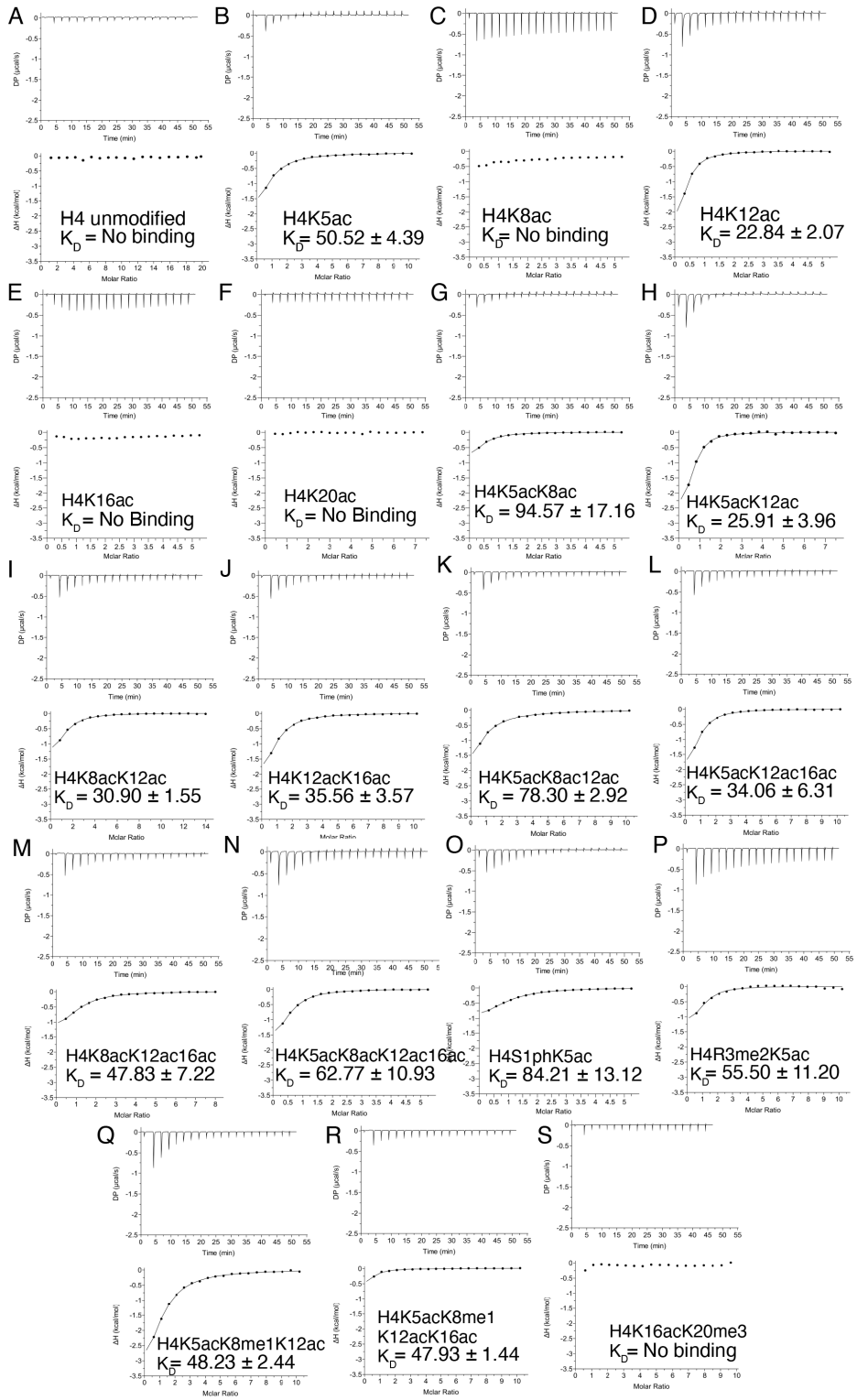

Fig. S2: Histone H4 peptides with combinatorial PTMs binding to the ATAD2B bromodomain. A-S) Exothermic enthalpy ITC curves for the H4 peptides with various combinations of acetylation, methylation, and phosphorylation. The calculated binding constant is given in mM as K_D for each peptide. All peptides are 1-24 amino acids in length.

Table S1: Summary of the data collection and refinement statistics for the crystal structure of ATAD2B BRD in complex with H4K12ac (PDB ID: 8EOQ).

Wavelength	1
Resolution range	27.56 - 2.0 (2.072 - 2.0)
Space group	P 41 21 2
Unit cell	55.119 55.119 140.657 90 90 90
Total reflections	206211 (19202)
Unique reflections	15396 (1490)
Multiplicity	13.4 (12.9)
Completeness (%)	99.84 (99.67)
Mean I/sigma(I)	22.67 (1.68)
Wilson B-factor	34.01
R-merge	0.1008 (1.635)
R-meas	0.1048 (1.702)
R-pim	0.02856 (0.471)
$CC_{1/2}$	0.999 (0.755)
CC*	1 (0.928)
Reflections used in refinement	15385 (1489)
Reflections used for R-free	729 (65)
R-work	0.1979 (0.2587)
R-free	0.2191 (0.2728)
CC(work)	0.968 (0.865)
CC(free)	0.949 (0.830)
Number of non-hydrogen atoms	1332
macromolecules	1232
solvent	100
Protein residues	151
RMS(bonds)	0.011
RMS(angles)	1.26
Ramachandran favored (%)	99.30
Ramachandran allowed (%)	0.70
Ramachandran outliers (%)	0.00
Rotamer outliers (%)	0.00
Clashscore	3.20
Average B-factor	41.69
macromolecules	41.64
solvent	42.26

Statistics for the highest-resolution shell are shown in parentheses.

Table S2: Summary of data collection and refinement statistics for the crystal structure of ATAD2 BRD in complex with H4S1phK5ac (PDBID: 8SDQ).

Wavelength	1.072
Resolution range	44.34 - 1.85 (1.916 - 1.85)
Space group	44.34 - 1.85 (1.916 - 1.85)
Unit cell	52.893 52.893 162.602 90 90 90
Total reflections	283313 (25897)
Unique reflections	20634 (1659)
Multiplicity	13.7 (12.8)
Completeness (%)	97.37 (82.12)
Mean I/sigma(I)	26.44 (3.15)
Wilson B-factor	23.67
R-merge	0.08953 (0.9309)
R-meas	0.09301 (0.9695)
R-pim	0.02498 (0.2679)
$CC_{1/2}$	1 (0.913)
CC*	1 (0.977)
Reflections used in refinement	20095 (1658)
Reflections used for R-free	996 (74)
R-work	0.2047 (0.3835)
R-free	0.2379 (0.4538)
CC(work)	0.959 (0.608)
CC(free)	0.956 (0.256)
Number of non-hydrogen atoms	1396
macromolecules	1186
solvent	210
Protein residues	140
RMS(bonds)	0.011
RMS(angles)	1.10
Ramachandran favored (%)	97.73
Ramachandran allowed (%)	2.27
Ramachandran outliers (%)	0.00
Rotamer outliers (%)	0.00
Clashscore	3.81
Average B-factor	34.24
macromolecules	32.79
solvent	42.40

Statistics for the highest-resolution shell are shown in parentheses.

Table S3: Summary of data collection and refinement statistics for the crystal structure of ATAD2B BRD in complex with H4S1phK5ac (PDBID: 8ESJ).

Wavelength	1.072
Resolution range	31.37 - 1.4 (1.45 - 1.4)
Space group	P 21 21 21
Unit cell	41.08 48.58 83.32 90 90 90
Total reflections	397691 (37316)
Unique reflections	33447 (3285)
Multiplicity	11.9 (11.4)
Completeness (%)	99.51 (99.57)
Mean I/sigma(I)	28.93 (2.50)
Wilson B-factor	18.27
R-merge	0.05652 (1.989)
R-meas	0.05916 (2.082)
R-pim	0.01714 (0.6077)
$CC_{1/2}$	1 (0.873)
CC*	1 (0.965)
Reflections used in refinement	33431 (3275)
Reflections used for R-free	1678 (154)
R-work	0.1784 (0.2520)
R-free	0.2023 (0.2784)
CC(work)	0.968 (0.895)
CC(free)	0.964 (0.832)
Number of non-hydrogen atoms	1399
macromolecules	1131
solvent	268
Protein residues	138
RMS(bonds)	0.011
RMS(angles)	1.04
Ramachandran favored (%)	97.71
Ramachandran allowed (%)	2.29
Ramachandran outliers (%)	0.00
Rotamer outliers (%)	0.00
Clashscore	3.10
Average B-factor	29.77
macromolecules	27.88
solvent	37.77

Statistics for the highest-resolution shell are shown in parentheses.

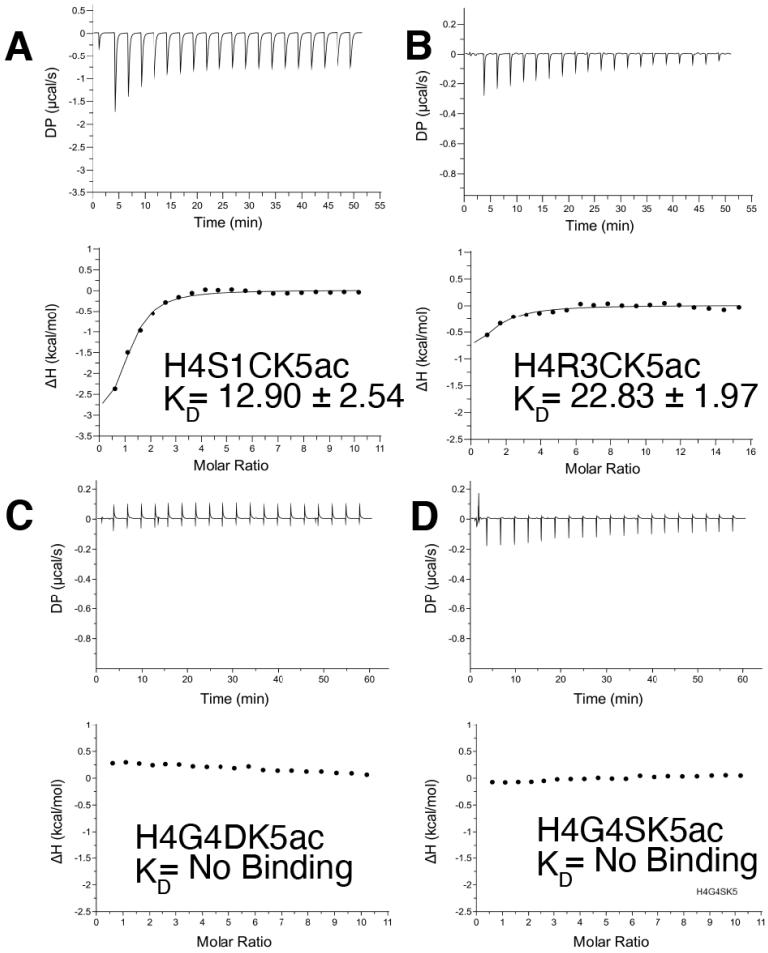

Fig. S3: Binding of 'oncohistone' H4 peptides to the ATAD2 bromodomain. A-D) ITC enthalpy plots for the binding of the ATAD2 BRD with mutant mono-acetylated histone H4 ligands (residues 1-15) as indicated. The calculated binding constant (K_D) for each peptide is shown in their respective plots.

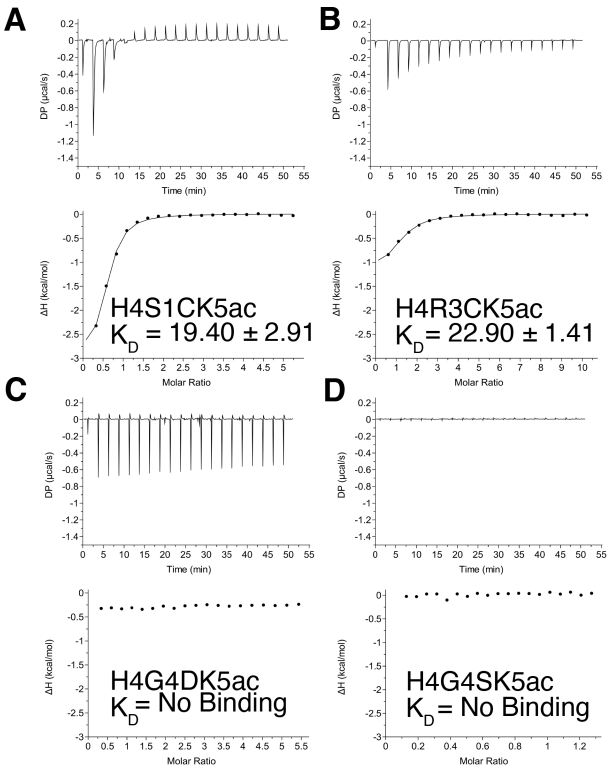

Fig. S4: Binding of 'oncohistone' H4 peptides to the ATAD2B bromodomain. A-D) ITC enthalpy plots for the binding of the ATAD2B BRD with mutant mono-acetylated histone H4 ligands (residues 1-15) as indicated. The calculated binding constant (K_D) for each peptide is shown in their respective plots.

Table S4: Summary of data collection and refinement statistics for the crystal structure of ATAD2 BRD in complex with H4S1CK5ac (PDBID: 8SDO).

Wavelength	1.072
Resolution range	27.46 - 2.01 (2.082 - 2.01)
Space group	P 43 2 2
Unit cell	53.941 53.941 159.522 90 90 90
Total reflections	220898 (21350)
Unique reflections	16480 (1529)
Multiplicity	13.4 (13.4)
Completeness (%)	99.51 (96.10)
Mean I/sigma(I)	18.91 (0.65)
Wilson B-factor	43.36
R-merge	0.1117 (4.016)
R-meas	0.1162 (4.175)
R-pim	0.0316 (1.133)
$CC_{1/2}$	0.999 (0.374)
CC*	1 (0.738)
Reflections used in refinement	16410 (1529)
Reflections used for R-free	762 (67)
R-work	0.2009 (0.3077)
R-free	0.2306 (0.3278)
CC(work)	0.966 (0.665)
CC(free)	0.966 (0.711)
Number of non-hydrogen atoms	1309
macromolecules	1141
ligands	0
solvent	168
Protein residues	136
RMS(bonds)	0.007
RMS(angles)	0.95
Ramachandran favored (%)	98.46
Ramachandran allowed (%)	1.54
Ramachandran outliers (%)	0.00
Rotamer outliers (%)	1.59
Clashscore	3.97
Average B-factor	56.87
macromolecules	55.63
solvent	65.29

Statistics for the highest-resolution shell are shown in parentheses.

Table S5: Summary of data collection and refinement statistics for the crystal structure of ATAD2B BRD in complex with H4S1CK5ac (PDBID: 7TZQ).

Wavelength	1.00
Resolution range	33.52 - 2.79 (2.89 - 2.79)
Space group	P 1 21 1
Unit cell	47.687 79.629 64.348 90 105.141 90
Total reflections	42819 (3969)
Unique reflections	11594 (1060)
Multiplicity	3.7 (3.5)
Completeness (%)	98.41 (92.81)
Mean I/sigma(I)	8.41 (1.21)
Wilson B-factor	65.79
R-merge	0.1152 (1.246)
R-meas	0.1351 (1.474)
R-pim	0.06988 (0.782)
$CC_{1/2}$	0.994 (0.524)
CC*	0.998 (0.829)
Reflections used in refinement	11481 (1059)
Reflections used for R-free	598 (53)
R-work	0.2208 (0.3775)
R-free	0.2563 (0.4409)
CC(work)	0.960 (0.678)
CC(free)	0.968 (0.503)
Number of non-hydrogen atoms	2342
macromolecules	2311
ligands	5
solvent	26
Protein residues	284
RMS(bonds)	0.011
RMS(angles)	1.41
Ramachandran favored (%)	93.70
Ramachandran allowed (%)	5.93
Ramachandran outliers (%)	0.37
Rotamer outliers (%)	1.56
Clashscore	15.65
Average B-factor	73.62
macromolecules	73.77
ligands	66.62
solvent	61.46

Statistics for the highest-resolution shell are shown in parentheses.

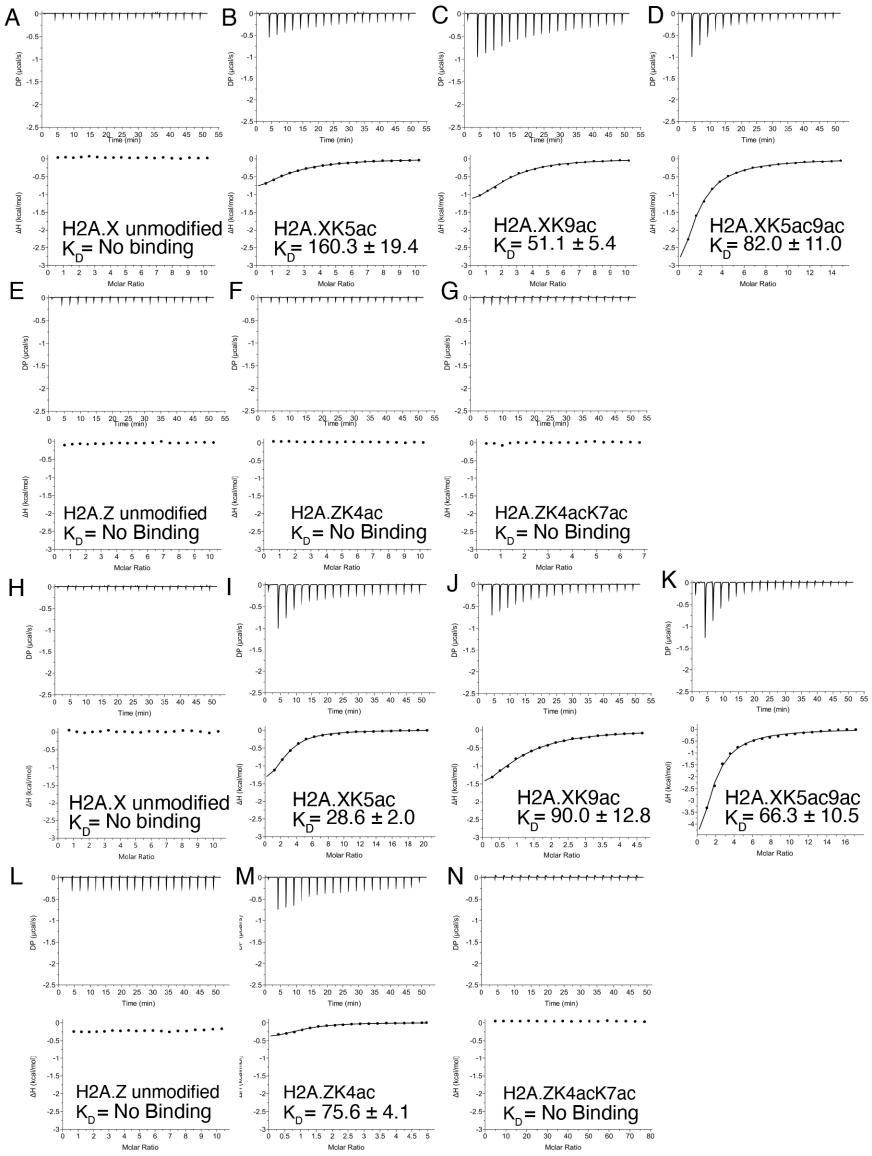

Fig. S5: Histone H2A.X and H2A.Z variant peptides with combinatorial PTMs binding to the ATAD2/B bromodomain. A-G) Exothermic enthalpy ITC curves for the H2A.X and H2A.Z histone variant peptides with mono- and di-acetylation marks binding to ATAD2 bromodomain. H-N) Exothermic enthalpy ITC curves for the H2A.X and H2A.Z histone variant peptides with mono- and di-acetylation marks binding to ATAD2B bromodomain. The calculated binding constant is given in mM as K_D for each peptide.

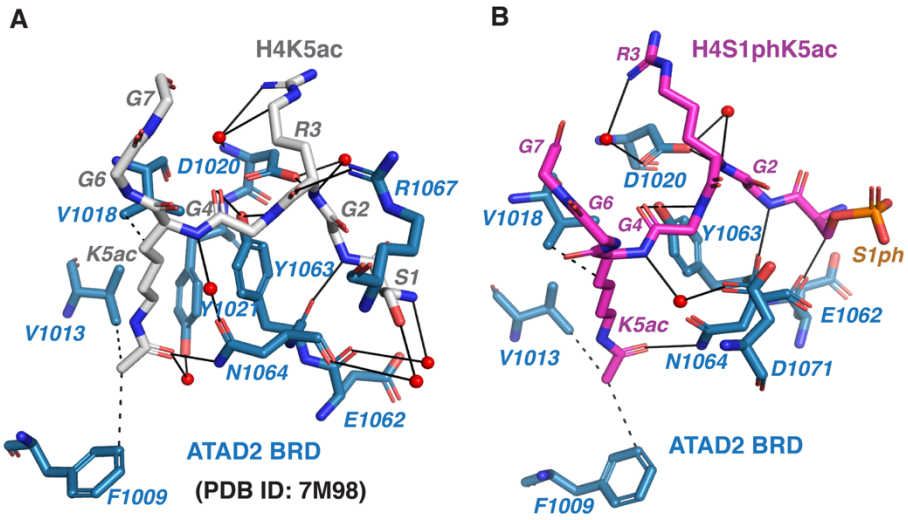

Figure S6: Coordination of the histone H4 ligand with K5ac by the ATAD2 bromodomain. (A) Coordination of the H4K5ac (residues 1-10) by the ATAD2 BRD observed in the previously solved crystal structure PDB ID: 7M98(9). ATAD2 BRD residues are in blue, while the histone H4K5ac ligand residues are in grey. (B) Coordination of the H4S1phK5ac ligand (residues 1-7) by the ATAD2 BRD. ATAD2 BRD residues are displayed in dark blue, while the H4S1phK5ac ligand residues are shown in magenta. Solid black lines represent hydrogen bonds, while dashed black lines show hydrophobic interactions. Water molecules are shown in red. All figures were made using the PyMOL Molecular Graphics system using version 2.3, Schrödinger, LLC, and all contacts were determined using the PLIP program (6).

References:

1. W. Kabsch, Xds. *Acta Crystallogr D Biol Crystallogr* **66**, 125-132 (2010).
2. A. J. McCoy *et al.*, Phaser crystallographic software. *Journal of applied crystallography* **40**, 658-674 (2007).
3. P. Emsley, K. Cowtan, Coot: model-building tools for molecular graphics. *Acta Crystallogr D Biol Crystallogr* **60**, 2126-2132 (2004).
4. P. D. Adams *et al.*, PHENIX: a comprehensive Python-based system for macromolecular structure solution. *Acta Crystallogr D Biol Crystallogr* **66**, 213-221 (2010).
5. V. B. Chen *et al.*, MolProbity: all-atom structure validation for macromolecular crystallography. *Acta Crystallogr D Biol Crystallogr* **66**, 12-21 (2010).
6. M. F. Adasme *et al.*, PLIP 2021: expanding the scope of the protein-ligand interaction profiler to DNA and RNA. *Nucleic Acids Res* **49**, W530-W534 (2021).
7. M. V. Holt, T. Wang, N. L. Young, Expeditious Extraction of Histones from Limited Cells or Tissue Samples and Quantitative Top-Down Proteomic Analysis. *Curr Protoc* **1**, e26 (2021).
8. P. A. DiMaggio, Jr., N. L. Young, R. C. Baliban, B. A. Garcia, C. A. Floudas, A mixed integer linear optimization framework for the identification and quantification of targeted post-translational modifications of highly modified proteins using multiplexed electron transfer dissociation tandem mass spectrometry. *Mol Cell Proteomics* **8**, 2527-2543 (2009).
9. C. M. Evans *et al.*, Coordination of Di-Acetylated Histone Ligands by the ATAD2 Bromodomain. *Int J Mol Sci* **22** (2021).

Sample Name :H4 unmodified (1-24)
Sample ID :U344SGB120-1
Time Processed :23:59:55
Month-Day-Year Processed :02/27/2021

Pump A : 0.065% trifluoroacetic in 100% water (v/v)
Pump B : 0.05% trifluoroacetic in 100% acetonitrile (v/v)
Total Flow:1 ml/min
Wavelength:220 nm
<<LC Time Program>>

Time	Module	Command	Value
0.01	Pumps	B.Conc	5
25.00	Pumps	B.Conc	65
25.01	Pumps	B.Conc	95
27.00	Pumps	B.Conc	95
27.01	Pumps	B.Conc	5
35.00	Pumps	B.Conc	5
35.01	Controller	Stop	

<<Column Performance>>
<Detector A>
Column :Inertsil ODS-3 4.6 x 250 mm
Equipment: SS-CM-0309

<Chromatogram>

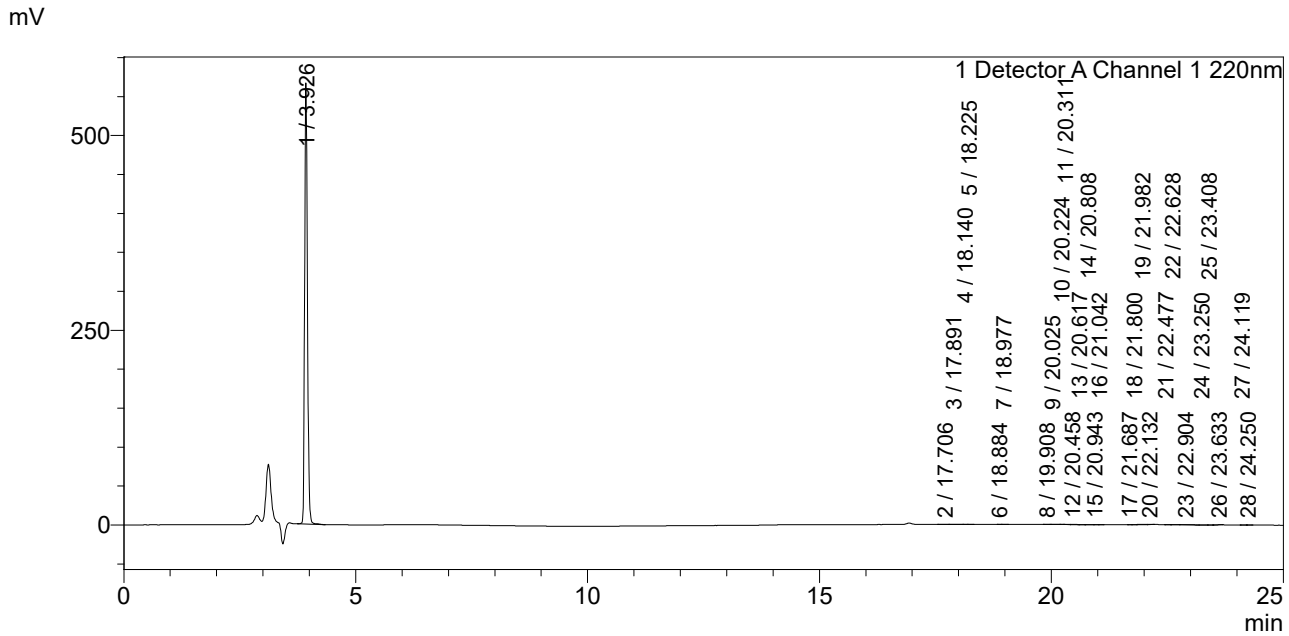

<Peak Table>

Detector A Channel 1 220nm

Peak#	Ret. Time	Area	Height	Area%
1	3.926	2387765	566467	99.576
2	17.706	1084	111	0.045
3	17.891	2205	199	0.092
4	18.140	200	48	0.008
5	18.225	108	29	0.005
6	18.884	115	32	0.005
7	18.977	162	44	0.007
8	19.908	198	52	0.008
9	20.025	147	13	0.006
10	20.224	136	45	0.006
11	20.311	356	56	0.015
12	20.458	459	58	0.019
13	20.617	170	34	0.007
14	20.808	535	77	0.022
15	20.943	253	49	0.011
16	21.042	153	44	0.006

Peak#	Ret. Time	Area	Height	Area%
17	21.687	100	35	0.004
18	21.800	177	37	0.007
19	21.982	787	83	0.033
20	22.132	325	77	0.014
21	22.477	255	65	0.011
22	22.628	309	57	0.013
23	22.904	1222	123	0.051
24	23.250	116	35	0.005
25	23.408	76	24	0.003
26	23.633	371	70	0.015
27	24.119	108	24	0.005
28	24.250	42	14	0.002
Total		2397933	567999	100.000

Sample Name : H4K5ac (1-24)
Sample ID : U3243HC210-3
Time Processed : 16:55:32
Month-Day-Year Processed : 04/25/2022

Pump A : 0.065% trifluoroacetic in 100% water (v/v)
Pump B : 0.05% trifluoroacetic in 100% acetonitrile (v/v)
Total Flow:1 ml/min
Wavelength:220 nm

Time	Module	Command	Value
0.01	Pumps	B.Conc	5
25.00	Pumps	B.Conc	65
25.01	Pumps	B.Conc	95
27.00	Pumps	B.Conc	95
27.01	Pumps	B.Conc	5
35.00	Pumps	B.Conc	5
35.01	Controller	Stop	

<<Column Performance>>
<Detector A>
Column : Inertsil ODS-3 4.6 x 250 mm
Equipment: GK11010017

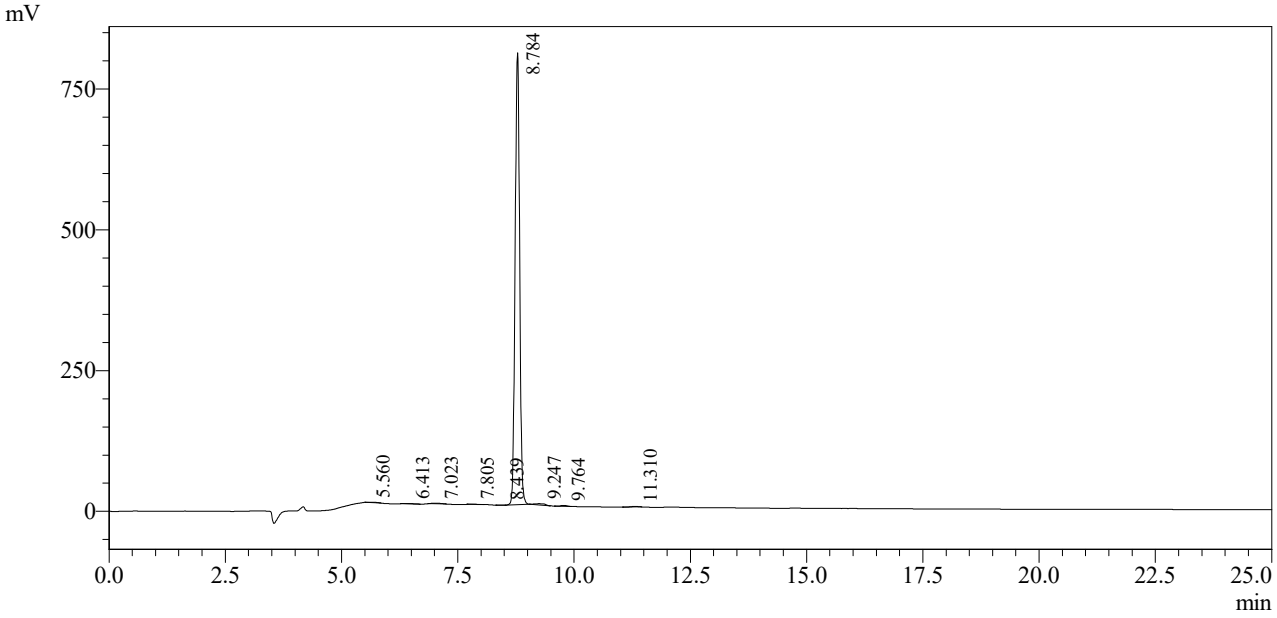

1 Detector A Channel 1 / 220nm

Peak Table

Detector A Channel 1 220nm

Peak#	Ret. Time	Area	Height	Area %
1	5.560	8616	507	0.155
2	6.413	8358	642	0.151
3	7.023	16639	1202	0.300
4	7.805	3840	469	0.069
5	8.439	465	110	0.008
6	8.784	5448115	802354	98.256
7	9.247	35949	2345	0.648
8	9.764	12242	1479	0.221
9	11.310	10613	1035	0.191
Total		5544837	810142	100.000

Sample Name :H4(1-24)K8ac
Sample ID :U3145DJ160-3
Time Processed : 8:54:00
Month-Day-Year Processed :10/25/2018

Pump A : 0.065% trifluoroacetic in 100% water (v/v)
Pump B : 0.05% trifluoroacetic in 100% acetonitrile (v/v)
Total Flow:1 ml/min
Wavelength:220 nm

Time	Unit	Command	Value	Comment
0.01	Pumps	Pump A B.Conc	5	
25.00	Pumps	Pump A B.Conc	65	
25.01	Pumps	Pump A B.Conc	95	
27.00	Pumps	Pump A B.Conc	95	
27.01	Pumps	Pump A B.Conc	5	
35.00	Pumps	Pump A B.Conc	5	
35.01	Controller	Stop		

<<Column Performance>>
<Detector A>
Column : Inertsil ODS-3 4.6 x 250 mm
Equipment:SS-CM-0286

Chromatogram

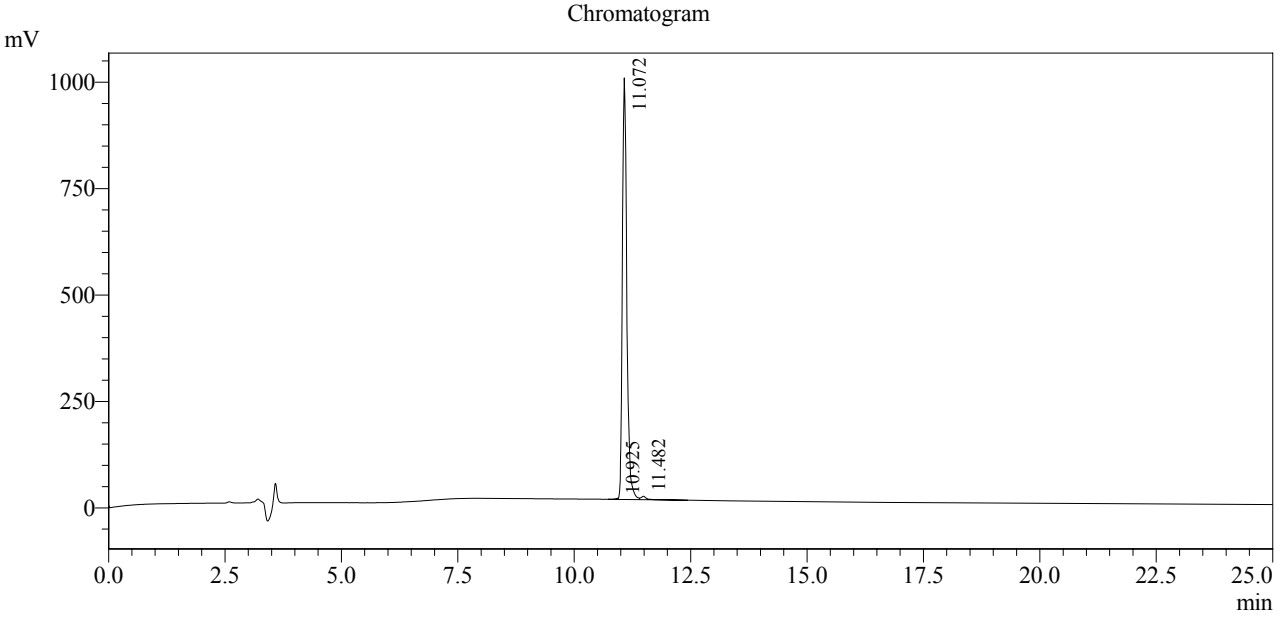

1 Det.A Ch1 / 220nm

Peak Table

Detector A Ch1 220nm

Peak#	Ret. Time	Area	Height	Area %
1	10.925	9790	2533	0.147
2	11.072	6554973	990334	98.741
3	11.482	73772	8070	1.111
Total		6638536	1000936	100.000

Sample Name : H4K12ac (1-24)
Sample ID : U638AGC310-1
Time Processed : 14:41:40
Month-Day-Year Processed : 05/28/2021

Pump A : 0.065% trifluoroacetic in 100% water (v/v)
Pump B : 0.05% trifluoroacetic in 100% acetonitrile (v/v)
Total Flow:1 ml/min
Wavelength:220 nm

Time	Module	Command	Value
0.01	Pumps	Pump A B.Conc	15
25.00	Pumps	Pump A B.Conc	75
25.01	Pumps	Pump A B.Conc	95
32.00	Pumps	Pump A B.Conc	95
32.01	Pumps	Pump A B.Conc	15
40.00	Pumps	Pump A B.Conc	15
45.00	Controller	Stop	

<<Column Performance>>
<Detector A>
Column : Inertsil ODS-3 4.6 x 250 mm
Equipment: GK11010017

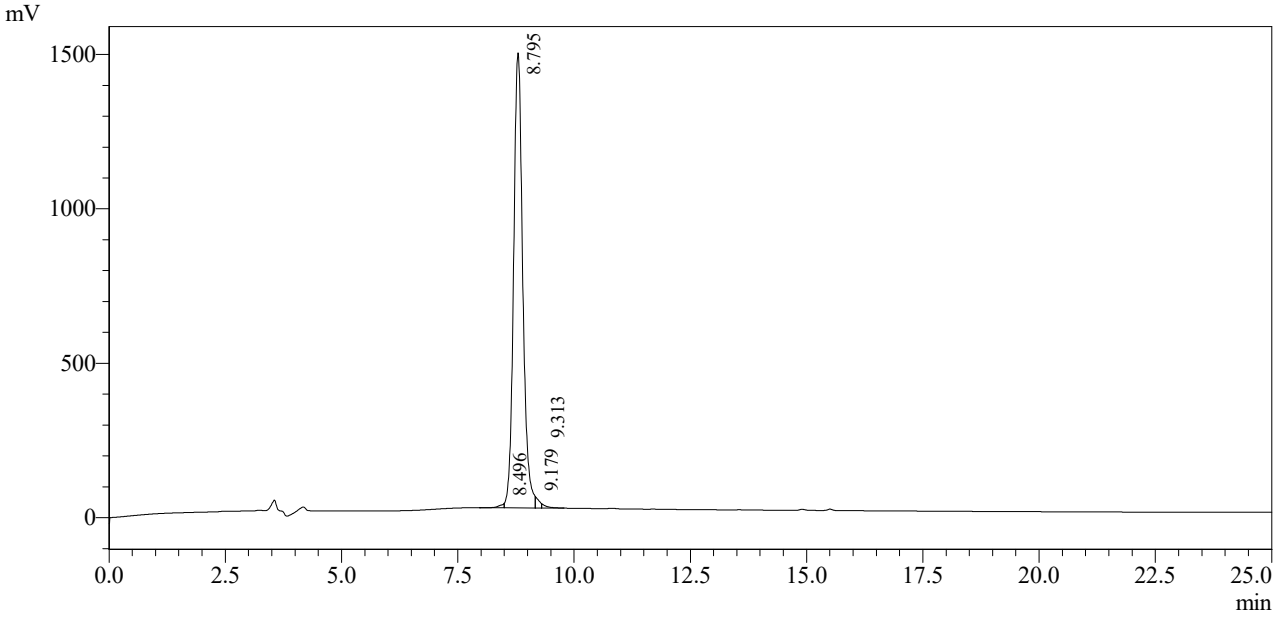

1 Detector A Channel 1 / 220nm

Peak Table

Detector A Channel 1 220nm

Peak#	Ret. Time	Area	Height	Area %
1	8.496	96374	13023	0.469
2	8.795	20162788	1473462	98.140
3	9.179	197323	35822	0.960
4	9.313	88479	13438	0.431
Total		20544966	1535746	100.000

Sample Name : H4K16ac (1-24)
Sample ID : U344SGB120-9
Time Processed : 1:44:40 AM
Month-Day-Year Processed : 02/28/2021

Pump A : 0.065% trifluoroacetic in 100% water (v/v)
Pump B : 0.05% trifluoroacetic in 100% acetonitrile (v/v)
Total Flow:1 ml/min
Wavelength:220 nm

Time	Module	Command	Value
0.01	Pumps	Pump A B.Conc	15
25.00	Pumps	Pump A B.Conc	75
25.01	Pumps	Pump A B.Conc	95
32.00	Pumps	Pump A B.Conc	95
32.01	Pumps	Pump A B.Conc	15
40.00	Pumps	Pump A B.Conc	15
40.00	Controller	Stop	

<<Column Performance>>
<Detector A>
Column : Inertsil ODS-3 4.6 x 250 mm
Equipment: GK11010017

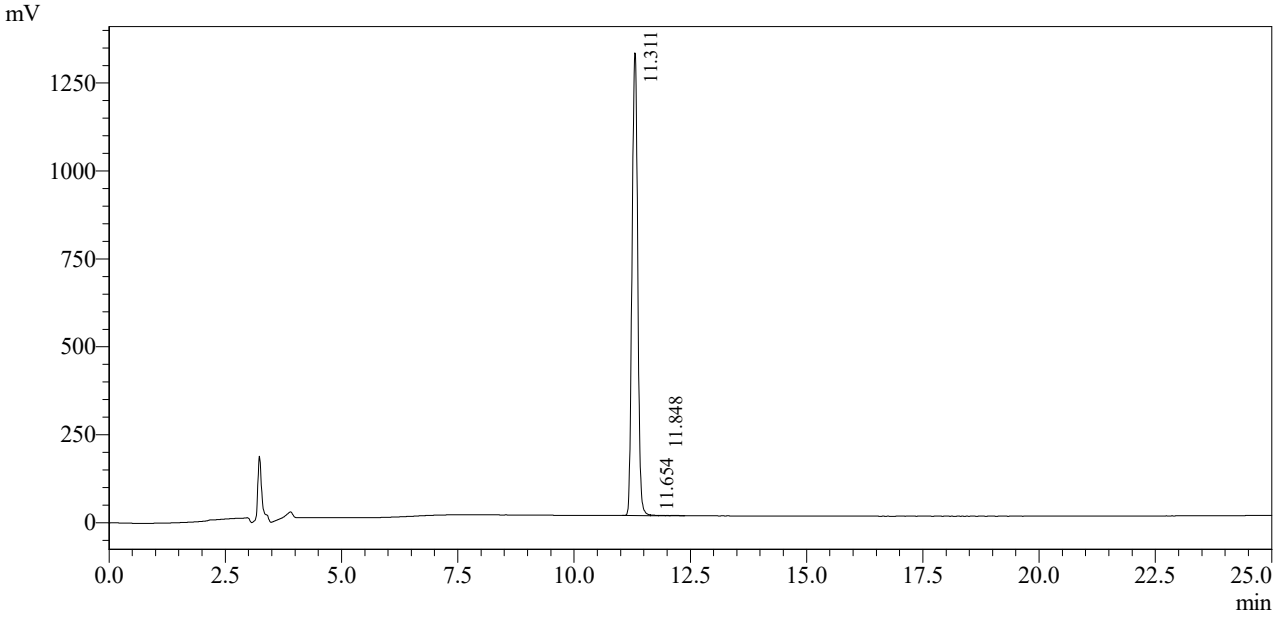

1 Detector A Channel 1 / 220nm

Peak Table

Detector A Channel 1 220nm

Peak#	Ret. Time	Area	Height	Area %
1	11.311	11169694	1315526	99.834
2	11.654	11007	1825	0.098
3	11.848	7559	563	0.068
Total		11188260	1317914	100.000

Sample Name :H4(1-24)K20ac
Sample ID :U3145DJ160-7
Time Processed : 17:16:39
Month-Day-Year Processed : 10/28/2018

Pump A : 0.065% trifluoroacetic in 100% water (v/v)
Pump B : 0.05% trifluoroacetic in 100% acetonitrile (v/v)
Total Flow:1 ml/min
Wavelength:220 nm

Time	Unit	Command	Value	Comment
0.01	Pumps	Pump A B.Conc	5	
25.00	Pumps	Pump A B.Conc	65	
25.01	Pumps	Pump A B.Conc	95	
32.00	Pumps	Pump A B.Conc	95	
32.01	Pumps	Pump A B.Conc	5	
40.00	Pumps	Pump A B.Conc	5	
40.01	Controller	Stop		

<<Column Performance>>
<Detector A>
Column : Inertsil ODS-3 4.6 x 250 mm
Equipment: G09010878

Chromatogram

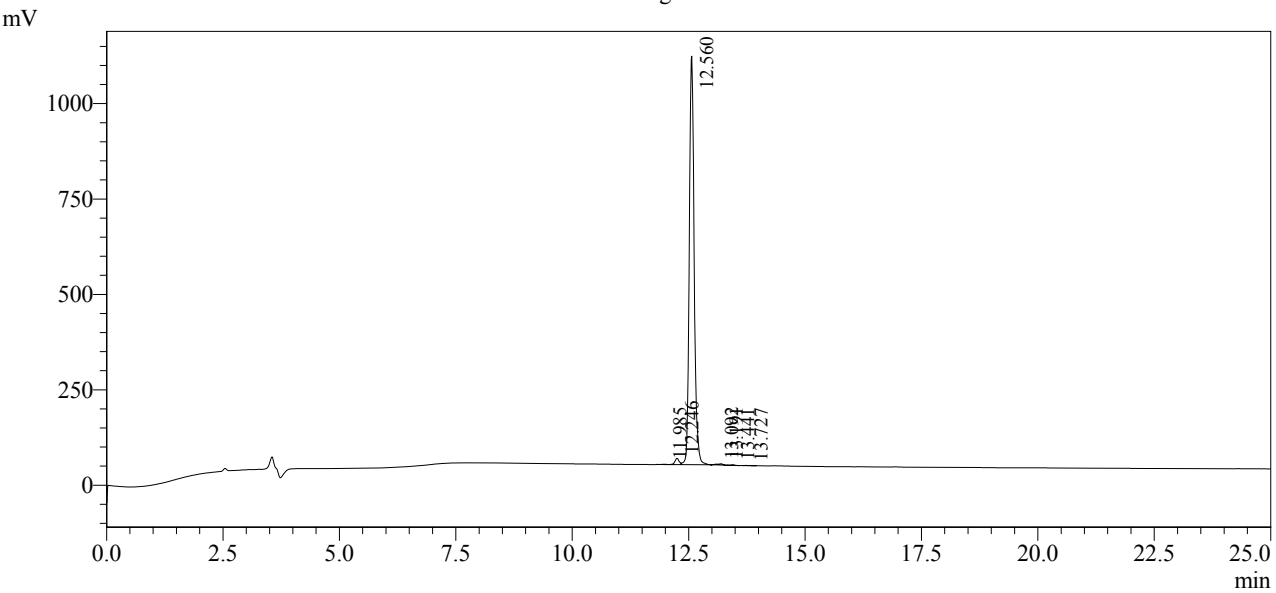

1 Det.A Ch1 / 220nm

Peak Table

Detector A Ch1 220nm

Peak#	Ret. Time	Area	Height	Area %
1	11.985	6677	796	0.084
2	12.246	105925	16627	1.333
3	12.560	7792712	1070467	98.035
4	13.092	12741	2232	0.160
5	13.191	19550	3365	0.246
6	13.441	8714	1435	0.110
7	13.727	2614	404	0.033
Total		7948932	1095325	100.000

Sample Name :H4K5acK8ac (1-24)
Sample ID :U638AGC310-3
Time Processed :22:27:59
Month-Day-Year Processed :04/14/2021

Pump A : 0.065% trifluoroacetic in 100% water (v/v)
Pump B : 0.05% trifluoroacetic in 100% acetonitrile (v/v)
Total Flow:1 ml/min
Wavelength:220 nm
<<LC Time Program>>

Time	Module	Command	Value
0.01	Pumps	B.Conc	5
25.00	Pumps	B.Conc	65
25.01	Pumps	B.Conc	95
27.00	Pumps	B.Conc	95
27.01	Pumps	B.Conc	5
35.00	Pumps	B.Conc	5
35.01	Controller	Stop	

<<Column Performance>>
<Detector A>
Column :Inertsil ODS-3 4.6 x 250 mm
Equipment: SS-CM-0309

<Chromatogram>

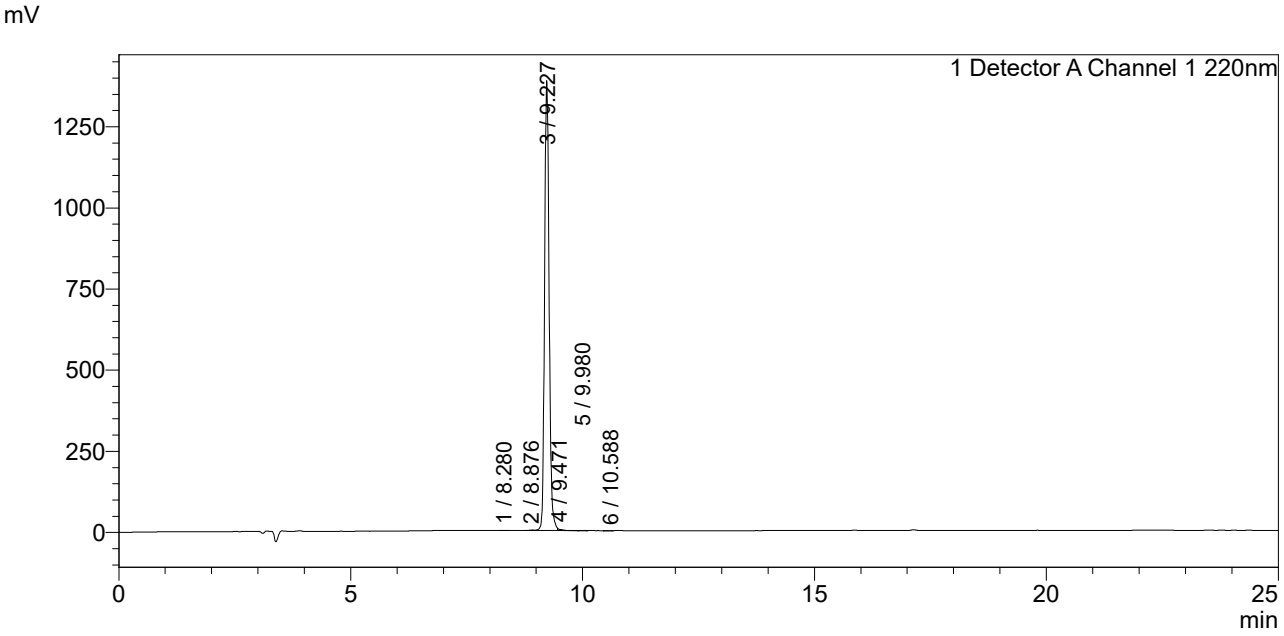

<Peak Table>

Detector A Channel 1 220nm

Peak#	Ret. Time	Area	Height	Area%
1	8.280	1503	211	0.016
2	8.876	6767	1154	0.071
3	9.227	9512752	1386908	99.537
4	9.471	34017	6174	0.356
5	9.980	1045	203	0.011
6	10.588	877	144	0.009
Total		9556961	1394795	100.000

Sample Name :H4(1-24)K5acK12ac,
Sample ID :U6685DL060-3
Time Processed : 20:32:46
Month-Day-Year Processed : 12/17/2018

Pump A : 0.065% trifluoroacetic in 100% water (v/v)
Pump B : 0.05% trifluoroacetic in 100% acetonitrile (v/v)
Total Flow:1 ml/min
Wavelength:220 nm

Time	Unit	Command	Value	Comment
0.01	Pumps	Pump A B.Conc	5	
25.00	Pumps	Pump A B.Conc	65	
25.01	Pumps	Pump A B.Conc	95	
27.00	Pumps	Pump A B.Conc	95	
27.01	Pumps	Pump A B.Conc	5	
35.00	Pumps	Pump A B.Conc	5	
35.01	Controller	Stop		

<<Column Performance>>
<Detector A>
Column : Inertsil ODS-3 4.6 x 250 mm
Equipment: GK11010017

Chromatogram

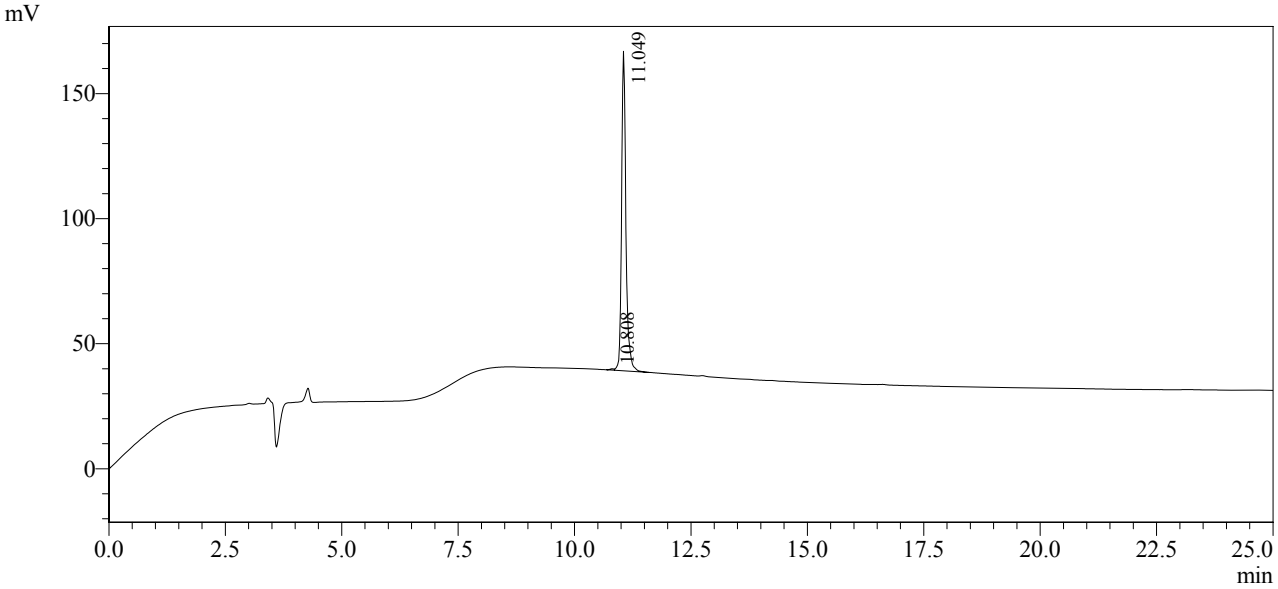

1 Det.A Ch1 / 220nm

Peak Table

Detector A Ch1 220nm

Peak#	Ret. Time	Area	Height	Area %
1	10.808	3109	534	0.374
2	11.049	827102	127737	99.626
Total		830210	128271	100.000

Sample Name :H4(1-24)K8acK12ac
Sample ID :U3145DJ160-11
Time Processed : 11:31:14
Month-Day-Year Processed : 10/31/2018

Pump A : 0.065% trifluoroacetic in 100% water (v/v)
Pump B : 0.05% trifluoroacetic in 100% acetonitrile (v/v)
Total Flow:1 ml/min
Wavelength:220 nm

Time	Unit	Command	Value	Comment
0.01	Pumps	Pump A B.Conc	5	
25.00	Pumps	Pump A B.Conc	65	
25.01	Pumps	Pump A B.Conc	95	
32.00	Pumps	Pump A B.Conc	95	
32.01	Pumps	Pump A B.Conc	5	
40.00	Pumps	Pump A B.Conc	5	
40.01	Controller	Stop		

<<Column Performance>>
<Detector A>
Column : Inertsil ODS-3 4.6 x 250 mm
Equipment: G09010878

Chromatogram

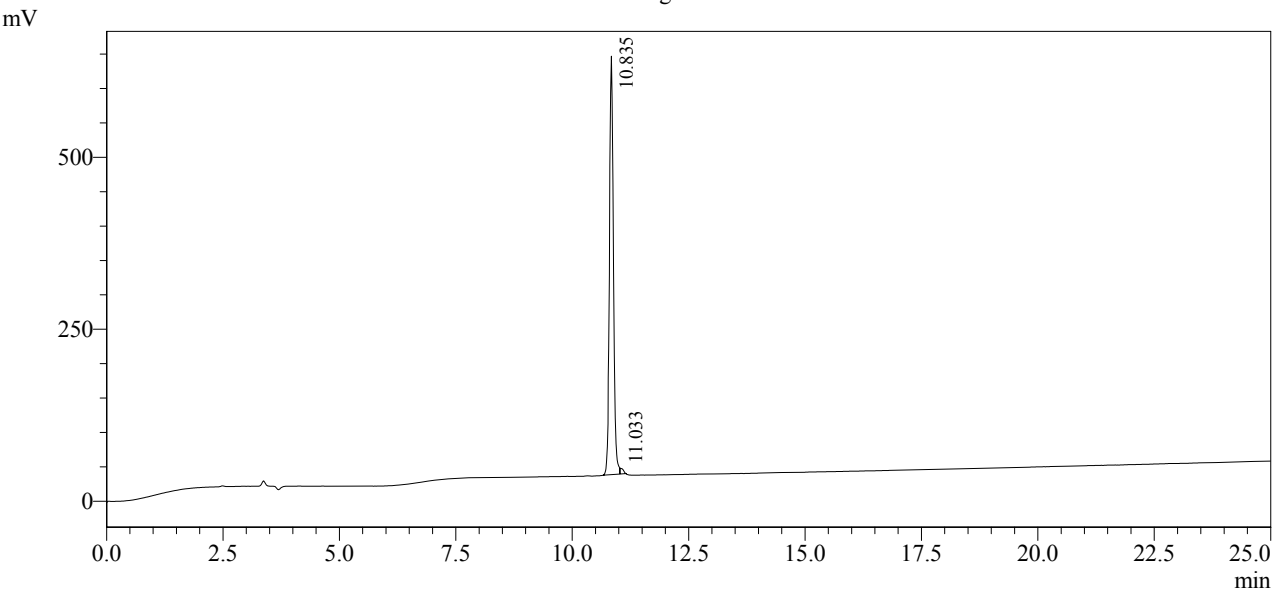

1 Det.A Ch1 / 220nm

Peak Table

Detector A Ch1 220nm

Peak#	Ret. Time	Area	Height	Area %
1	10.835	3630454	608307	98.963
2	11.033	38051	8342	1.037
Total		3668505	616649	100.000

Sample Name :H4(1-24)K12acK16ac
Sample ID :U6685DL060-1
Time Processed : 14:23:25
Month-Day-Year Processed : 12/18/2018

Pump A : 0.065% trifluoroacetic in 100% water (v/v)
Pump B : 0.05% trifluoroacetic in 100% acetonitrile (v/v)
Total Flow:1 ml/min
Wavelength:220 nm

Time	Unit	Command	Value	Comment
0.01	Pumps	Pump A B.Conc	5	
25.00	Pumps	Pump A B.Conc	65	
25.01	Pumps	Pump A B.Conc	95	
32.00	Pumps	Pump A B.Conc	95	
32.01	Pumps	Pump A B.Conc	5	
40.00	Pumps	Pump A B.Conc	5	
40.01	Controller	Stop		

<<Column Performance>>
<Detector A>
Column : Inertsil ODS-3 4.6 x 250 mm
Equipment: G09010878

Chromatogram

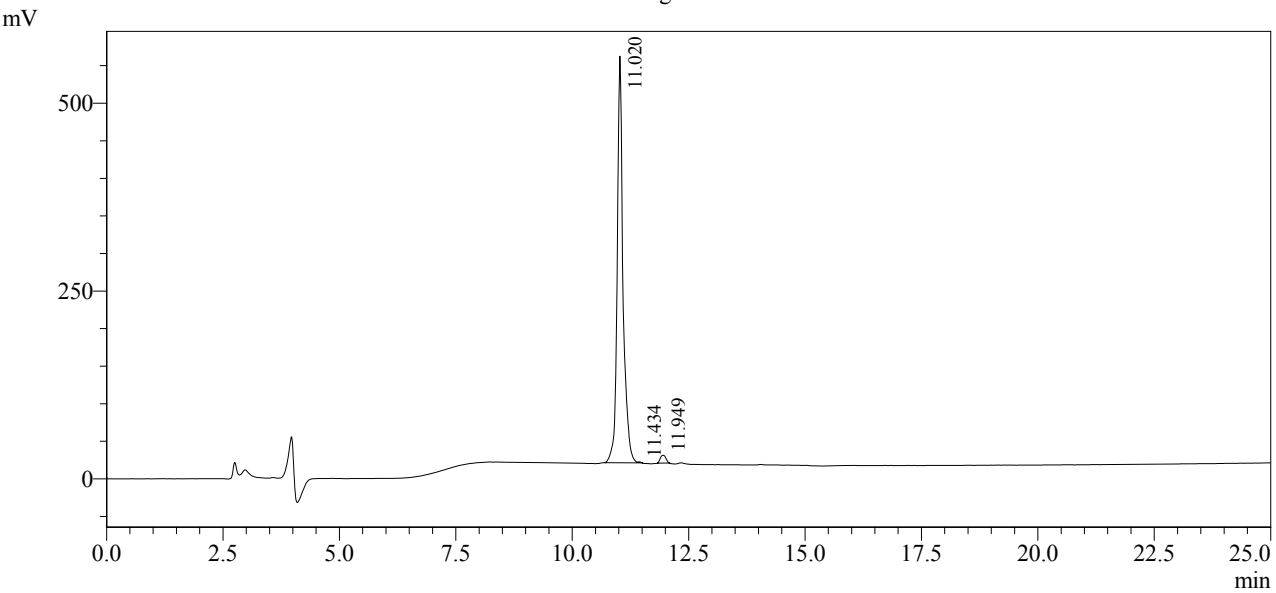

1 Det.A Ch1 / 220nm

Peak Table

Detector A Ch1 220nm

Peak#	Ret. Time	Area	Height	Area %
1	11.020	4698610	541065	98.071
2	11.434	5083	1202	0.106
3	11.949	87344	10268	1.823
Total		4791038	552534	100.000

Sample Name :H4(1-24)K12acK20ac
Sample ID :U6685DL060-7
Time Processed : 11:05:08
Month-Day-Year Processed :12/19/2018

Pump A : 0.065% trifluoroacetic in 100% water (v/v)
Pump B : 0.05% trifluoroacetic in 100% acetonitrile (v/v)
Total Flow:1 ml/min
Wavelength:220 nm
<<LC Time Program>>

Time	Module	Command	Value
0.01	Pumps	Solvent B Conc.	5
25.00	Pumps	Solvent B Conc.	65
25.01	Pumps	Solvent B Conc.	95
27.00	Pumps	Solvent B Conc.	95
27.01	Pumps	Solvent B Conc.	5
33.00	Pumps	Solvent B Conc.	5
33.01	Controller	Stop	

<<Column Performance>>
<Detector A>
Column : Inertsil ODS-3 4.6 x 250 mm
Equipment:ZJ17010507

<Chromatogram>

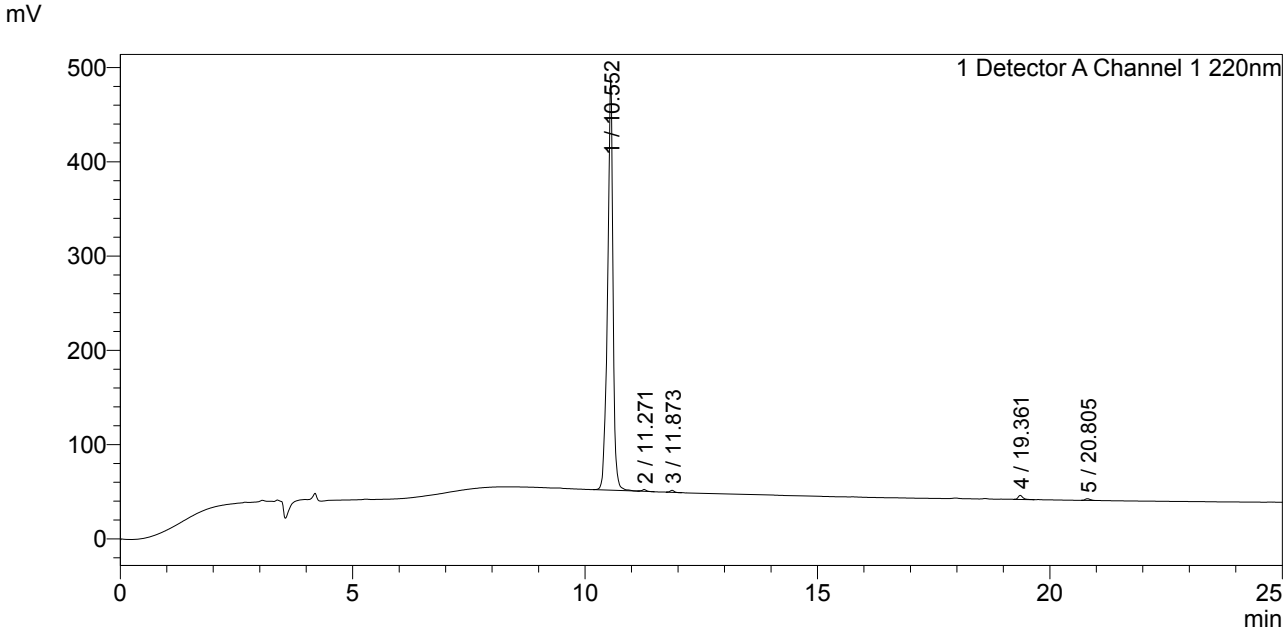

<Peak Table>

Detector A Channel 1 220nm

Peak#	Ret. Time	Area	Height	Area%
1	10.552	3501096	435014	98.078
2	11.271	11886	1941	0.333
3	11.873	12751	2191	0.357
4	19.361	29777	4294	0.834
5	20.805	14210	1883	0.398
Total		3569720	445323	100.000

Sample Name :H4K5acK12ac (1-15)
Sample ID :U344SGB120-15
Time Processed :4:45:02 PM
Month-Day-Year Processed :02/23/2021

Pump A : 0.065% trifluoroacetic in 100% water (v/v)
Pump B : 0.05% trifluoroacetic in 100% acetonitrile (v/v)
Total Flow:1 ml/min
Wavelength:220 nm
<<LC Time Program>>

Time	Module	Command	Value
0.01	Pumps	Pump A B.Conc	5
25.00	Pumps	Pump A B.Conc	65
25.01	Pumps	Pump A B.Conc	95
27.00	Pumps	Pump A B.Conc	95
27.01	Pumps	Pump A B.Conc	5
35.00	Pumps	Pump A B.Conc	5
35.01	Controller	Stop	

<<Column Performance>>
<Detector A>
Column :Inertsil ODS-3 4.6 x 250 mm
Equipment: SS-CM-0286

<Chromatogram>

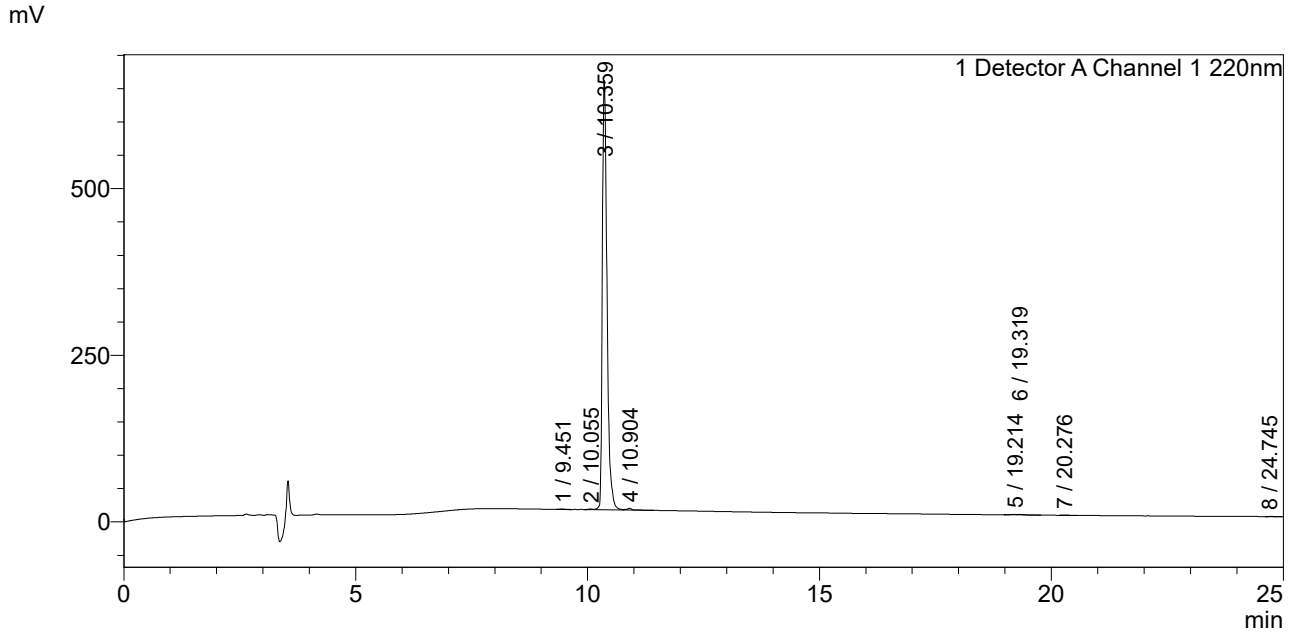

<Peak Table>

Detector A Channel 1 220nm

Peak#	Ret. Time	Area	Height	Area%
1	9.451	5531	848	0.120
2	10.055	6649	897	0.145
3	10.359	4546051	643982	98.830
4	10.904	22164	2774	0.482
5	19.214	7717	825	0.168
6	19.319	6693	957	0.146
7	20.276	3281	397	0.071
8	24.745	1785	224	0.039
Total		4599872	650903	100.000

Sample Name :H4(1-24)K5acK12acK16ac
Sample ID :U8184DL060-1
Time Processed : 20:34:34
Month-Day-Year Processed :12/18/2018

Pump A : 0.065% trifluoroacetic in 100% water (v/v)
Pump B : 0.05% trifluoroacetic in 100% acetonitrile (v/v)
Total Flow:1 ml/min
Wavelength:220 nm
<<LC Time Program>>

Time	Module	Command	Value
0.01	Pumps	Pump A B.Conc	5
25.00	Pumps	Pump A B.Conc	65
25.01	Pumps	Pump A B.Conc	95
32.00	Pumps	Pump A B.Conc	95
32.01	Pumps	Pump A B.Conc	5
40.00	Pumps	Pump A B.Conc	5
40.00	Controller	Stop	

<<Column Performance>>
<Detector A>
Column : Inertsil ODS-3 4.6 x 250 mm
Equipment:ZJ17010507

<Chromatogram>

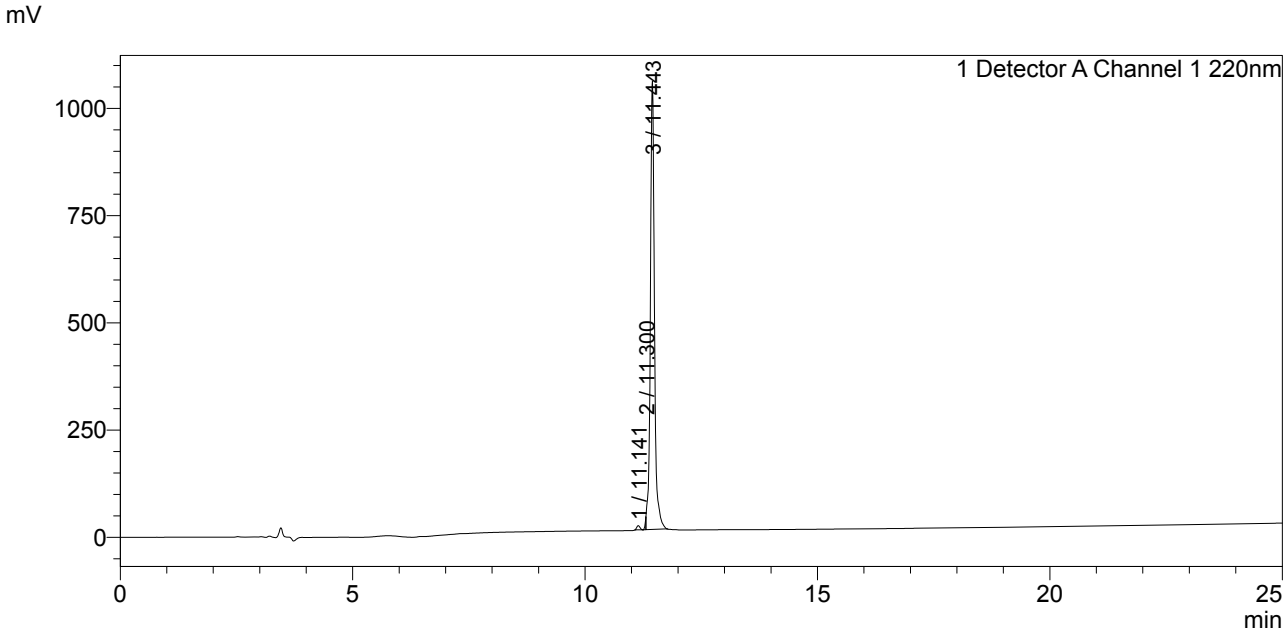

<Peak Table>

Detector A Channel 1 220nm

Peak#	Ret. Time	Area	Height	Area%
1	11.141	46339	9761	0.713
2	11.300	39155	20761	0.603
3	11.443	6410371	1045483	98.684
Total		6495865	1076005	100.000

Sample Name :H4K5acK8acK12ac (1-24)
Sample ID :U344SGB120-3
Time Processed :3:54:45 AM
Month-Day-Year Processed :03/06/2021

Pump A : 0.065% trifluoroacetic in 100% water (v/v)
Pump B : 0.05% trifluoroacetic in 100% acetonitrile (v/v)
Total Flow:1 ml/min
Wavelength:220 nm
<<LC Time Program>>

Time	Module	Command	Value
0.01	Pumps	B.Conc	5
25.00	Pumps	B.Conc	65
25.01	Pumps	B.Conc	95
27.00	Pumps	B.Conc	95
27.01	Pumps	B.Conc	5
35.00	Pumps	B.Conc	5
35.01	Controller	Stop	

<<Column Performance>>
<Detector A>
Column :Inertsil ODS-3 4.6 x 250 mm
Equipment: GK11010009

<Chromatogram>

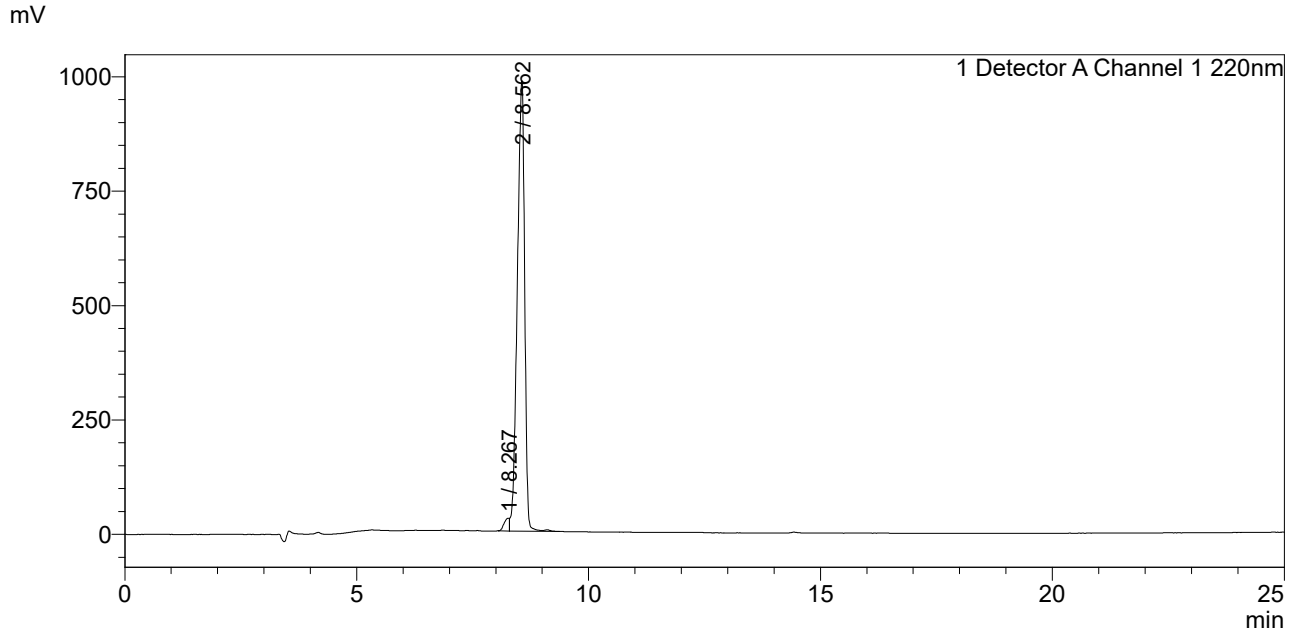

<Peak Table>

Detector A Channel 1 220nm

Peak#	Ret. Time	Area	Height	Area%
1	8.267	215155	27992	1.951
2	8.562	10815202	984366	98.049
Total		11030357	1012357	100.000

Sample Name : H4K8acK12acK16ac (1-24)
Sample ID : U344SGB120-5
Time Processed : 15:04:56
Month-Day-Year Processed : 02/25/2021

Pump A : 0.065% trifluoroacetic in 100% water (v/v)
Pump B : 0.05% trifluoroacetic in 100% acetonitrile (v/v)
Total Flow:1 ml/min
Wavelength:220 nm

Time	Module	Command	Value
0.01	Pumps	B.Conc	5
25.00	Pumps	B.Conc	65
25.01	Pumps	B.Conc	95
32.00	Pumps	B.Conc	95
32.01	Pumps	B.Conc	5
40.00	Pumps	B.Conc	5
60.00	Controller	Stop	

<<Column Performance>>
<Detector A>
Column : Inertsil ODS-3 4.6 x 250 mm
Equipment: GK11010017

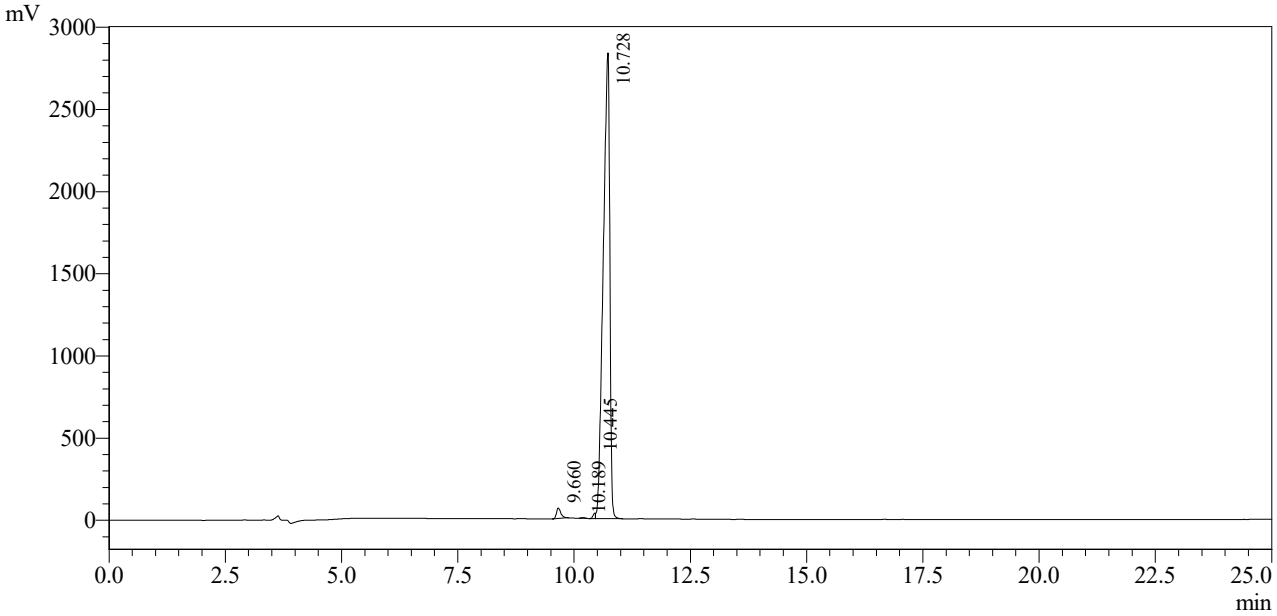

1 Detector A Channel 1 / 220nm

Peak Table

Detector A Channel 1 220nm

Peak#	Ret. Time	Area	Height	Area %
1	9.660	410851	63247	1.451
2	10.189	19101	4432	0.067
3	10.445	113720	32133	0.402
4	10.728	27773613	2833803	98.080
Total		28317287	2933615	100.000

Sample Name : H4K8acK12acK16ac (1-24)
Sample ID : U344SGB120-5
Time Processed : 15:04:56
Month-Day-Year Processed : 02/25/2021

Pump A : 0.065% trifluoroacetic in 100% water (v/v)
Pump B : 0.05% trifluoroacetic in 100% acetonitrile (v/v)
Total Flow:1 ml/min
Wavelength:220 nm

Time	Module	Command	Value
0.01	Pumps	B.Conc	5
25.00	Pumps	B.Conc	65
25.01	Pumps	B.Conc	95
32.00	Pumps	B.Conc	95
32.01	Pumps	B.Conc	5
40.00	Pumps	B.Conc	5
60.00	Controller	Stop	

<<Column Performance>>
<Detector A>
Column : Inertsil ODS-3 4.6 x 250 mm
Equipment: GK11010017

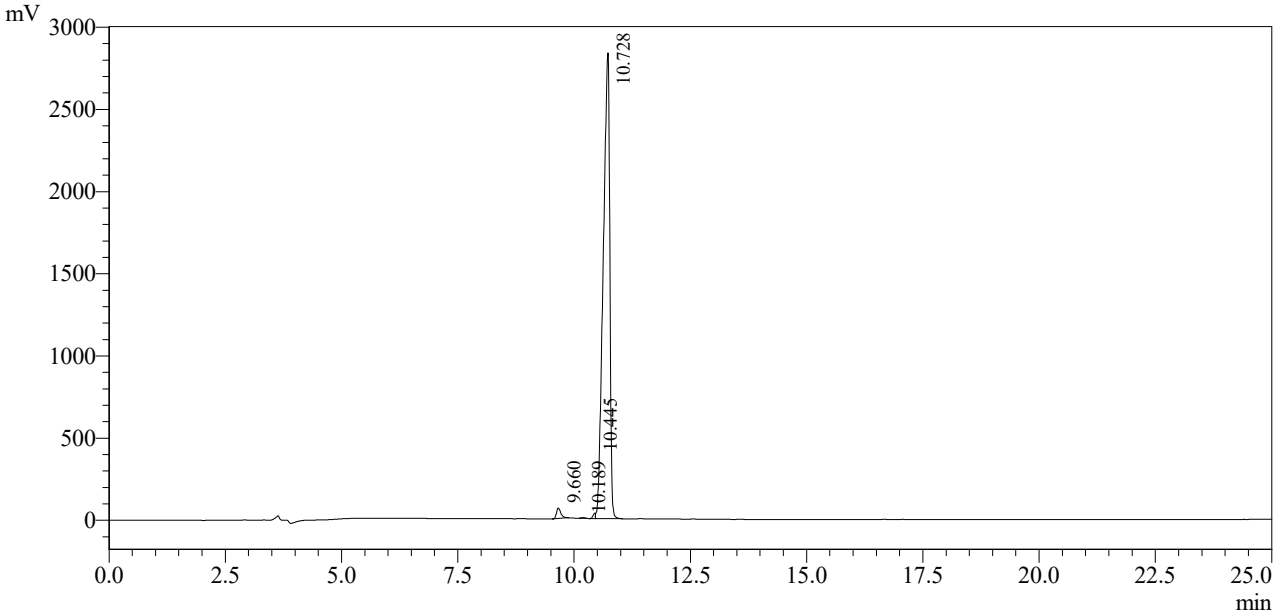

1 Detector A Channel 1 / 220nm

Peak Table

Detector A Channel 1 220nm

Peak#	Ret. Time	Area	Height	Area %
1	9.660	410851	63247	1.451
2	10.189	19101	4432	0.067
3	10.445	113720	32133	0.402
4	10.728	27773613	2833803	98.080
Total		28317287	2933615	100.000

Sample Name : H4 (1-24)K5acK8ac12acK16ac
Sample ID : U512SGJ190-1
Time Processed : 3:57:50 PM
Month-Day-Year Processed : 10/24/2021

Pump A : 0.065% trifluoroacetic in 100% water (v/v)
Pump B : 0.05% trifluoroacetic in 100% acetonitrile (v/v)
Total Flow:1 ml/min
Wavelength:220 nm

Time	Module	Command	Value
0.01	Pumps	B.Conc	5
25.00	Pumps	B.Conc	65
25.01	Pumps	B.Conc	95
32.00	Pumps	B.Conc	95
32.01	Pumps	B.Conc	5
40.00	Pumps	B.Conc	5
40.01	Controller	Stop	

<<Column Performance>>
<Detector A>
Column : Inertsil ODS-3 4.6 x 250 mm
Equipment: GK11010017

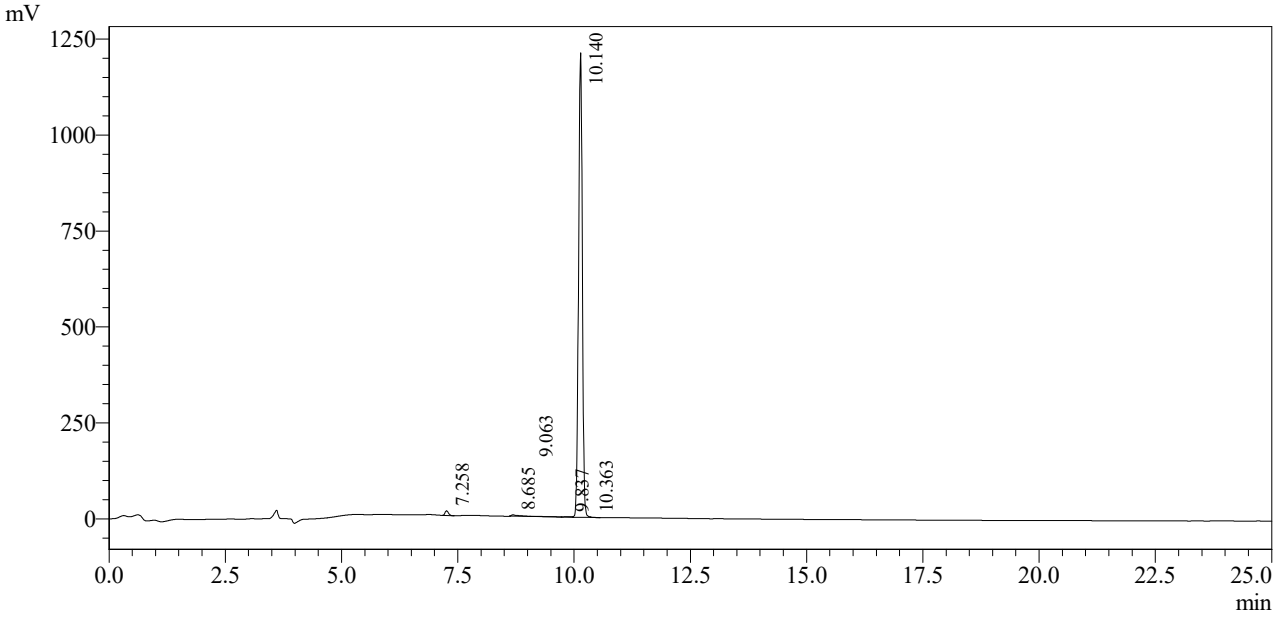

1 Detector A Channel 1 / 220nm

Peak Table

Detector A Channel 1 220nm

Peak#	Ret. Time	Area	Height	Area %
1	7.258	61408	12231	0.887
2	8.685	40626	3623	0.587
3	9.063	11990	388	0.173
4	9.837	11612	1059	0.168
5	10.140	6790417	1210014	98.136
6	10.363	3358	1021	0.049
Total		6919411	1228337	100.000

Sample Name : H4R3me2aK5ac 1-24
Sample ID : U5293GC180-3
Time Processed : 9:43:30 AM
Month-Day-Year Processed : 04/12/2021

Pump A : 0.065% trifluoroacetic in 100% water (v/v)
Pump B : 0.05% trifluoroacetic in 100% acetonitrile (v/v)
Total Flow:1 ml/min
Wavelength:220 nm

Time	Module	Command	Value
0.01	Pumps	Pump A B.Conc	0
25.00	Pumps	Pump A B.Conc	50
25.01	Pumps	Pump A B.Conc	95
32.00	Pumps	Pump A B.Conc	95
32.01	Pumps	Pump A B.Conc	0
40.00	Pumps	Pump A B.Conc	0
45.00	Controller	Stop	

<<Column Performance>>
<Detector A>
Column : Inertsil ODS-3 4.6 x 250 mm
Equipment: GK11010017

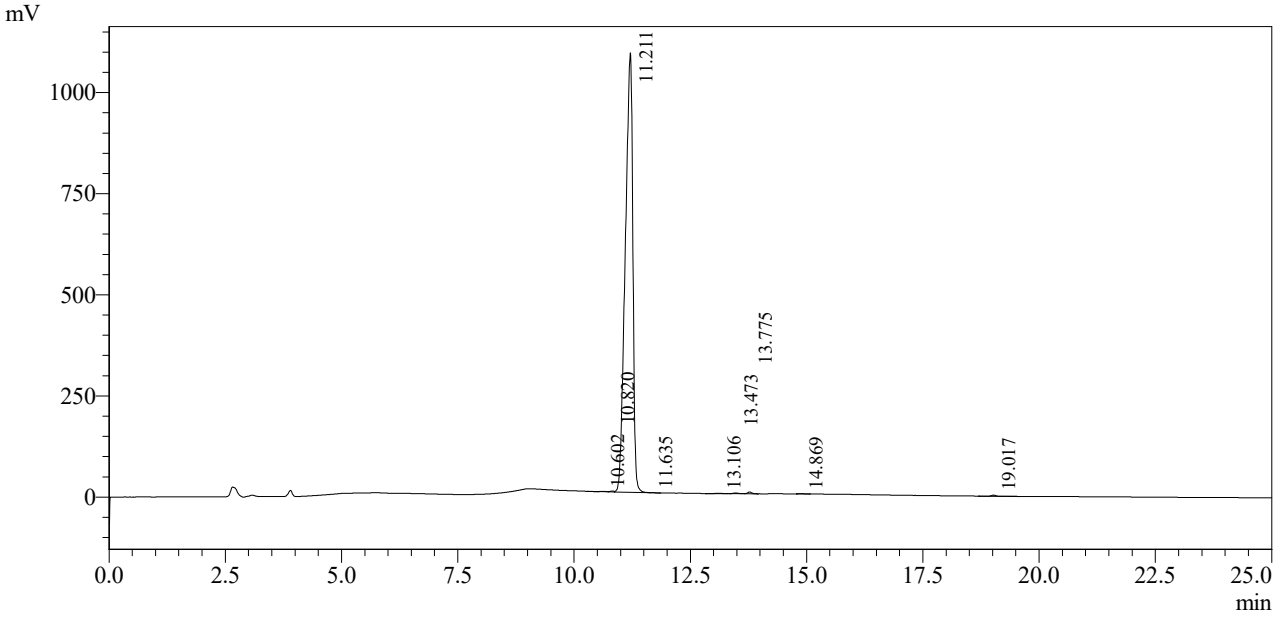

1 Detector A Channel 1 / 220nm

Peak Table

Detector A Channel 1 220nm

Peak#	Ret. Time	Area	Height	Area %
1	10.602	2939	965	0.024
2	10.820	11935	2081	0.097
3	11.211	12213408	1086465	99.302
4	11.635	2236	425	0.018
5	13.106	6573	801	0.053
6	13.473	13335	1788	0.108
7	13.775	25627	4257	0.208
8	14.869	7027	975	0.057
9	19.017	16158	2779	0.131
Total		12299237	1100537	100.000

Sample Name :H4(1-24)K5acK8me1K12ac
Sample ID :U8184DL060-3
Time Processed : 21:15:17
Month-Day-Year Processed :12/18/2018

Pump A : 0.065% trifluoroacetic in 100% water (v/v)
Pump B : 0.05% trifluoroacetic in 100% acetonitrile (v/v)
Total Flow:1 ml/min
Wavelength:220 nm
<<LC Time Program>>

Time	Module	Command	Value
0.01	Pumps	Pump A B.Conc	5
25.00	Pumps	Pump A B.Conc	65
25.01	Pumps	Pump A B.Conc	95
31.00	Pumps	Pump A B.Conc	95
31.01	Pumps	Pump A B.Conc	5
40.00	Pumps	Pump A B.Conc	5
40.00	Controller	Stop	

<<Column Performance>>
<Detector A>
Column : Inertsil ODS-3 4.6 x 250 mm
Equipment:ZJ17010507

<Chromatogram>

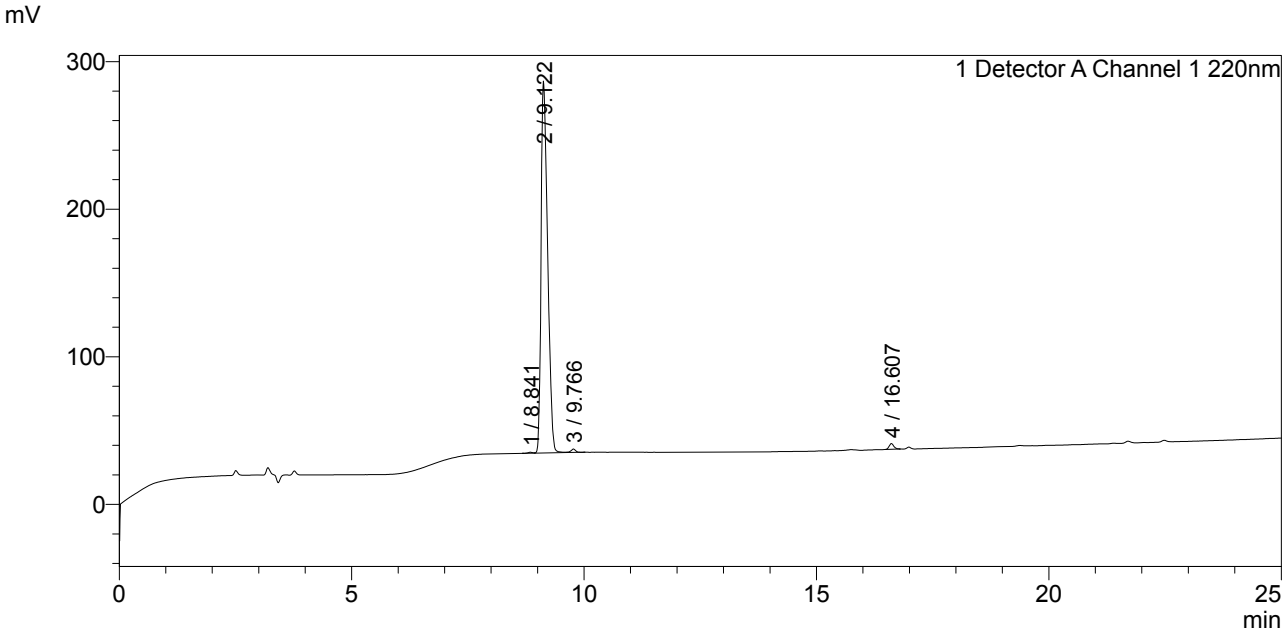

<Peak Table>

Detector A Channel 1 220nm

Peak#	Ret. Time	Area	Height	Area%
1	8.841	4589	679	0.184
2	9.122	2444872	251995	98.101
3	9.766	15880	2297	0.637
4	16.607	26868	3895	1.078
Total		2492209	258866	100.000

Sample Name :H4K5acK8me1K12acK16ac (1-24)
Sample ID :U7543GC050-25
Time Processed : 15:29:22
Month-Day-Year Processed : 04/13/2021

Pump A : 0.065% trifluoroacetic in 100% water (v/v)
Pump B : 0.05% trifluoroacetic in 100% acetonitrile (v/v)
Total Flow:1 ml/min
Wavelength:220 nm

Time	Module	Command	Value
0.01	Pumps	B.Conc	5
25.00	Pumps	B.Conc	65
25.01	Pumps	B.Conc	95
31.00	Pumps	B.Conc	95
31.01	Pumps	B.Conc	5
40.00	Pumps	B.Conc	5
40.01	Controller	Stop	

<<Column Performance>>
<Detector A>
Column : Inertsil ODS-3 4.6 x 250 mm
Equipment: GK11010017

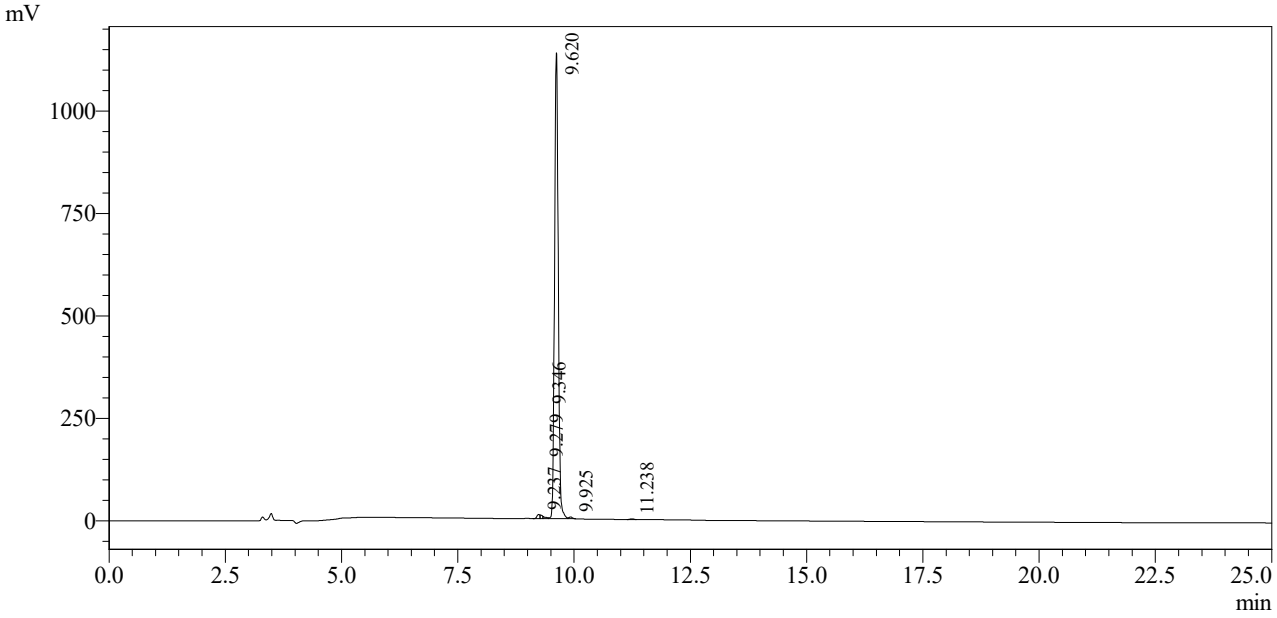

1 Detector A Channel 1 / 220nm

Peak Table

Detector A Channel 1 220nm

Peak#	Ret. Time	Area	Height	Area %
1	9.237	45884	10231	0.706
2	9.279	30274	8859	0.466
3	9.346	22518	4695	0.346
4	9.620	6373427	1137317	98.014
5	9.925	22150	4565	0.341
6	11.238	8327	1532	0.128
Total		6502579	1167199	100.000

Sample Name : H4 (1-24)K16acK20me3
Sample ID : U512SGJ190-7
Time Processed :21:32:30
Month-Day-Year Processed :10/28/2021

Pump A : 0.065% trifluoroacetic in 100% water (v/v)
Pump B : 0.05% trifluoroacetic in 100% acetonitrile (v/v)
Total Flow:1 ml/min
Wavelength:220 nm

Time	Module	Command	Value
0.01	Pumps	B.Conc	5
25.00	Pumps	B.Conc	65
25.01	Pumps	B.Conc	95
27.00	Pumps	B.Conc	95
27.01	Pumps	B.Conc	5
35.00	Pumps	B.Conc	5
35.01	Controller	Stop	

<<Column Performance>>
<Detector A>
Column : Inertsil ODS-3 4.6 x 250 mm

Chromatogram

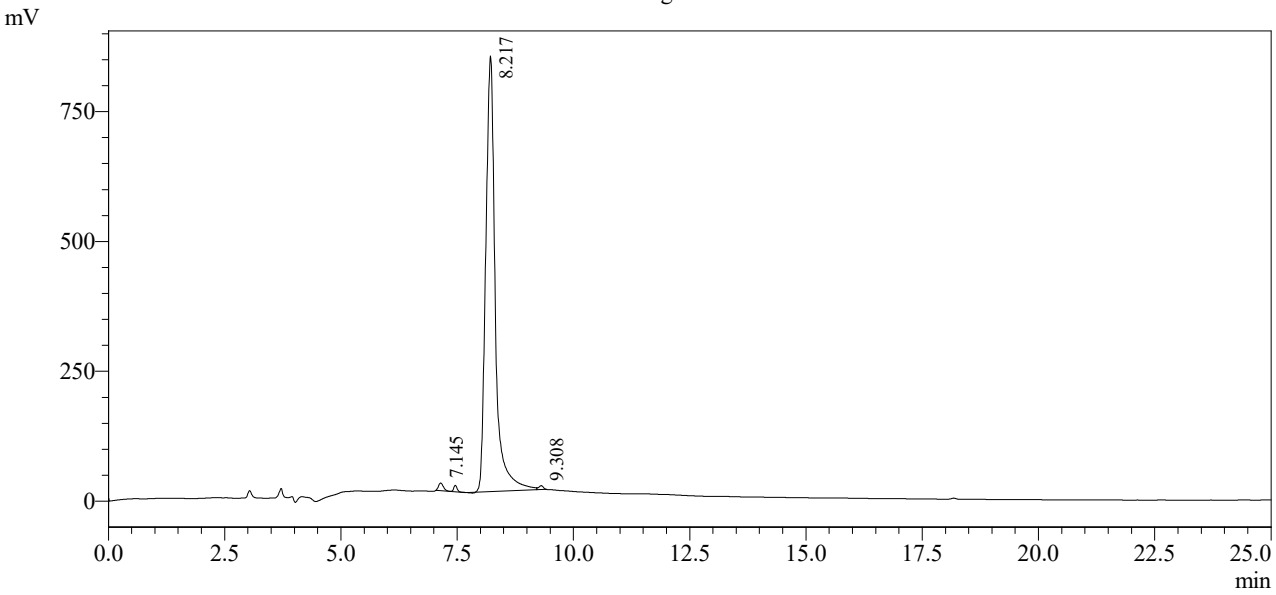

1 Detector A Channel 1 / 220nm

Peak Table

Detector A Channel 1 220nm

Peak#	Ret. Time	Area	Height	Area %
1	7.145	169223	14739	1.391
2	8.217	11949534	838903	98.206
3	9.308	49118	7373	0.404
Total		12167875	861015	100.000

Sample Name :H4 1-24)S1phK5ac
Sample ID :U3003IC220-5
Time Processed :10:18:24
Month-Day-Year Processed :04/11/2023

Pump A : 0.065% trifluoroacetic in 100% water (v/v)
Pump B : 0.05% trifluoroacetic in 100% acetonitrile (v/v)
Total Flow:1 ml/min
Wavelength:220 nm
<<LC Time Program>>

Time	Module	Command	Value
0.01	Pumps	B.Conc	5
25.00	Pumps	B.Conc	65
25.01	Pumps	B.Conc	95
27.00	Pumps	B.Conc	95
27.01	Pumps	B.Conc	5
35.00	Pumps	B.Conc	5
35.01	Controller	Stop	

<<Column Performance>>
<Detector A>
Column :Inertsil ODS-SP 4.6 x 250 mm
Equipment: GR11010440

<Chromatogram>

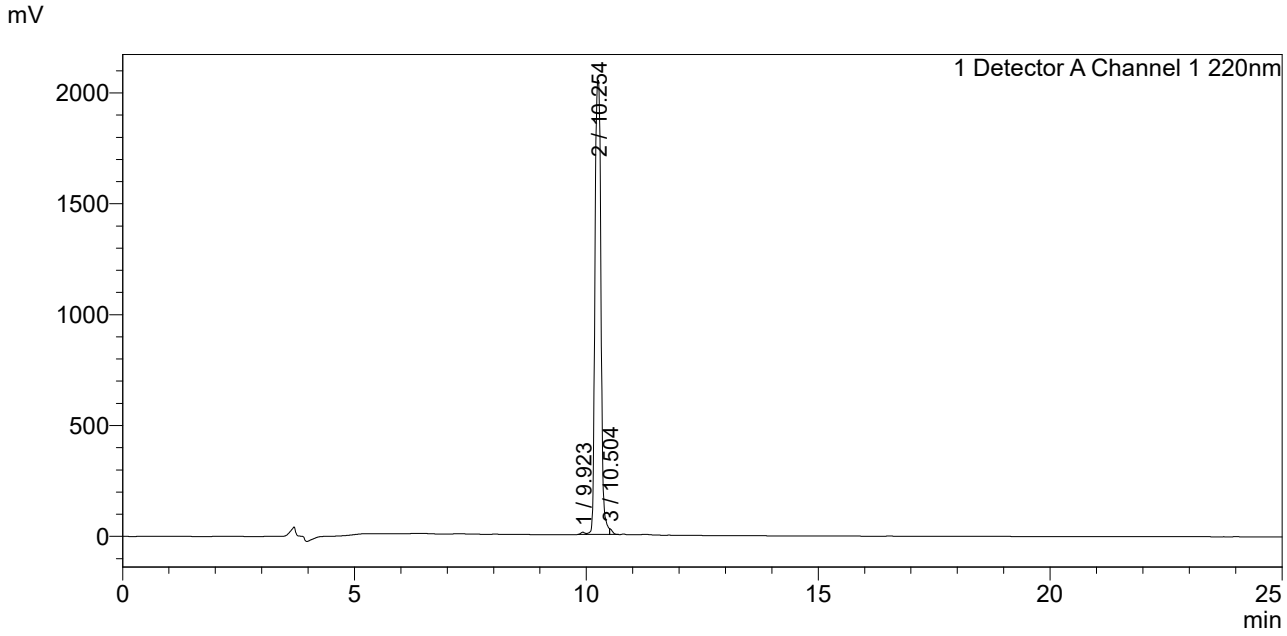

<Peak Table>

Detector A Channel 1 220nm

Peak#	Ret. Time	Area	Height	Area%
1	9.923	61902	10091	0.338
2	10.254	18157245	2048570	99.122
3	10.504	98852	26651	0.540
Total		18317999	2085312	100.000

Sample Name:H4K5ac (1-15)
Sample ID :U2819EJ240-1
Time Processed: 19:48:19
Month-Day-Year Processed :10/30/2019

Pump A : 0.065% trifluoroacetic in 100% water (v/v)
Pump B : 0.05% trifluoroacetic in 100% acetonitrile (v/v)
Total Flow:1 ml/min
Wavelength:220 nm
<<LC Time Program>>

Time	Module	Command	Value
0.01	Pumps	Pump A B.Conc	5
25.00	Pumps	Pump A B.Conc	65
25.01	Pumps	Pump A B.Conc	95
31.00	Pumps	Pump A B.Conc	95
31.01	Pumps	Pump A B.Conc	5
40.00	Pumps	Pump A B.Conc	5
40.01	Controller	Stop	

<<Column Performance>>
<Detector A>
Column : AlltimaTM C18 4.6 x 250 mm
Equipment:ZJ19010324

<Chromatogram>

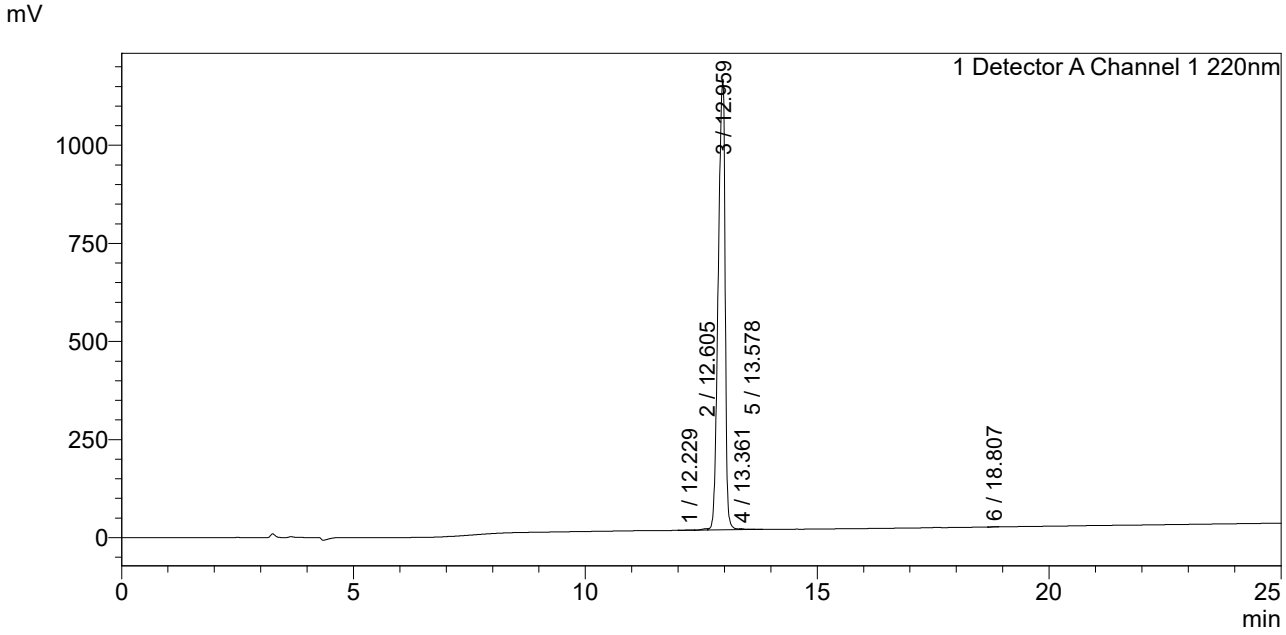

<Peak Table>

Detector A Channel 1 220nm

Peak#	Ret. Time	Area	Height	Area%
1	12.229	11546	1144	0.097
2	12.605	33865	3648	0.286
3	12.959	11807221	1149152	99.563
4	13.361	2802	621	0.024
5	13.578	1550	289	0.013
6	18.807	2072	383	0.017
Total		11859057	1155237	100.000

Sample Name :H4G4DK5ac (res 1-15)
Sample ID :U4531FI020-7
Time Processed :18:26:54
Month-Day-Year Processed :09/18/2020

Pump A : 0.065% trifluoroacetic in 100% water (v/v)
Pump B : 0.05% trifluoroacetic in 100% acetonitrile (v/v)
Total Flow:1 ml/min
Wavelength:220 nm
<<LC Time Program>>

Time	Module	Command	Value
0.01	Pumps	Solvent B Conc.	15
25.00	Pumps	Solvent B Conc.	75
25.01	Pumps	Solvent B Conc.	95
30.00	Pumps	Solvent B Conc.	95
30.01	Pumps	Solvent B Conc.	15
41.00	Pumps	Solvent B Conc.	15
41.00	Controller	Stop	

<<Column Performance>>
<Detector A>
Column :Inertsil ODS-3 4.6 x 250 mm
Equipment: ZJ19010324

<Chromatogram>

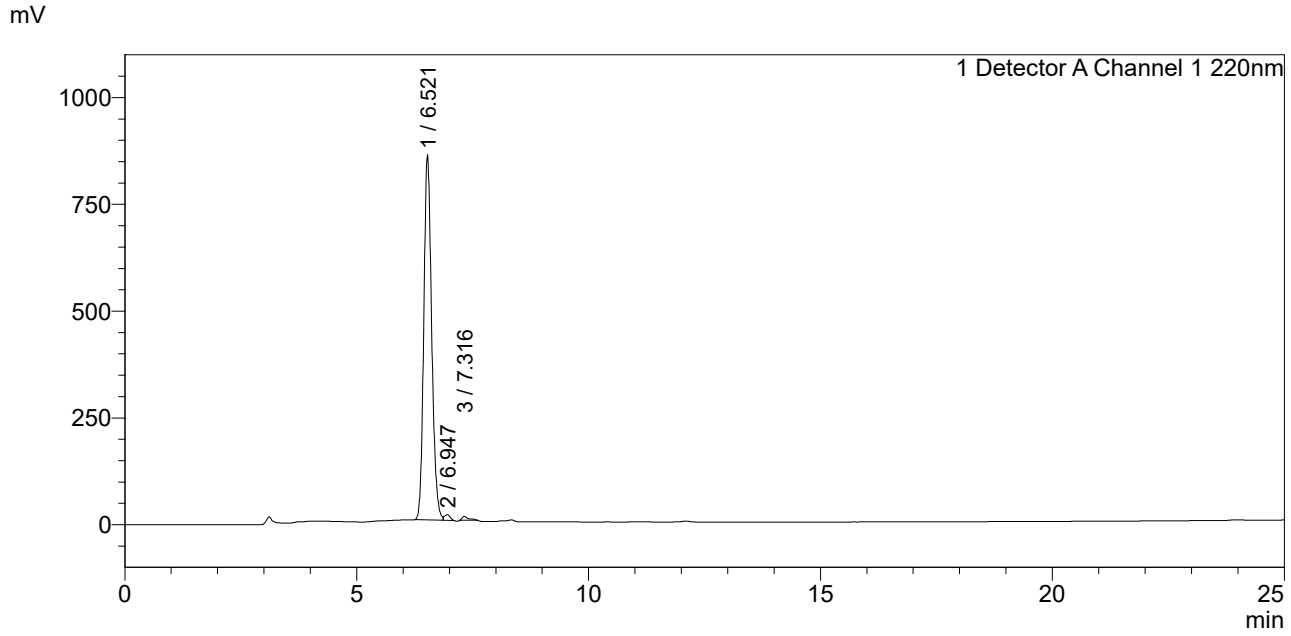

<Peak Table>

Detector A Channel 1 220nm

Peak#	Ret. Time	Area	Height	Area%
1	6.521	10082362	855137	98.100
2	6.947	108066	13256	1.051
3	7.316	87208	8961	0.849
Total		10277636	877354	100.000

Sample Name :H4G4SK5ac (res 1-15)
Sample ID :U4531FI020-5
Time Processed :6:59:59
Month-Day-Year Processed :08/25/2020

Pump A : 0.065% trifluoroacetic in 100% water (v/v)
Pump B : 0.05% trifluoroacetic in 100% acetonitrile (v/v)
Total Flow:1 ml/min
Wavelength:220 nm
<<LC Time Program>>

Time	Module	Command	Value
0.01	Pumps	Pump A B.Conc	5
25.00	Pumps	Pump A B.Conc	65
25.01	Pumps	Pump A B.Conc	95
27.00	Pumps	Pump A B.Conc	95
27.01	Pumps	Pump A B.Conc	5
35.00	Pumps	Pump A B.Conc	5
35.01	Controller	Stop	

<<Column Performance>>
<Detector A>
Column :Inertsil ODS-3 4.6 x 250 mm
Equipment: ZJ19010324

<Chromatogram>

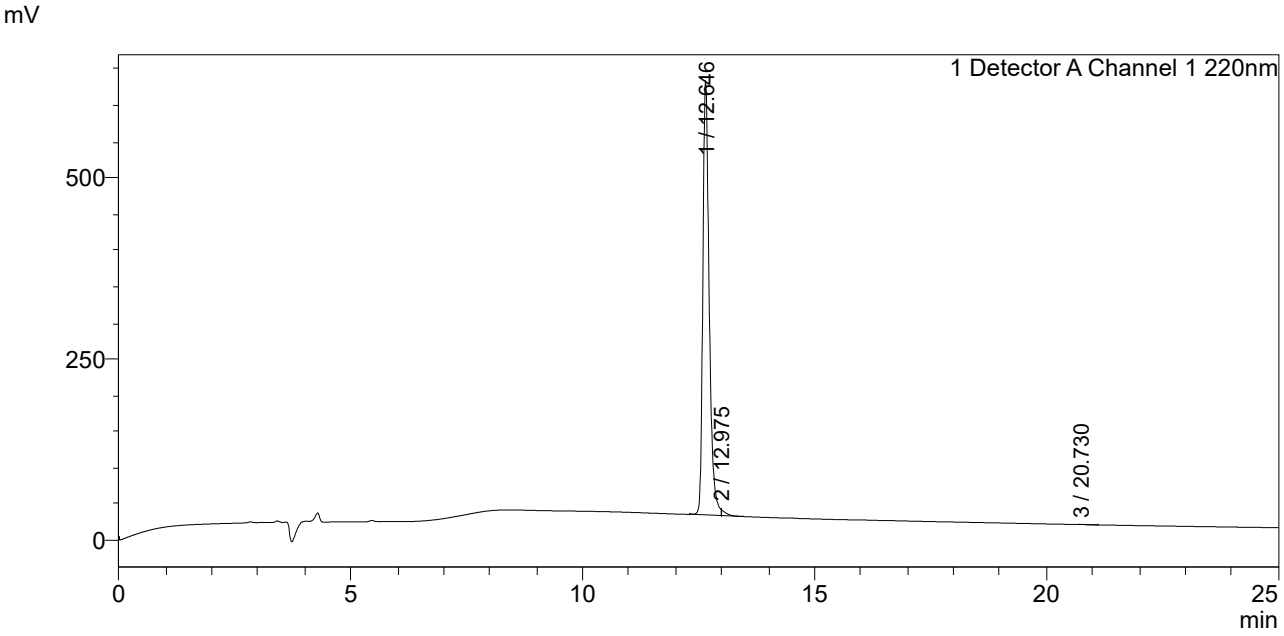

<Peak Table>

Detector A Channel 1 220nm

Peak#	Ret. Time	Area	Height	Area%
1	12.646	5687624	599317	98.874
2	12.975	63647	9084	1.106
3	20.730	1125	46	0.020
Total		5752396	608447	100.000

Sample Name :H4R3CK5ac (res 1-15)
Sample ID :U4531FI020-3
Time Processed :23:47:30
Month-Day-Year Processed :09/05/2020

Pump A : 0.065% trifluoroacetic in 100% water (v/v)
Pump B : 0.05% trifluoroacetic in 100% acetonitrile (v/v)
Total Flow:1 ml/min
Wavelength:220 nm
<<LC Time Program>>

Time	Module	Command	Value
0.01	Pumps	Pump A B.Conc	5
25.00	Pumps	Pump A B.Conc	65
25.01	Pumps	Pump A B.Conc	95
27.00	Pumps	Pump A B.Conc	95
27.01	Pumps	Pump A B.Conc	5
35.00	Pumps	Pump A B.Conc	5
35.01	Controller	Stop	

<<Column Performance>>
<Detector A>
Column :Inertsil ODS-3 4.6 x 250 mm
Equipment: ZJ19010324

<Chromatogram>

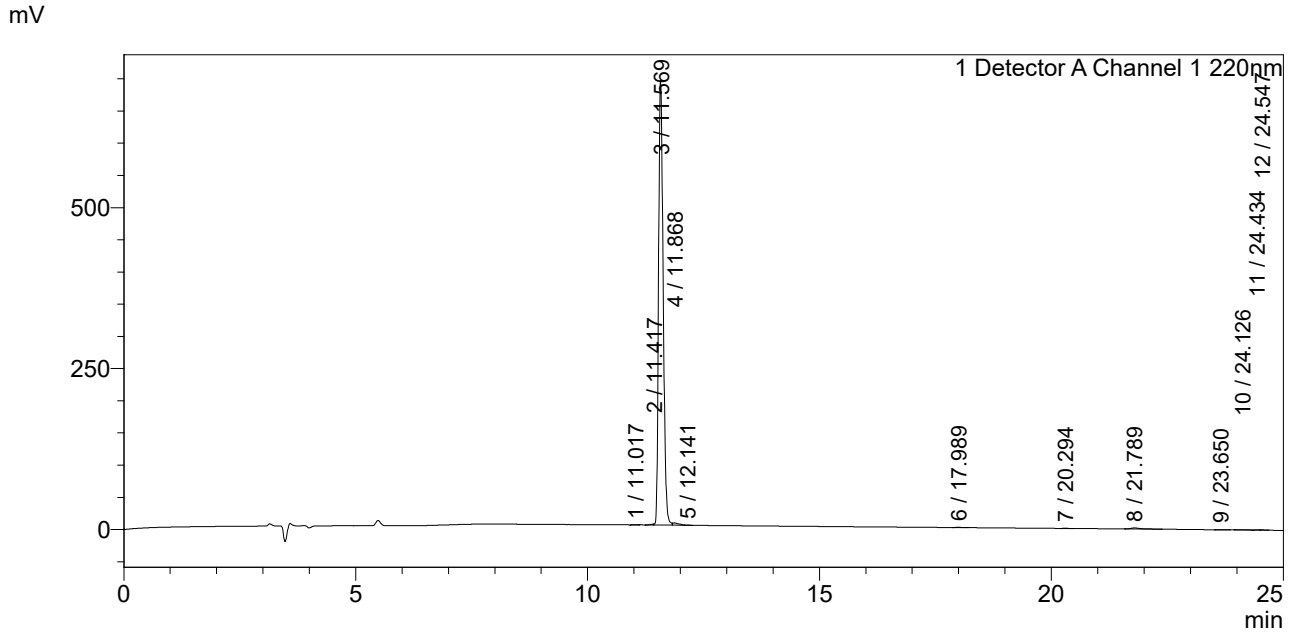

<Peak Table>

Detector A Channel 1 220nm

Peak#	Ret. Time	Area	Height	Area%
1	11.017	1566	283	0.033
2	11.417	6196	1247	0.129
3	11.569	4737527	690405	98.338
4	11.868	32248	3437	0.669
5	12.141	2307	421	0.048
6	17.989	3792	530	0.079
7	20.294	1988	288	0.041
8	21.789	23387	1648	0.485
9	23.650	1676	178	0.035
10	24.126	3855	292	0.080
11	24.434	1376	205	0.029
12	24.547	1686	316	0.035
Total		4817605	699250	100.000

Sample Name :H4S1CK5ac (res 1-15)
Sample ID :U4531FI020-1
Time Processed :16:11:11
Month-Day-Year Processed :09/23/2020

Pump A : 0.065% trifluoroacetic in 100% water (v/v)
Pump B : 0.05% trifluoroacetic in 100% acetonitrile (v/v)
Total Flow:1 ml/min
Wavelength:220 nm

Time	Module	Command	Value
0.01	Pumps	Pump A B.Conc	0
25.00	Pumps	Pump A B.Conc	30
25.01	Pumps	Pump A B.Conc	95
31.00	Pumps	Pump A B.Conc	95
31.01	Pumps	Pump A B.Conc	0
40.00	Pumps	Pump A B.Conc	0
70.01	Controller	Stop	

<<Column Performance>>
<Detector A>
Column : Inertsil ODS-3 4.6 x 250 mm

Chromatogram

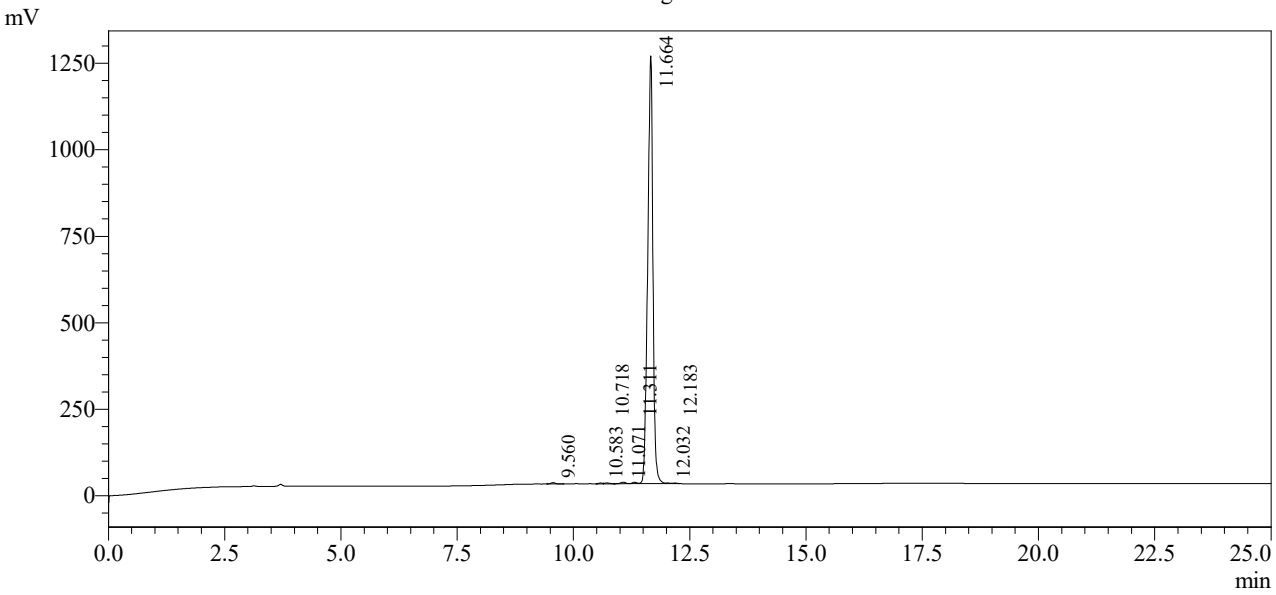

1 Detector A Channel 1 / 220nm

Peak Table

Detector A Channel 1 220nm

Peak#	Ret. Time	Area	Height	Area %
1	9.560	27040	3820	0.276
2	10.583	12542	2236	0.128
3	10.718	17638	2205	0.180
4	11.071	33750	4569	0.345
5	11.311	29608	4459	0.303
6	11.664	9648610	1236259	98.582
7	12.032	10058	1488	0.103
8	12.183	8129	1452	0.083
Total		9787376	1256487	100.000

Sample Name :H2A.X (1-17) unmod
Sample ID :U5313GL230-1
Time Processed :4:19:30 PM
Month-Day-Year Processed :01/14/2022

Pump A : 0.065% trifluoroacetic in 100% water (v/v)
Pump B : 0.05% trifluoroacetic in 100% acetonitrile (v/v)
Total Flow:1 ml/min
Wavelength:220 nm
<<LC Time Program>>

Time	Module	Command	Value
0.01	Pumps	B.Conc	0
5.00	Pumps	B.Conc	0
25.00	Pumps	B.Conc	60
25.01	Pumps	B.Conc	95
27.00	Pumps	B.Conc	95
27.01	Pumps	B.Conc	0
35.00	Pumps	B.Conc	0
35.01	Controller	Stop	

<<Column Performance>>
<Detector A>
Column :Inertsil ODS-3 4.6 x 250 mm
Equipment: ZJ20010139

<Chromatogram>

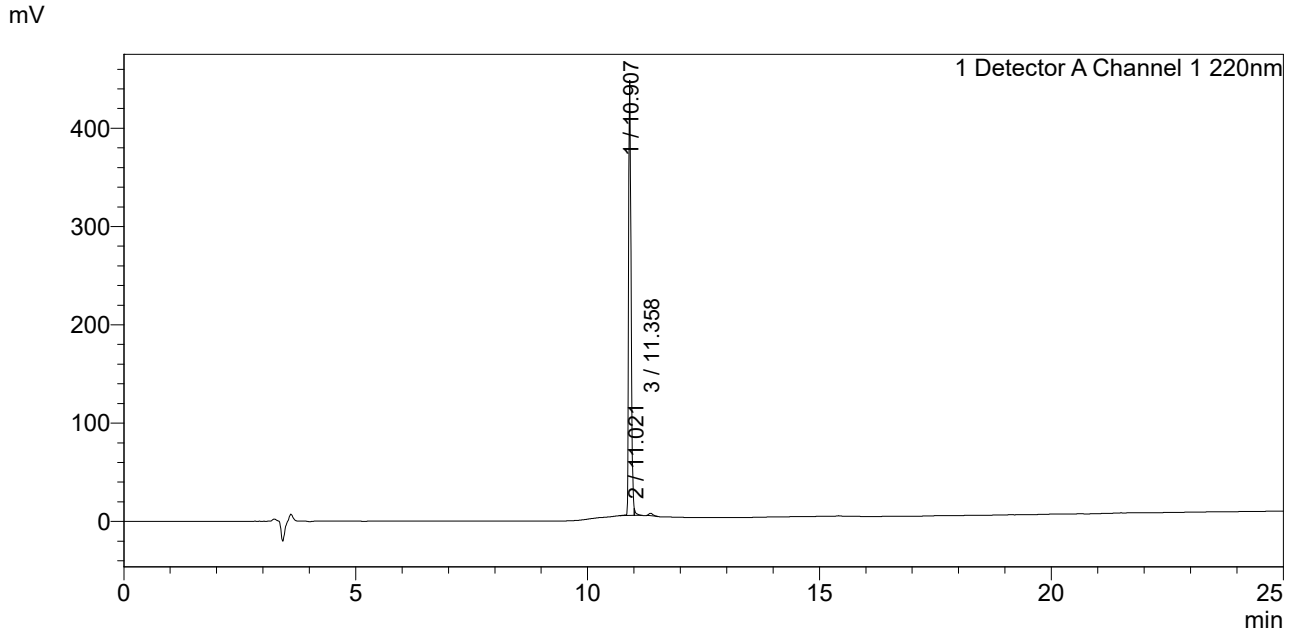

<Peak Table>

Detector A Channel 1 220nm

Peak#	Ret. Time	Area	Height	Area%
1	10.907	1621322	442769	98.377
2	11.021	11531	4910	0.700
3	11.358	15222	2573	0.924
Total		1648075	450253	100.000

Sample Name : H2A.XK9ac (1-17)
Sample ID : U5313GL230-3
Time Processed : 20:17:28
Month-Day-Year Processed : 01/07/2022

Pump A : 0.065% trifluoroacetic in 100% water (v/v)
Pump B : 0.05% trifluoroacetic in 100% acetonitrile (v/v)
Total Flow:1 ml/min
Wavelength:220 nm

Time	Module	Command	Value
0.01	Pumps	B.Conc	5
25.00	Pumps	B.Conc	65
25.01	Pumps	B.Conc	95
27.00	Pumps	B.Conc	95
27.01	Pumps	B.Conc	5
35.00	Pumps	B.Conc	5
35.01	Controller	Stop	

<<Column Performance>>
<Detector A>
Column : Inertsil ODS-3 4.6 x 250 mm
Equipment: GK11010017

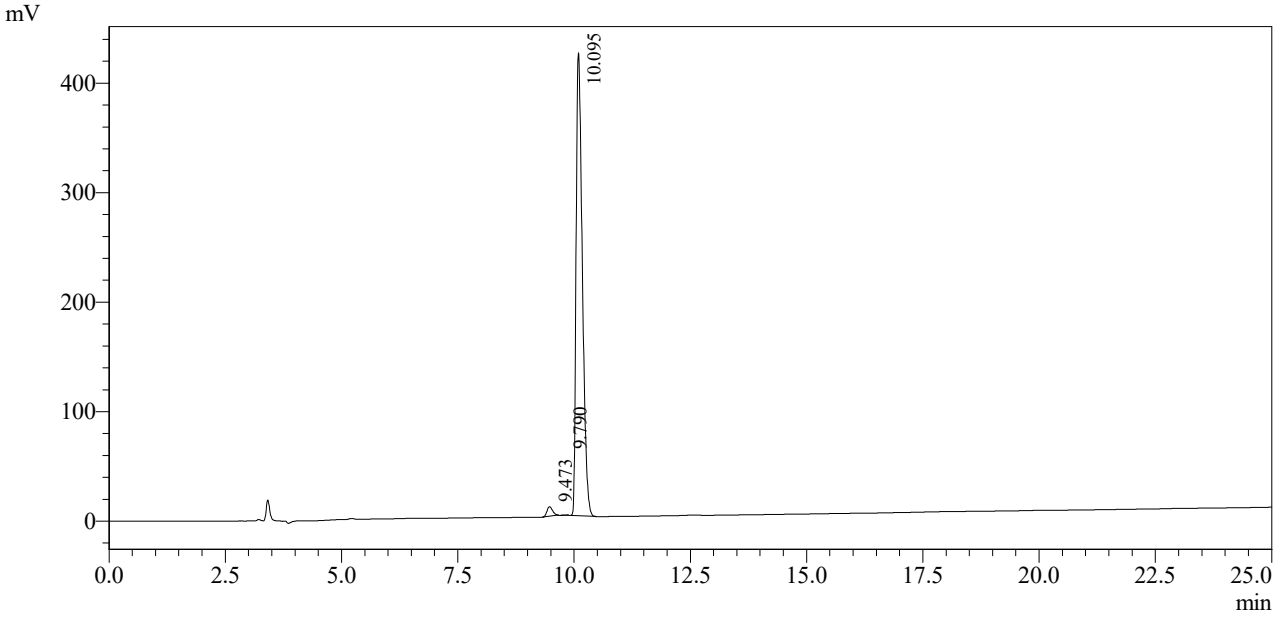

1 Detector A Channel 1 / 220nm

Peak Table

Detector A Channel 1 220nm

Peak#	Ret. Time	Area	Height	Area %
1	9.473	72623	8657	1.803
2	9.790	1030	191	0.026
3	10.095	3953769	422572	98.171
Total		4027422	431420	100.000

Sample Name :H2A.XK5acK9ac (1-17)
Sample ID :U5313GL230-5
Time Processed :12:00:33 AM
Month-Day-Year Processed :01/12/2022

Pump A : 0.065% trifluoroacetic in 100% water (v/v)
Pump B : 0.05% trifluoroacetic in 100% acetonitrile (v/v)
Total Flow:1 ml/min
Wavelength:220 nm
<<LC Time Program>>

Time	Module	Command	Value
0.01	Pumps	B.Conc	5
25.00	Pumps	B.Conc	65
25.01	Pumps	B.Conc	95
27.00	Pumps	B.Conc	95
27.01	Pumps	B.Conc	5
35.00	Pumps	B.Conc	5
35.01	Controller	Stop	

<<Column Performance>>
<Detector A>
Column :Inertsil ODS-SP 4.6 x 250 mm
Equipment: ZJ21010376

<Chromatogram>

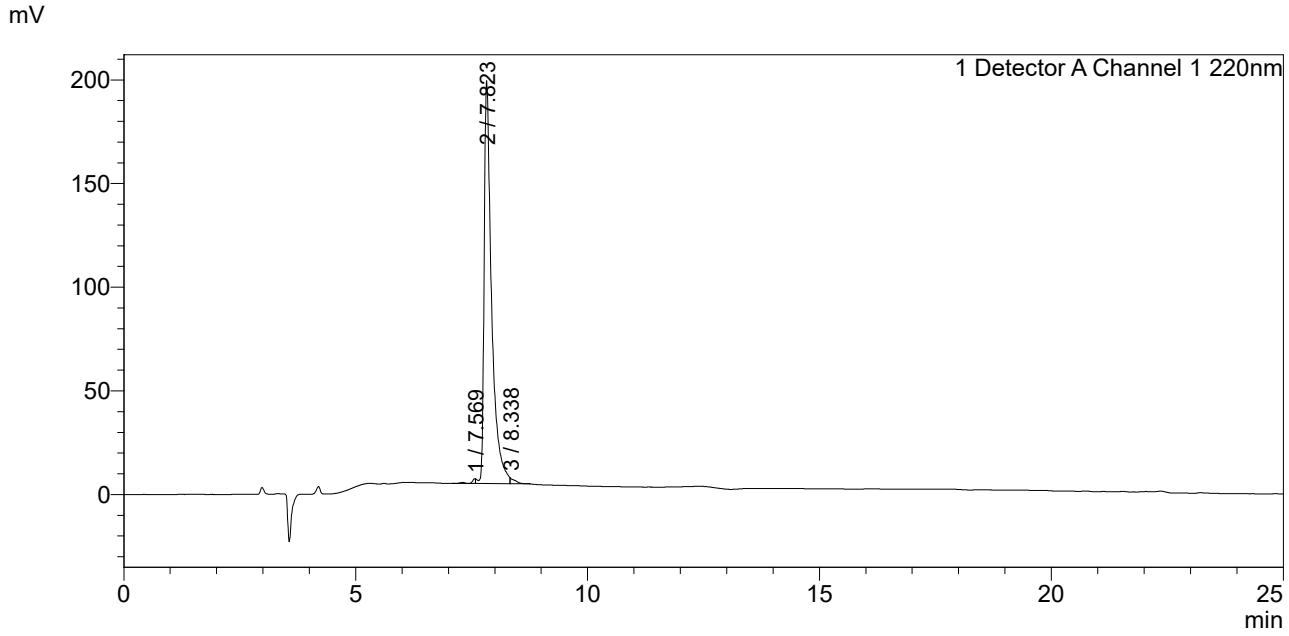

<Peak Table>

Detector A Channel 1 220nm

Peak#	Ret. Time	Area	Height	Area%
1	7.569	13883	2338	0.629
2	7.823	2173618	194420	98.449
3	8.338	20355	2756	0.922
Total		2207855	199513	100.000

Sample Name : H2A.Z unmod (1-15)
Sample ID : U5313GL230-7
Time Processed : 19:35:05
Month-Day-Year Processed : 01/15/2022

Pump A : 0.065% trifluoroacetic in 100% water (v/v)
Pump B : 0.05% trifluoroacetic in 100% acetonitrile (v/v)
Total Flow:1 ml/min
Wavelength:220 nm

Time	Module	Command	Value
0.01	Pumps	B.Conc	5
25.00	Pumps	B.Conc	65
25.01	Pumps	B.Conc	95
27.00	Pumps	B.Conc	95
27.01	Pumps	B.Conc	5
31.00	Pumps	B.Conc	5
31.01	Controller	Stop	

<<Column Performance>>
<Detector A>
Column : Inertsil ODS-3 4.6 x 250 mm
Equipment: GK11010017

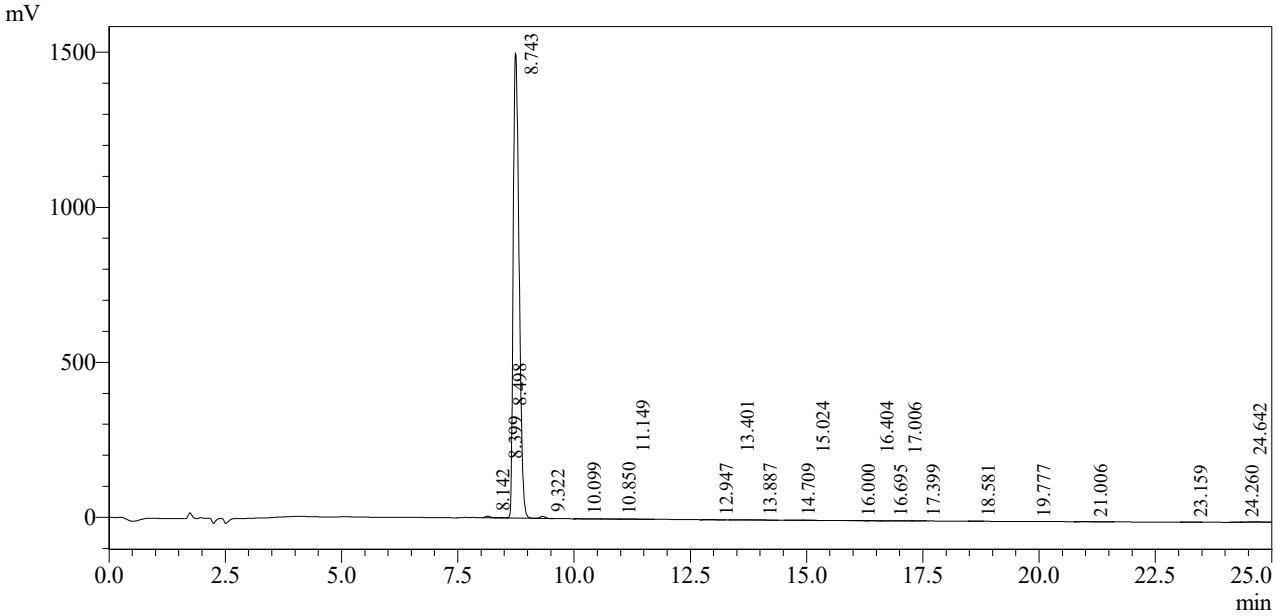

1 Detector A Channel 1 / 220nm

Peak Table

Detector A Channel 1 220nm

Peak#	Ret. Time	Area	Height	Area %
1	8.142	38765	5067	0.288
2	8.399	8199	1143	0.061
3	8.498	8274	1265	0.062
4	8.743	13228812	1500681	98.349
5	9.322	51571	6506	0.383
6	10.099	5716	362	0.042
7	10.850	8760	575	0.065
8	11.149	20079	808	0.149
9	12.947	4938	307	0.037
10	13.401	1197	176	0.009
11	13.887	7835	368	0.058
12	14.709	3539	318	0.026
13	15.024	2153	191	0.016
14	16.000	4952	357	0.037
15	16.404	1615	193	0.012
16	16.695	1069	160	0.008
17	17.006	2397	166	0.018
18	17.399	1734	213	0.013
19	18.581	1222	112	0.009
20	19.777	3225	283	0.024
21	21.006	12497	616	0.093
22	23.159	2636	235	0.020
23	24.260	2007	217	0.015
24	24.642	27681	1243	0.206

Peak#	Ret. Time	Area	Height	Area %
Total		13450875	1521560	100.000

Sample Name : H2A.Z.1.K4ac (res 1-15)
Sample ID : U3243HC210-1
Time Processed :11:44:54
Month-Day-Year Processed :04/28/2022

Pump A : 0.065% trifluoroacetic in 100% water (v/v)
Pump B : 0.05% trifluoroacetic in 100% acetonitrile (v/v)
Total Flow:1 ml/min
Wavelength:220 nm

Time	Module	Command	Value
0.01	Pumps	B.Conc	5
25.00	Pumps	B.Conc	65
25.01	Pumps	B.Conc	95
27.00	Pumps	B.Conc	95
27.01	Pumps	B.Conc	5
35.00	Pumps	B.Conc	5
35.01	Controller	Stop	

<<Column Performance>>
<Detector A>
Column : Inertsil ODS-3 4.6 x 250 mm

Chromatogram

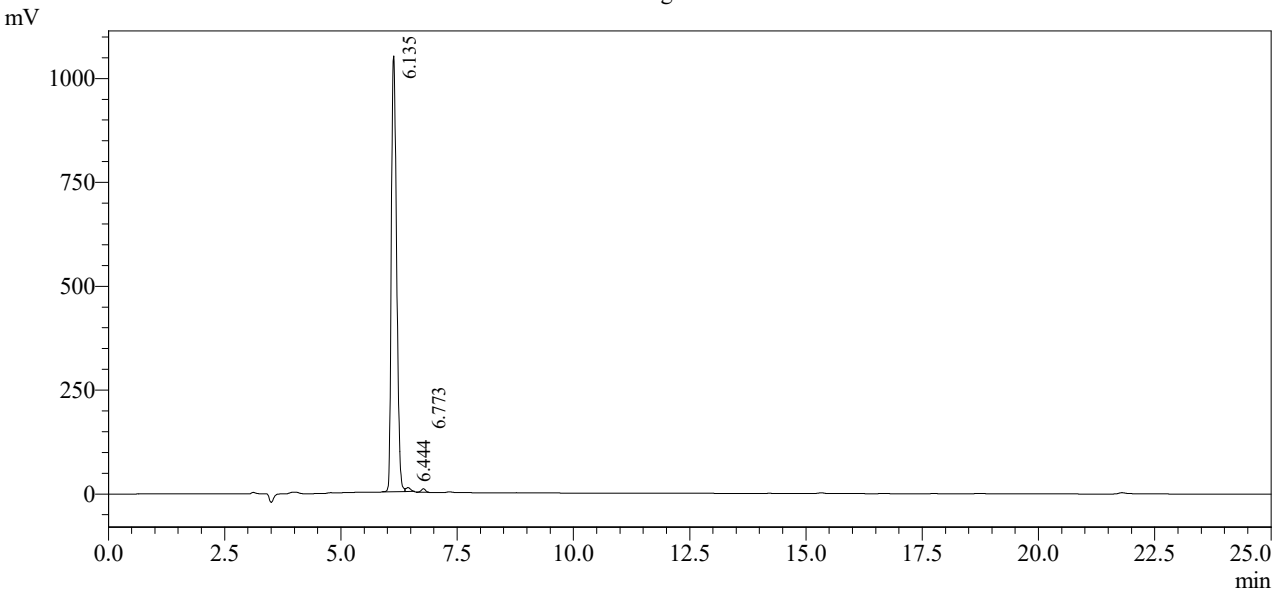

1 Detector A Channel 1 / 220nm

Peak Table

Detector A Channel 1 220nm

Peak#	Ret. Time	Area	Height	Area %
1	6.135	8224258	1028322	98.645
2	6.444	64906	9146	0.778
3	6.773	48100	7963	0.577
Total		8337264	1045431	100.000

Sample Name : H2A.Z K4acK7ac (1-15)
Sample ID : U5313GL230-11
Time Processed : 19:24:38
Month-Day-Year Processed : 01/15/2022

Pump A : 0.065% trifluoroacetic in 100% water (v/v)
Pump B : 0.05% trifluoroacetic in 100% acetonitrile (v/v)
Total Flow:1 ml/min
Wavelength:220 nm

Time	Module	Command	Value
0.01	Pumps	B.Conc	5
25.00	Pumps	B.Conc	65
25.01	Pumps	B.Conc	95
27.00	Pumps	B.Conc	95
27.01	Pumps	B.Conc	5
35.00	Pumps	B.Conc	5
35.01	Controller	Stop	

<<Column Performance>>
<Detector A>
Column : Inertsil ODS-3 4.6 x 250 mm
Equipment: GK11010017

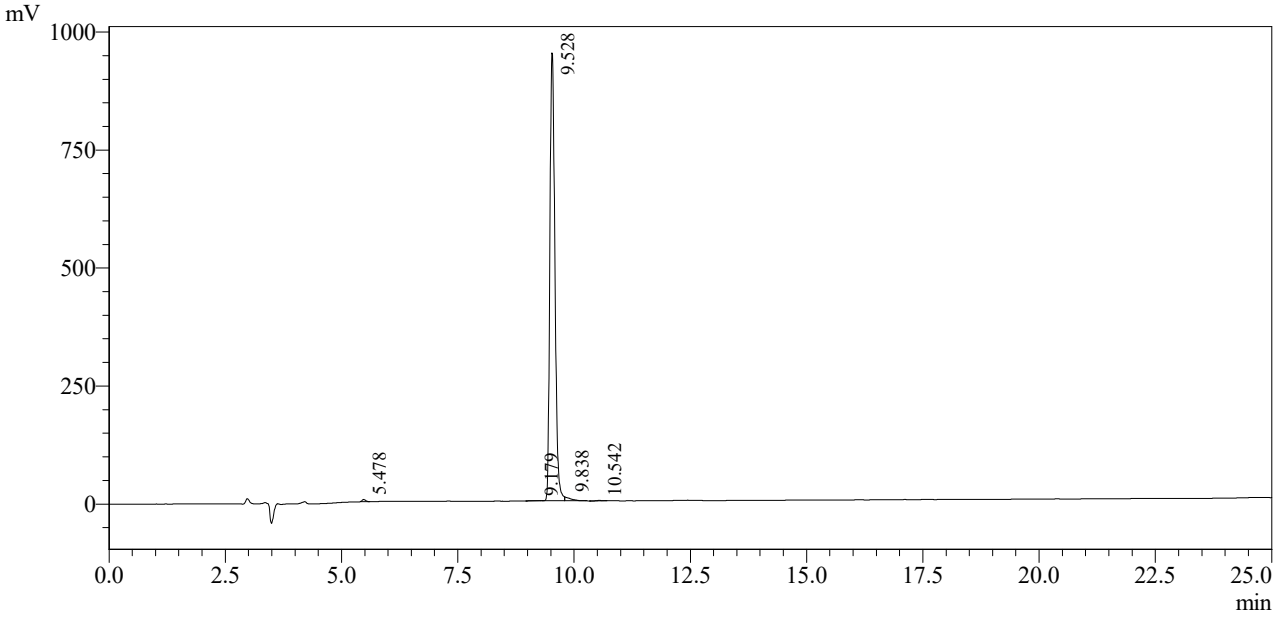

1 Detector A Channel 1 / 220nm

Peak Table

Detector A Channel 1 220nm

Peak#	Ret. Time	Area	Height	Area %
1	5.478	21057	4333	0.290
2	9.179	7724	622	0.106
3	9.528	7156018	946923	98.611
4	9.838	67486	7112	0.930
5	10.542	4505	784	0.062
Total		7256791	959773	100.000